

MODELING AND EXPERIMENTAL TESTING OF TWIST
ACTUATED SINGLE CELL COMPOSITE BEAMS FOR
HELICOPTER BLADE CONTROL

by

ANDRIES J. DU PLESSIS

Submitted to the Department of Aeronautics and Astronautics
in Partial Fulfillment of the Requirements for the Degree of

MASTER OF SCIENCE
IN AERONAUTICS AND ASTRONAUTICS

at the
MASSACHUSETTS INSTITUTE OF TECHNOLOGY
February 1996

© 1996 Massachusetts Institute of Technology
All rights reserved

Signature of Author

.....

Department of Aeronautics and Astronautics

February 2, 1996

Certified by

.....

Associate Professor Nesbitt W. Hagood

Thesis Supervisor

Accepted by

.....

MASSACHUSETTS INSTITUTE
OF TECHNOLOGY

Professor Harold Y. Wachman
Chairman, Department Graduate Committee

FEB 21 1996

Aero

LIBRARIES

MODELING AND EXPERIMENTAL TESTING OF TWIST ACTUATED SINGLE CELL COMPOSITE BEAMS FOR HELICOPTER BLADE CONTROL

by

Andries J. du Plessis

Submitted to the Department of Aeronautics and Astronautics on January 19, 1996
in Partial Fulfillment of the Requirements for the Degree of Master of Science in
Aeronautics and Astronautics

Abstract

An adaptive beam model of anisotropically actuated, single cell, composite beams is formulated to determine the twist actuation capabilities of anisotropic linear piezoelectric actuators as related to the potential application for helicopter blade control. The model allows for the inclusion of planar anisotropic actuation piezoelectric media anywhere in the cross-section of the composite beam. Model state variables are the displacement, rotations, twist, and twist rate of the beam cross-section. The adaptive beam model is used in a twist actuation parameter study to determine anisotropic actuator properties which result in maximum non-dimensionalized twist of a twist actuated composite box beam. The study indicates that actuators should either have no stiffness anisotropy with negative actuation anisotropy, or high stiffness anisotropy with no actuation anisotropy. The objective of the adaptive, single cell, composite beam model is to predict the static displacement response of an anisotropically actuated beam. To obtain the static displacement response of an actuated beam, the model governing differential equations are solved with the finite element method. The element used in the analysis is a high order adaptive beam finite element formulated based on the analytical adaptive beam model. The simulation capabilities of the adaptive beam finite element is validated with displacement comparisons for both passive and adaptive beams. Finally, a proof of concept 1/16th scale adaptive model blade, constructed from composite materials, is tested for twist actuation performance. Experimentally measured twist levels proves the anisotropic actuation concept and validates the adaptive beam model and associated adaptive beam element.

Thesis Supervisor: Dr. Nesbitt W. Hagood

Title: Associate Professor of Aeronautics and Astronautics

Acknowledgments

I wish to thank for Prof. Nesbitt Hagood for giving me the opportunity to conduct research at MIT in the Active Materials and Structures Laboratory. To all the AMSLers: Thank you for the friendship, support, and laughter during the past two years (it made all those late nights bearable!). The actuators that were used for the experimental part of this study was manufactured by Aaron A. Bent, John P. Rodgers and Alessandro Pizzochero. You saved my life, guys! Thank you John for proof reading the thesis. To all the friends and family back home in South Africa and in Boston: Baie dankie vir julle ondersteuning/Thanks for your support. To her that suffered with me these two years at MIT: Thanks Berrie.

Life in Boston according to Jaco:

"Alles is COOL tot die wit kak in swart kak verander"

Everything is COOL until the white s... (stuff) turns into black s... (stuff)

Biographical Note

Andries Jacobus du Plessis is a native of Pretoria, Gauteng, Republic of South Africa. He graduated from the University of Pretoria with a degree in Mechanical Engineering. Since August 1993 he has been living in Boston, Massachusetts in an effort to deprive himself of sunlight, beer, braaivleis (BBQ), and to get a master's degree from MIT.

Table of Contents

Abstract	3
Table of Contents	9
List of Figures	13
List of Tables	17
Nomenclature	19
Chapter 1: Introduction	23
1.1 Motivation.....	23
1.2 Objectives	26
1.3 Background.....	27
1.3.1 Active Materials	27
1.3.2 Anisotropic Actuators	30
1.3.3 Adaptive Structures.....	34
1.3.4 Aeroelastic Control for Aircraft	35
1.3.5 Helicopter Blade Control.....	36
1.4 Thesis Overview.....	38

Chapter 2: Modeling of Actuated Single Cell Composite Beams	41
2.1 Introduction.....	41
2.2 Actuated Beam Description and Assumptions	42
2.3 Strain-Displacement Relations.....	44
2.3.1 Position Vector and Normal Projection	44
2.3.2 Beam Cross-Section Kinematics.....	46
2.3.3 Torsional Warping Function	48
2.3.4 Strain Relations	51
2.4 Constitutive Relations	52
2.4.1 Linear Piezoelectric Constitutive Relations	52
2.4.2 Plane Stress Problem.....	54
2.4.3 Property Rotations.....	55
2.4.4 Plate Formulation.....	57
2.5 Equations of Motion	59
2.5.1 Internal Strain Energy.....	59
2.5.2 External Work.....	61
2.5.3 Equilibrium Equations and Boundary Conditions	62
2.5.4 Force-Displacement Relations.....	63
2.5.5 Structural Coupling.....	66
2.5.6 Solution of the Governing Equations	67
2.6 Summary.....	67
Chapter 3: Twist Actuator Parameter Study	69
3.1 Composite Box Beam Description	70
3.1.1 Laminate Membrane Stiffness.....	71
3.1.2 Box Beam Stiffnesses for Parameter Study	73
3.2 Actuator Description	73
3.2.1 Actuator Package Induced Stress Resultants	74
3.2.2 Maximized Induced Shear Stress Resultants	75
3.3 Non-Dimensional Actuated Box Beam Twist.....	77
3.3.1 Induced Torque and Beam Torsional Stiffness	77
3.3.2 Beam Tip Twist.....	80
3.3.3 Non-Dimensional Tip Twist Parameter	85

3.4 Parameter Study	87
3.4.1 Influence of the Actuator Stiffness Anisotropy on Twist	88
3.4.2 Influence of the Actuator Free Strain Anisotropy on Twist.....	89
3.4.3 Twist Parameter Contour Plots.....	90
3.5 Actuator Comparison	92
3.6 Summary	93
Chapter 4: Finite Element Displacement Simulation	95
4.1 Adaptive High Order Beam Element	96
4.1.1 Adaptive Single Cell Composite Beam Element Description	97
4.1.2 Displacement and Voltage Interpolation.....	99
4.1.3 Element Strains and Electrical Fields	101
4.1.5 Constitutive Relations	102
4.1.6 Governing Equations.....	104
4.1.7 Actuated Beam Displacement Simulation	106
4.2 Non-Actuated Beam Model Verification.....	108
4.2.1 Previous Experimental Work.....	108
4.2.2 Cross-Ply Beam Results	110
4.2.3 Symmetric Beam.....	111
4.2.4 Anti-Symmetric Beam Results	116
4.2.5 Results Discussion.....	118
4.3 Actuated Beam Model Verification	119
4.3.1 Chinook CH-47D Blade	119
4.3.2 Approximate Blade Description	120
4.3.3 Actuated Blade	122
4.3.4 CH-47D Blade Spar Twist Results	123
4.4 Summary	125
Chapter 5: Experimental Beam Manufacturing and Testing	127
5.1 Manufacture of Passive Composite Box Beams.....	128
5.1.1 Laminate Manufacturing	128
5.1.2 Laminate Panel and Edge-fitting Preparation	129
5.1.3 Mandrel Assembly and Secondary Cure	130
5.2 Box Beam Experimental Setup and Results.....	133

5.2.1 Experimental Setup.....	133
5.2.2 Cross-ply Beam Results.....	137
5.2.3 Symmetric Beam Results.....	138
5.3 Twist Actuated Model Helicopter Blade.....	141
5.3.1 IDEPFC Actuators.....	141
5.3.2 E-Glass Properties.....	145
5.3.3 Non-Active Scale Model Blade Manufacturing.....	147
5.3.4 Twist Actuated Model Blade Manufacturing.....	149
5.3.5 Experimental Setup.....	152
5.3.6 Actuated Model Blade Twist.....	153
5.4 Summary.....	155
Chapter 6: Conclusions and Recommendations	157
6.1 Conclusions.....	157
6.2 Recommendations.....	160
References	163
Appendix A: MATLAB Code	169
Appendix B: ANSYS Code	195

List of Figures

Figure 1-1. Piezoelectric Material Coordinate System.....	29
Figure 1-2. Piezoelectric Fiber Composite.....	31
Figure 1-3. Anisotropic Actuation	32
Figure 1-4. IDEPFC Actuation System	33
Figure 2-1. Global and Local Coordinate Systems	43
Figure 2-2. Position Vector of a Point in the Beam Wall.....	44
Figure 2-3. Global Displacement Variables.....	46
Figure 2-4. Normal Displacements Associated with Beam Out-of-Plane Rotation.....	47
Figure 2-5. Structural and Material Coordinate Systems.....	55
Figure 3-1. General Box Beam for Parameter Study	70
Figure 3-2. Twist Actuator Package	74
Figure 3-3. Beam Cross-Section with Actuator Package Included.....	77
Figure 3-4. Influence of Actuator Stiffness Anisotropy, R_{Q22} , on the Twist Parameter.....	89
Figure 3-5. Influence of Free Strain Actuation Anisotropy, R_d , on the Twist Parameter.....	90
Figure 3-6. Non-Dimensionalized Twist Parameter Contour Plots	91
Figure 3-7. Actuator Comparison based on Actuator Anisotropies	94
Figure 4-1. Adaptive Single Cell Composite Beam Element.....	98
Figure 4-2. Displacement Simulation Code Outline.....	107
Figure 4-3. Experimental Passive Box Beam Geometry	109
Figure 4-4. Cross-Ply Beam Bending Slope, $W_{,x}$, for a Unit Tip Shear Force, \bar{Q}_z	110
Figure 4-5. Cross-Ply Beam Twist , ϕ , for a Unit Tip Torque, \bar{M}_x	111

Figure 4-6. Symmetric Box Beam Schematic	112
Figure 4-7. Symmetric Layup Beam - Bending Slope and Twist for a Unit Tip Shear Load, \bar{Q}_2 (Top $[-15]_6$ & Bottom $[15]_6$)	113
Figure 4-8. Symmetric Layup Beam - Bending Slope and Twist for a Unit Tip Shear Load, \bar{Q}_2 (Top $[-30]_6$ & Bottom $[30]_6$)	114
Figure 4-9. Symmetric Layup Beam - Bending Slope and Twist for a Unit Tip Shear Load, \bar{Q}_2 (Top $[-45]_6$ & Bottom $[45]_6$)	115
Figure 4-10. Anti-symmetric Box Beam Schematic	116
Figure 4-11. Anti-Symmetric Layup Beam - Bending Slope for a Unit Tip Shear Load, \bar{Q}_2 (Top $[15]_6$ & Bottom $[15]_6$)	117
Figure 4-12. Anti-Symmetric Layup Beam - Bending Slope for a Unit Tip Shear Load, \bar{Q}_2 (Top $[0/30]_3$ & Bottom $[0/30]_3$)	117
Figure 4-13. Anti-Symmetric Layup Beam - Bending Slope for a Unit Tip Shear Load, \bar{Q}_2 (Top $[0/45]_3$ & Bottom $[0/45]_3$)	118
Figure 4-14. CH-47D Blade Spar Approximation	120
Figure 4-15. CH-47D Actuated Spar Laminate Construction	122
Figure 4-16. ANSYS Model of the Twist Actuated CH-47D Blade	124
Figure 4-17. CH-47D Actuated Spar Twist	124
Figure 5-1. Aluminum Edge-Fitting Cross-Section	130
Figure 5-2. Aluminum Mandrel used for Passive Box Beam Manufacture	130
Figure 5-3. Mandrel Manufacturing Assembly	131
Figure 5-4. Experimental and Model Box Beam Cross-Sections	132
Figure 5-5. Experimental Setup Base, Base Mount, and Top Mount	134
Figure 5-6. Beam Shear Force and Torque Application Systems	135
Figure 5-7. Laser Displacement Measurement System	136
Figure 5-8. Cross-Ply Beam Transverse Displacement, W , for a Tip Shear Load	137
Figure 5-9. Cross-Ply Beam Twist, ϕ , for a Tip Torque	138
Figure 5-10. Symmetric Beam Transverse Displacement, W , and Twist, ϕ , for a Tip Shear Force	139
Figure 5-11. Symmetric Beam Twist, ϕ , for a Tip Moment	140
Figure 5-12. Electrode Pattern of the 45° IDEPFC Actuators	142
Figure 5-13. IDEPFC Actuators used for Updating of	144
Figure 5-14. Twist Actuated Model Blade Manufacturing	150
Figure 5-15. Twist Actuated Model Helicopter Blade	151

Figure 5-16. Adaptive Model Blade with Dimensions and Actuator Locations..... 152
Figure 5-17. Angular Indicator Twist Measurement Setup..... 152
Figure 5-18. Laser Twist Measurement Setup..... 153
Figure 5-19. Tip Twist of the Active Blade as a Function of Applied Voltage 154
Figure C-1. ANSYS Code Flowchart 195

List of Tables

TABLE 3-1. INVARIANT SYSTEM PARAMETERS FOR TWIST PARAMETER STUDY.....	88
TABLE 3-2. TWIST ACTUATOR MATERIAL PROPERTIES	93
TABLE 4-1. AS4/3506-1 MATERIAL PROPERTIES	109
TABLE 4-2. CROSS-PLY BOX BEAM DIMENSIONS AND LAYUPS	110
TABLE 4-3. SYMMETRIC BOX BEAM DIMENSIONS AND LAYUPS	112
TABLE 4-4. ANTI-SYMMETRIC BOX BEAM DIMENSIONS AND LAYUPS	116
TABLE 4-5. CH-47D SPAR MATERIAL PLY PROPERTIES	121
TABLE 4-6. CH-47D MODEL AND ACTUAL BLADE STIFFNESSES	122
TABLE 5-1. AS4/3501-6 PLY PROPERTIES.....	129
TABLE 5-2. T6061-T6 ALUMINUM PROPERTIES	129
TABLE 5-3. EXPERIMENTAL BOX BEAM DIMENSIONS AND LAYUPS.....	132
TABLE 5-4. IDEPFC STIFFNESS PROPERTIES.....	144
TABLE 5-5. IDEPFC ACTUATION PROPERTIES	145
TABLE 5-6. CURED E-GLASS (#120) PROPERTIES.....	146
TABLE 5-7. NON-ACTIVE MODEL BLADE SCALING PARAMETERS.....	148

Nomenclature

A	cross sectional area
A, B, D	laminated plate elastic coefficients matrices
B_u, B_v	strain and electrical field interpolation matrices
C_{ij}	3-D ply elastic constants
c	blade chord
d	blade thickness
d_{ij}	ij^{th} piezoelectric strain-field coupling constant
D	electrical displacement vector
e_{ij}	ij^{th} piezoelectric stress-field coupling constant
E_i	applied electric field, Young's modulus in the i^{th} direction
F	internal beam force vector, adaptive beam element forcing matrix
G_{ij}	ij^{th} shear modulus
K_{ij}	beam stiffness constants
K	adaptive beam element stiffness matrix
L_{ij}	reduced plate stiffness coefficients
L_u, L_v	displacement, voltage differential matrix operator
l	blade length
m_i	distributed moment around the i -axis
M_i	i^{th} beam moment, torque
M_{ij}	ij^{th} moment stress resultant
n_x	distributed beam normal force
N	beam normal force
N_i	i^{th} interpolation function

N_{ij}	ij^{th} force stress resultant
N	reduced plate stress resultant vector
N_u	displacement interpolation function matrix
N_v	voltage interpolation function matrix
p_{ijk}	rotated piezoelectric stress coupling parameter
P_ϕ	non-dimensional twisting parameter
P	poling vector, induced stress coefficient matrix
q	shear flow
q_i	i^{th} distributed shear force or bimoment
Q_i	i^{th} beam shear force, bimoment
Q_{ij}	2-D plane stress ply elastic constants
r	position vector
R_i	non-dimensional system parameter for i^{th} variable
R_{ij}	rotated plane stress ply elastic constants
s	mid-plane circumferential coordinate
s	material compliance matrix
S	Voigt's contracted strain vector
t	wall thickness
T	Voigt's stress vector, tensor rotation matrix
u, v, w	displacements in x, y, z system
u_t	mid-plane tangential displacement
u	beam displacement variables, adaptive beam displacement vector
U	internal system energy
U, V, W	cross-section centerline displacements
v_i^j	voltage on the i^{th} side of the j^{th} composite ply
W_{ext}	external system work
α	cross sectional warping parameter
β_i	cross sectional rotation around i^{th} -axis
ϵ_{ij}	ij^{th} normal strain
ϵ	material dielectric matrix, reduced plate strain vector
ϕ	twist angle
Γ	center line
γ_{ij}	ij^{th} shear strain
κ_{ij}	ij^{th} curvature

λ	beam torsional warping constant
Λ	induced strain
ν_{ij}	ij^{th} poisson's ratio
θ	material angle
Θ	adaptive beam element electro-mechanical coupling matrix
σ_{ij}	ij^{th} normal stress
Σ, Π	force and moment induced stress resultant coefficient matrices
τ_{ij}	ij^{th} shear stress
ξ	normalized spanwise coordinate
ψ	warping function

Superscripts and Subscripts

1,2	nodal points
<i>a</i>	actuation, actuator
<i>act</i>	actuator
<i>b</i>	blade
<i>eff</i>	thickness averaged effective value
<i>E</i>	variable measured at constant electrical field
<i>k</i>	k^{th} ply in a composite laminate
<i>s</i>	structure
<i>S</i>	variable measured at constant stress field
$(\cdot)^T$	transpose
$(\cdot)_{,ij}$	ij^{th} derivative
$(\bar{\cdot})$	end point values, nodal values
$(\hat{\cdot})$	unit vector
\circ	midplane value
*	reduced values

Coordinates

1,2,3	local material cartesian coordinate system
<i>x, y, z</i>	general cartesian coordinate system
<i>X, Y, Z</i>	center line coordinates
<i>x, t, n</i>	local coordinate system at center line

In recent decades researchers have been investigating the application of new material system developments to existing engineering systems in an effort to improve these systems. There is a drive toward systems with improved performance, less parts, lower maintenance costs, and higher reliability. This thesis focuses on the application of new materials technology to flight control mechanisms, and in particular helicopter blade control mechanisms for the suppression of vibration experienced during forward flight and the potential reduction of helicopter noise.

1.1 Motivation

The basic operating principle of a helicopter is a thrust vectoring rotor which not only supplies lifting forces, but also the forces needed for forward flight. Problems associated with the usage of a rotor in forward flight include high vibration, noise and limited speed. Vibration is one of the more important factors due to ride comfort and maintenance requirements on the helicopter.

During helicopter forward flight, the main rotor operates in an unsteady, complex aerodynamic field which leads to high levels of vibration in both the fuselage and the rotor. As the blades change angle during rotation, the aerodynamic conditions change as well. This causes aerodynamic forcing on the blades at higher harmonics of the rotor base rotational speed, Ω . Through aeroelastic interaction, these forcings are transmitted to the fuselage as forces and moments which results in the vibration of the helicopter. For a N

bladed rotor the $(N \pm 1)\Omega$ and $N\Omega$ blade loads leads to $N\Omega$ forcings on the fuselage [Loewy, 1984].

A good overview of vibration attenuation devices was given by Loewy [Loewy, 1984]. These systems include both passive and active vibration reduction devices. Passive devices have an associated bandwidth restriction and can not address the whole vibration frequency spectrum. Most of the active vibration reduction devices acts as isolation systems between the fuselage and the rotor. None of the existing systems are capable of isolating vibrations in the vertical direction between the rotor and the fuselage.

The most recent development for helicopter vibration reduction at the source, is higher harmonics control (HHC). Shaw [Shaw and Albion, 1980] showed that HHC can be accomplished by $\pm 3^\circ$, high frequency, pitch angle changes of the blades. This method directly controls the higher harmonic disturbances at the excitation through blade pitch changes instead of using the fuselage as the point of vibration reduction. The easiest HHC scheme is to actuate the swashplate, normally used for conventional flight control, to introduce the required blade pitch angle changes [Shaw et al., 1985]. There are some problems associated with using the swashplate for HHC. The swashplate is a low frequency device which is incapable of introducing $(N + 1)\Omega$ frequency pitch angle changes. Another drawback of the swashplate is that only certain pitch frequencies can be independently introduced into the system. The final limitation of the swashplate is the inability to vary the spanwise pitch angle which would provide a stall area reduction mechanism for the helicopter rotor [Fenn et al., 1993].

Individual blade control (IBC) schemes offer a solution to the HHC objective. There are no limit on the type of the blade pitch angle changes which can be imposed during a blade revolution. Another advantage of IBC is potential for higher bandwidth control. The bandwidth of IBC systems is determined by the control mechanisms used in the systems and is not prescribed any standard helicopter systems (for example the swashplate). IBC also offers the possibility of controlling the spanwise blade lift. In order to provide a IBC scheme for the helicopter vibration problem, it is necessary to examine control mechanisms used for flight vehicles. To control a flight vehicle it is necessary to have control over the aerodynamic forces on the vehicle [Bisplinghoff and Ashley, 1962]. This control can be accomplished in various ways, but the two most effective ways available are to change the aerodynamic shape of the lifting structure or to change the angle of incidence of the lifting

structure. In most flight vehicles this control is achieved by the deflection or deformation of lift generating control surfaces. These deformations can be local (flaps) or global (swashplate), but in all cases the goal of the deformation is to change the air flow around the control surface or attached structure. Therefore either shape control, or incidence control (control of the effective angle of attack) is required for the control of a flight structure.

Thus to enable IBC control, some means of shape or incidence control must be implemented on the helicopter blade. Active materials which strain when exposed to an external excitation, whether it be temperature, electrical field or magnetic field, offer a means to accomplish IBC. Some trailing edge flap actuation schemes have been proposed for IBC [Spangler and Hall, 1990; Fenn et al., 1993; Walz and Chopra, 1994]. A very effective means to attain either shape or incidence control is through planar shear or bending actuation schemes. An example of this is a helicopter blade which is twisted with shear inducing actuators embedded in the wall of the blade.

There are two methods for active materials to induce planar shear in a structure: the first is through structural couplings and the second is by inducing direct shear. To obtain direct shear stresses the active material must exhibit planar anisotropic actuation behavior. Barrett [Barrett, 1992] showed that it is possible to induce twist in a lifting structure by using Directionally Applied Piezoelectric (DAP) elements for actuation. These in-plane, isotropic actuation elements induced shear through a shear lag effect in the attachment of the element to the structure. Chen [Chen and Chopra, 1995] also used shear lag to induce shear stresses to twist a blade with embedded monolithic piezoelectric elements. The maximum static blade tip twist reported was 0.6° . The insufficient actuation levels of these elements excludes these actuation schemes from IBC.

The Piezoelectric Fiber Composite (PFC) [Hagood and Bent, 1993] is an anisotropic actuation material which has the capability of inducing direct, planar, distributed shear stresses in a structure. The PFC actuators consist of piezoelectric fibers which are embedded in a soft epoxy matrix. This composite active layer is sandwiched between two electrode layers to supply the necessary through-thickness applied electrical field for operation (a more detailed description of PFC actuator operation is given in the background section). PFC's have several advantages over monolithic piezoelectric wafers. Some of these are tailorability, conformability, and improved reliability. This actuator system is also easily integrated with composite material manufacturing techniques which are widely used

in the aerospace environment [Rodgers and Hagood, 1995]. PFC actuation performance is improved with the usage of Interdigitated Electrodes (IDE) [Hagood et al., 1993; Bent and Hagood, 1995]. These electrodes enable distributed, planar, anisotropic actuation which utilize the primary piezoelectric effect instead of the transverse piezoelectric effect. This material system can be used to twist a helicopter blade or deflect a secondary control surface on the blade for IBC. The need thus exists to investigate the possibility of using this new anisotropic actuation material system, Interdigitated Electrode Piezoelectric Fiber Composite (IDEPFC), for the control of helicopter blades to accomplish IBC.

1.2 Objectives

The first objective of this study is to construct an analytical model of anisotropically actuated, single cell, composite beams to predict the static displacement response of such beams. This model is required to investigate the potential application of twist actuated composite beams for helicopter blade control. Associated with the adaptive beam model, an effective boundary value problem solution technique, such as the finite difference or finite element method, should be numerically implemented for actual blade design purposes. New developments in actuation material technologies enable planar anisotropic actuation, and the model should reflect this. Aerodynamic control surfaces are of different cross-sectional shapes and the model should not have any restrictions on the cross-sectional shape of the composite beam. At this stage of the study it is only necessary to be able to predict the static displacement response of the actuated composite beam.

The second objective of the study is to determine what the properties of an anisotropic actuator should be to obtain the maximum level of twist deformation for a single cell, composite beam. IDEPFC is an active material with tailorable stiffness and actuation properties. The designer has some freedom in choosing the stiffness and actuation properties when designing the actuator, therefore it is critical to have a priori knowledge of properties which is best for the twist application.

A mathematical model is not of any use if it does not reflect reality to a satisfactory level. Therefore the final objective of the study is to prove the twist concept experimentally and to verify the accuracy of the analytical model of the actuated, single cell, composite beam.

1.3 Background

The actuation of single cell composite beams with IDEPFC's has roots in a number of research fields. These fields are: active materials, anisotropic actuators, adaptive structures, aeroelastic control of aircraft using active materials, and helicopter blade control. The next sections look at relevant research that has previously been completed in these fields.

1.3.1 Active Materials

Active materials are materials which have some property which is controllable by the application of an external excitation. The simplest example is metals which change shape when exposed to variable temperature levels. Other examples of controllable properties are stiffness (shape memory alloys [Bueller and Wiley, 1965; Hurtado et al., 1995]) and viscosity (electrorheological fluid [Wang et al., 1994]). There are a number of external excitations which causes shape changes, but the most important ones are electrical and magnetic excitations. For this study, the interest is in piezoelectric materials which form the basis for IDEPFC's. A general discussion of shape-controllable materials will follow, along with a more in depth look into piezoelectric material.

Magnetostrictive materials are materials which strain when they are exposed to a magnetic field. "Terfenol-D" is a commercially available magnetostrictive material with high strain actuation values. The strain behavior of the material is quadratic with applied magnetic field and the maximum actuated strain level is on the order of 0.15% at room temperature [Butler, 1988]. The primary disadvantages of these materials for actuation are the low stiffness and associated systems needed to supply the magnetic field for actuation.

Electrostrictive ceramics are lead based active materials with a quadratic strain response with applied electrical field. Maximum strain levels are on the order of 0.1% [Fripp et al., 1995]. A big problem with these materials is the temperature dependence of the actuation properties. Another lead based active material is shape memory ceramics. This material composition is on the phase boundary between ferroelectric and anti-ferroelectric materials. When exposed to a high enough electrical field the material undergoes a phase transition between anti-ferroelectric to ferroelectric. Associated with this phase change is a large volume change. The maximum strains during the phase transition is on the order of 0.3%. Once the phase change is imposed, an opposite field must be applied to reverse the phase

transition [Ghandi and Hagood, 1994]. The material thus acts as a binary memory which can be switched between strain states.

Piezoelectricity is the ability of certain crystalline materials to develop an electrical charge proportional to an applied mechanical stress. The converse effect can also be seen in these materials where strain is developed proportional to an applied electrical field. It was originally discovered by the Curie's in the 1880's. Today piezoelectric materials for industrial applications are lead based ceramics available in wide array of properties. Maximum in-plane actuation strains are on the order of 0.1% [Chan and Hagood, 1994]. Piezoelectric materials have high actuation authority due to the high Young's modulus. Another advantage of piezoelectric ceramics is the high associated bandwidth which enables dynamic control applications. The biggest draw backs of these materials are their brittleness and high densities. Piezoelectric materials are the most well known active material typically used for transducers as well as in adaptive structures.

The virgin ceramic material must be poled first to utilize the complete piezoelectric effect. Poling consists of applying a high electrical field to the material. During the poling process the crystal dipoles in the material are aligned with the applied electrical field and the material strains in the direction of the electrical field. By applying a field of the opposite direction, strain of the opposite sign is observed. If the magnitude of this opposite field is increased, the material first depoles and finally repoles.

Poled piezoelectric material is transversely isotropic. That is: one plane is isotropic while the out-of-plane direction has different properties. The standard coordinate convention adopted by the IEEE [IEEE, 1978] assigns the 1-2 plane as the plane of symmetry and the 3-direction as the-out of-plane poling direction. Figure 1-1 shows the standard coordinate system. Vector \mathbf{P} is the poling vector, and \mathbf{E} is the applied electrical field. If the applied field is in the same direction as the poling vector the piezoelectric piece expands in the 3-direction and contracts in the transverse (1-2) directions (as shown in Figure 1-1).

For a small applied electrical field, the response of the piezoelectric ceramic can be modeled by the following linear piezoelectric constitutive relations [Jaffe et al., 1971], expressed in engineering matrix notation as:

$$\begin{Bmatrix} \mathbf{S} \\ \mathbf{D} \end{Bmatrix} = \begin{bmatrix} \mathbf{s}^E & (\mathbf{d})^T \\ \mathbf{d} & \boldsymbol{\varepsilon}^T \end{bmatrix} \begin{Bmatrix} \mathbf{T} \\ \mathbf{E} \end{Bmatrix} \quad (1.1)$$

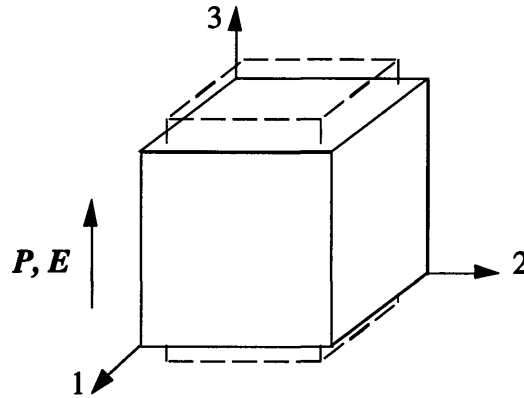


Figure 1-1. Piezoelectric Material Coordinate System

The field variables are T , S , D , and E , the matrices of engineering stress and strain as well as the electrical displacement and electrical field. Voigt's contracted stress and strain notation is used to represent the stress and strain state in the material. The different field variables can be expressed in component form as:

$$T = \begin{Bmatrix} T_1 \\ T_2 \\ T_3 \\ T_4 \\ T_5 \\ T_6 \end{Bmatrix} = \begin{Bmatrix} \sigma_{11} \\ \sigma_{22} \\ \sigma_{33} \\ \tau_{23} \\ \tau_{31} \\ \tau_{12} \end{Bmatrix}, \quad S = \begin{Bmatrix} S_1 \\ S_2 \\ S_3 \\ S_4 \\ S_5 \\ S_6 \end{Bmatrix} = \begin{Bmatrix} \epsilon_{11} \\ \epsilon_{22} \\ \epsilon_{33} \\ \gamma_{23} \\ \gamma_{31} \\ \gamma_{12} \end{Bmatrix}, \quad D = \begin{Bmatrix} D_1 \\ D_2 \\ D_3 \end{Bmatrix}, \quad \text{and} \quad E = \begin{Bmatrix} E_1 \\ E_2 \\ E_3 \end{Bmatrix} \quad (1.2)$$

the stress and In this study bold faced variables denote either a vector or a matrix. The field variables are related through the material property matrices s , d , and ϵ which represent the material compliance, piezoelectric electromechanical coupling coefficients, and the material dielectric. Superscripts E and T denote constant electrical field and stress boundary conditions (typically short circuit and stress free boundaries), while $(\cdot)^T$ denote the matrix transpose. The complete matrix expansion of equation (1.1) for poled polycrystalline ceramic piezoelectric material is:

$$\begin{Bmatrix} S_1 \\ S_2 \\ S_3 \\ S_4 \\ S_5 \\ S_6 \\ D_1 \\ D_2 \\ D_3 \end{Bmatrix} = \begin{array}{cccccc|ccc} s_{11}^E & s_{12}^E & s_{13}^E & 0 & 0 & 0 & 0 & 0 & d_{31} \\ s_{12}^E & s_{11}^E & s_{13}^E & 0 & 0 & 0 & 0 & 0 & d_{32} \\ s_{13}^E & s_{13}^E & s_{33}^E & 0 & 0 & 0 & 0 & 0 & d_{33} \\ 0 & 0 & 0 & s_{44}^E & 0 & 0 & 0 & d_{24} & 0 \\ 0 & 0 & 0 & 0 & s_{44}^E & 0 & d_{15} & 0 & 0 \\ 0 & 0 & 0 & 0 & 0 & s_{66}^E & 0 & 0 & 0 \\ \hline 0 & 0 & 0 & 0 & d_{15} & 0 & \varepsilon_1^T & 0 & 0 \\ 0 & 0 & 0 & d_{24} & 0 & 0 & 0 & \varepsilon_2^T & 0 \\ d_{31} & d_{32} & d_{33} & 0 & 0 & 0 & 0 & 0 & \varepsilon_3^T \end{array} \begin{Bmatrix} T_1 \\ T_2 \\ T_3 \\ T_4 \\ T_5 \\ T_6 \\ E_1 \\ E_2 \\ E_3 \end{Bmatrix} \quad (1.3)$$

Depending on the problem, equation (1.1) can be manipulated into three other formats depending on the field variables used in the problem [IEEE, 1978]. The appropriate form used for this study is:

$$\begin{Bmatrix} T \\ D \end{Bmatrix} = \begin{bmatrix} c^E & -(e)^T \\ e & \varepsilon^S \end{bmatrix} \begin{Bmatrix} S \\ E \end{Bmatrix} \quad (1.4)$$

with

$$c^E = (s^E)^{-1}, \quad e = dc^E, \quad \text{and} \quad \varepsilon^S = \varepsilon^T - dc^E(d)^T \quad (1.5)$$

In equation (1.4), c^E are material elastic coefficients (stiffness coefficients) at constant electrical field and ε^S are the material dielectric constants at constant strain. The matrix e is the induced stress coefficient matrix.

1.3.2 Anisotropic Actuators

Before solving the problem at hand, it is necessary to have a clear understanding of what is meant by anisotropic actuation. The word anisotropic means “having physical properties that are different when measured along different axes” [Webster's, 1992]. For a completely anisotropic material, the elastic constants in Hooke's law, are all independent [Jones, 1975]. As the order in the material increases, the number of independent constants decreases up to the point where the material is isotropic and there are only two independent material constants. The same argument applies to actuation properties. For problems where the actuation is described in terms of induced stress (equation (1.4)), the actuation is described by the induced stress actuation matrix, e . An active material has anisotropic

actuation capabilities if the matrix entries are all independent. The origins of the induced stress matrix lies with both the stiffness properties and the actuation strain properties. Thus anisotropic actuation can either result from stiffness origins or from actuation origins, or a combination of both.

The major concern for this study is the ability to induce shear stresses in planar structures (i.e. plates and shells). Currently available planar actuation materials behave isotropically in both stiffness and actuation in the 1-2 plane. Directionally Applied Piezoelectric (DAP) elements were introduced by Barrett [Barrett, 1992] to construct an “anisotropic” actuator. For this actuation scheme a very thin (widthwise) bonding layer are used to attach the actuators to the structure. The large aspect ratio of the bonding layer area results in the transferal of strain in the direction parallel to the bonding layer and very low induced strain transverse to the thin bonding layer. Although this scheme does function, it is not an anisotropic actuator, but rather an anisotropic attachment driven by an isotropic actuator.

Piezoelectric Fiber Composites (PFC) were developed by Hagood [Hagood and Bent, 1993] to accomplish planar anisotropic actuation and increase the strength and reliability of piezoelectric actuators. The actuators consist of piezoelectric fibers which are embedded in a soft epoxy matrix. This composite active layer is sandwiched between two electrode layers to supply the necessary through-thickness applied electrical field for operation. The actuator layer is then included as an active ply in a composite panel during final structural integration. A schematic of the actuator is shown Figure 1-2. The anisotropic nature of the actuator comes from the fact that in the fiber direction, the response is dominated by the fiber properties (both stiffness and actuation). Transverse to the fibers, the response is dominated by the soft epoxy matrix. The final result is an actuator with stress actuation properties which differ in the longitudinal and transverse directions.

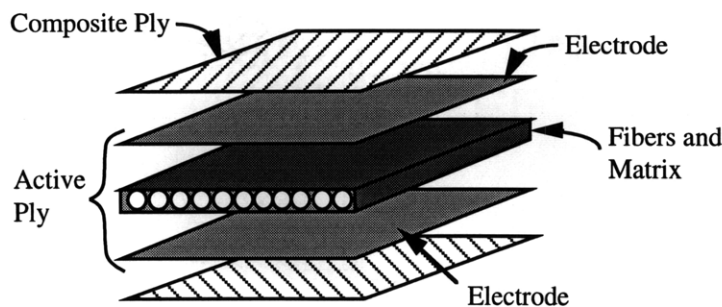


Figure 1-2. Piezoelectric Fiber Composite

Another advantage of the composite construction is that PFC's are much more conformable and less brittle than monolithic piezoelectric ceramic wafers. The soft epoxy matrix supports the brittle fibers and strengthens the actuator through load sharing.

The best way to get a physical understanding of anisotropic actuation is to look at what happens to single actuated PFC ply and then the response when attached to a structure. This explanation is exemplified in Figure 1-3.

A single PFC ply cantilevered at one end, with the major fiber axis aligned at some angle, responds as follows when actuated: along the major axis the highest levels of actuation strain is developed. Transverse to the major axis the actuated strain level is lower due to the fact that response is dominated by the epoxy matrix. In effect, the whole ply "shears". A mathematical description of this phenomena will be given in Chapter 2. If this single ply is attached to an isotropic substrate and then actuated, the laminated structure will bend, shear, and twist. If the same laminated structure is supplied with another actuator ply on the opposite side, oriented at the negative angle of the first ply, the actuated laminated structure will extend and twist if both active plies are excited in phase at the same the electrical field levels.

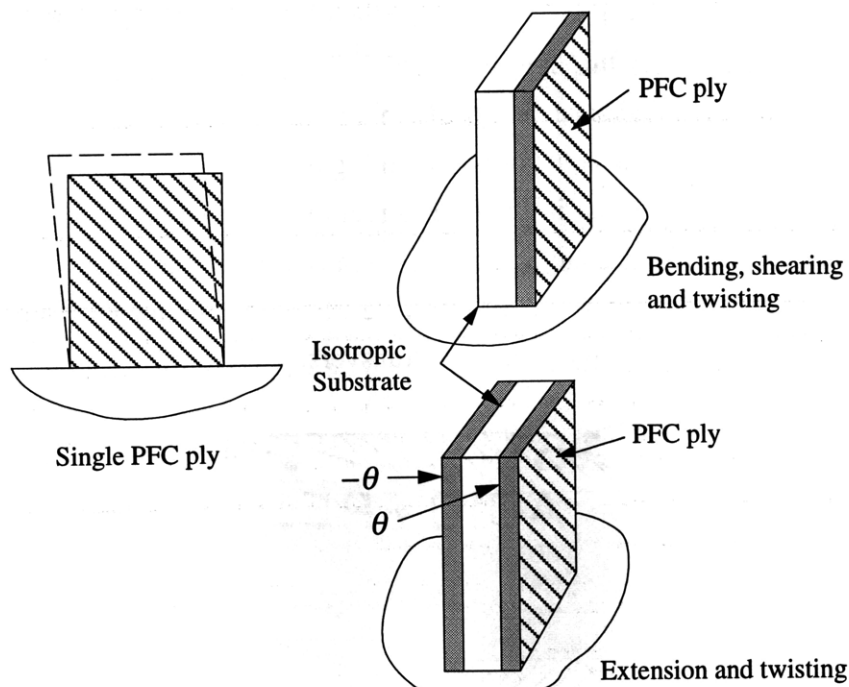


Figure 1-3. Anisotropic Actuation

Another development by Hagood [Hagood et al., 1993] is the Interdigitated Electrode Pattern (IDE). To supply the necessary field to either monolithic piezoelectric wafers or PFC's electrodes must be attached to the surfaces of the material. When using normal unpatterned electrodes, the electrical field is through the thickness of the piece. Assuming the actuators are also poled in the through-thickness direction, the in-plane actuation arises from the transverse piezoelectric effect. The schematic of the IDE system is shown in Figure 1-4. For proper operation of the IDE actuator, alternating electrode "fingers" are of different polarity. In this system with the appropriate poling, the major straining occurs in the plane of the actuator where it is most useful. Recent work published by Bent [Bent and Hagood, 1995] for IDEPFC reports strains of up to 0.17% in the fiber direction. This result is a significant improvement over conventional electrodes used on PFC's and the in-plane actuation capabilities of monolithic piezoceramic wafers.

To prove the concept of PFC's, Bent [Bent et al., 1995] constructed a laminated structure with PFC's and an isotropic substrate. The system was configured in such a fashion as to allow both bending actuation as well as twisting actuation. Close agreement with predicted values was reported. Rodgers [Rodgers and Hagood, 1995] took the work a step further with the inclusion of PFC plies in a composite structure. Again the system was configured to demonstrate twist actuation. Results from this study shows that the system can be used with composite materials to construct a planar structure actuated in twist.

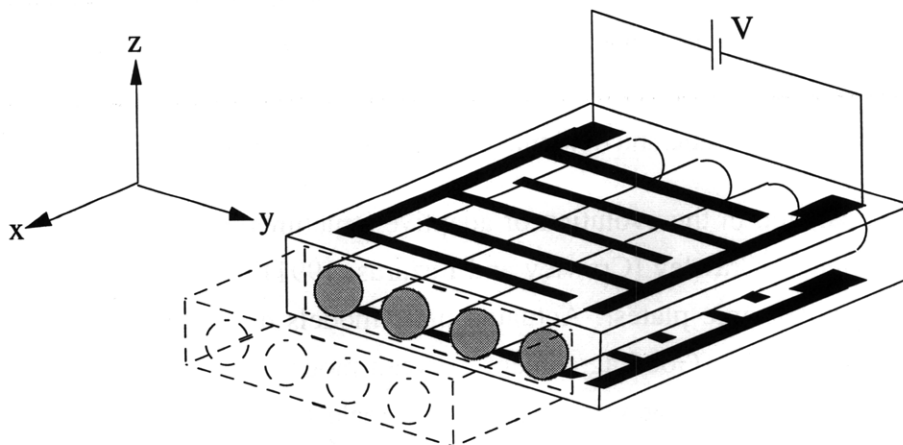


Figure 1-4. IDEPFC Actuation System

1.3.3 Adaptive Structures

Structures in the engineering sense, are elements of a system which are used for load transfer or elements which act as a “bus” for other devices like optical or transportation devices. In recent years there has been a concentrated effort to expand the operational envelope of structures through the use of active materials. The main characteristics of structures are mass, stiffness, static deflection under load and dynamic displacement, velocity, and acceleration behavior. Through the use of active materials, structural engineers are trying to improve the dynamic behavior of structures as well as to broaden the application regime of structures. In their review paper, Wada [Wada et al., 1989] gives a framework for classifying structures with active elements. The type of structures being dealt with in this study are adaptive structures. Adaptive structures are structures with actuators that “enable the alteration of system states or characteristics in a controlled manner”. Structures which use active elements as sensors are sensory structures and the intersection of these two classes is controlled structures. In the following sections, a basic background is given of adaptive structures, their evolution, and simple applications.

In the late seventies and mid eighties people started to consider using piezoelectric materials as direct actuators in structures. One of the first papers on adaptive structures by Crawley [Crawley and de Luis, 1986] reports on the use of piezoelectric actuators in simple beams. In this work, an analytical model is presented for the behavior of a bending actuated beam, and a study is conducted into the effects of bonding layers on the beam response. The final part of this work reports on experimental beams with surface bonded and embedded actuators to control the static and dynamic bending behavior of these beams.

The next logical step in the evolution of adaptive structures was to look at the isotropic actuation of plates. Crawley [Crawley and Lazarus, 1991] investigated the actuation of isotropic and anisotropic plates. Actuated plate models developed for the study were experimentally verified. Good agreement between model and experiment was reported. From this work, the conclusion was drawn that piezoelectric strain actuation is an effective means for controlling plate deformations. Lazarus [Lazarus and Crawley, 1992] took the actuation of plates further with the experimental demonstration of aeroelastic control of flexible plate-like adaptive structures. Throughout the literature, the only stresses and strains available, for planar actuators, were normal stresses and strains. To obtain twist deformations, structural coupling was used to transform bending and extension into twist.

It is the capability of PFC's and IDEPFC's to directly induce twist that makes it such promising material systems.

1.3.4 Aeroelastic Control for Aircraft

Aeroelastic control, which evolved with aircraft technology, is a technology which encompasses a lot of different aspects. In this section of the study, a report is given of the applicable background to adaptive aeroelastic control. The starting point is basic wing modeling followed by static aeroelastic control, and finally adaptive flutter control.

The wing of an aircraft can be modeled in several different ways. The easiest way is to model the wing as a plate made from isotropic material [Bisplinghoff and Ashley, 1962]. For composite wings, the plate models need be augmented to reflect the usage of composite materials. This is easily done through the use of Classical Laminated Plate Theory (CLPT) for transversely isotropic materials [Jones, 1975; Jensen et al., 1982]. The next level of modeling is to consider the wing to be a single cell composite box beam with thin walls [Rehfield, 1985; Libove, 1988; Librescu and Song, 1990; Chandra et al., 1990]. In these models, the thin-walled box beam problem is reduced to a high order, one-dimensional beam problem. An important feature of some of these models is the non-uniform twist distribution which is allowed in the model. This enables the inclusion of a torsional warping degree of freedom. Warping is the out-of-plane displacement during the twisting of a beam. Both the plate and the beam models can be used for static and dynamic modeling.

Static aeroelastic control for fixed wing aircraft consist of lift, roll, yaw and pitch control as well as divergence control. Weisshaar [Weisshaar, 1980; Weisshaar and Foist, 1985; Weisshaar, 1987] used a plate model of a composite wing to show that by tailoring the laminate layup, the divergence of forward swept, composite wings can be controlled. This work was continued by Librescu [Librescu and Thangjitham, 1991] by using higher order plate models of the forward swept wings. Ehlers [Ehlers and Weisshaar, 1990; Ehlers and Weisshaar, 1992] combined composite forward swept wing modeling and piezoelectrically actuated plates into a single topic of adaptive aeroelastic control of composite wings. The conclusion from this work was that torsional actuation is an important requirement for adaptive wings. This requirement effectively reduces to a shear inducing requirement for the active material. Another conclusion made by Ehlers was the need for new material systems with better performance. In answer to the induced shear stress requirement,

Barrett [Barrett, 1992] introduced DAP elements. DAP elements are capable of inducing shear stresses through a directional bonding layer. This concept was applied to a low aspect ratio wing for twist actuation [Barrett, 1993]. During experiments, the observed twist was small, which reaffirmed the need for new material systems.

In order to obtain better modeling accuracy for adaptive wings, Song [Song et al., 1992] used a high order beam model with active inclusions to model an adaptive wing. The outstanding feature of this work was the inclusion of primary and secondary warping into the model. Primary warping accounts for the out-of-plane displacements of the cross-section during twisting. Secondary warping accounts for through-thickness effects. This work showed that adaptive wings offer great potential for divergence control and the control of the spanwise lift distribution. Ehlers [Ehlers, 1994] used a similar model, but did not include any secondary warping effects. The major objective of this work was to explore different ways to actuate a wing to obtain twist deformations. One innovative way to obtain twist is to actuate the single cell, composite beam in warping. If the warping is restrained at one end, the other end twists when the beam is actuated.

The ultimate problem in aeroelasticity is flutter. Flutter is a dynamic instability which can lead to complete failure of wings during flight. Active materials are being considered as a means to control flutter in composite wings. Reich [Reich et al., 1995] described an active wing model used for an active model wing developed at MIT. In the associated results paper, Lin [Lin et al., 1995] reported on the results obtained during experimental testing of the active model wing. The implementation of the piezoelectrically induced flutter control mechanism led to a 12% increase in the passive model flutter dynamic pressure which proves the concept of using active materials for aeroelastic control.

1.3.5 Helicopter Blade Control

Control of helicopter rotors is normally accomplished through the use of a swashplate mechanism. As discussed earlier, the operating principles of the rotor leads to higher harmonic disturbances on the blades. Shaw [Shaw and Albion, 1980; Shaw et al., 1985] showed that higher harmonics control (HHC) of the disturbances can be achieved with a $\pm 3^\circ$ blade pitch change at specified blade harmonics. Most of the systems proposed for HHC operate on the individual blades. Individual blade control (IBC) can address the needs of every blade on an individual bases with no system-imposed frequency constraints.

IBC can be accomplished in various ways, but the two most promising solutions are offered by an actively controlled trailing edge flap or by actuating the whole blade in twist with distributed actuators. Spangler [Spangler and Hall, 1990] was the first to examine discrete actuation of the trailing edge flap. In this work a piezoelectric bender element is used to drive a trailing edge flap. Another trailing edge flap concept presented by Fenn [Fenn et al., 1993] uses magnetostrictive rods to drive a discrete trailing edge flap actuation mechanism. A very good overview of current discrete actuator technology was given by Giurgiutiu [Giurgiutiu et al., 1994]. The second possible solution for IBC is to actuate the whole helicopter blade with distributed actuators in twist or bending. Chen [Chen and Chopra, 1995] tested an active helicopter blade in hover. The blade was twisted during operation with embedded, monolithic piezoelectric elements which relied on shear lag to induce shear stresses in the blade. With the invention of PFC's and IDEPFC's, planar, distributed, shear actuation has become a reality. Therefore distributed anisotropic actuation needs to be investigated more thoroughly.

Helicopter blades are typically composite structures made from isotropic and composite materials. The significant length and cross-sectional dimensions make one-dimensional models appropriate for helicopter blades. For a complete review of composite blade modeling techniques refer to Hodges [Hodges, 1990]. The major advantage of analytical models is the physical understanding that accompanies these models. Rehfield [Rehfield, 1985; Rehfield et al., 1988; Rehfield and Atilgan, 1989] developed an analytical, high order, one-dimensional beam model for helicopter blades. This model is widely used to model both helicopter blades and aircraft wings. In this model the general rotor blade cross-section is approximated as a single-cell, composite section. A torsional warping function is used to describe the out-of-plane displacements during twist. Bauchau [Bauchau, 1985] used a series approach to model the warping. This modeling technique is more accurate than Rehfield's, but the gain in accuracy is not worth the price in computational effort needed for this model. Smith [Smith and Chopra, 1990] used a similar approach as Rehfield to model single cell, composite beams. The experimental results published by Smith show some of the structural couplings that can exist in composite helicopter blades. Ehlers [Ehlers, 1994] and Song [Song and Librescu, 1993] incorporated active material capabilities into Rehfield's model to model adaptive, single cell, composite beams. Except for Ehlers [Ehlers, 1994] nobody has considered anisotropic actuation of composite box beams. All of the models assume the actuators behave isotropically when actuated. The model by Ehlers is very general and the main

focus of the work was the investigation of different actuation schemes for single cell, composite beams (bending and torsion). Due to the generality of Ehlers's work, a more indepth investigation of distributed planar anisotropic actuation of single cell, composite beams is needed before this concept can be applied for integral helicopter blade control.

1.4 Thesis Overview

Chapter 1 served as an introduction to anisotropic actuation of single cell, composite beams. It provided a motivation, based on helicopter vibration reduction, for this study. It showed that the development of PFC technology allows the planar anisotropic actuation of structures. The background section provided an introduction to active materials and anisotropic actuators. The remainder of the section introduced adaptive structures, but more specifically adaptive aircraft wings and helicopter blades. At the end of each of these sections an overview was given of the current implementation of active materials in these structures. The introductory chapter showed what the shortcomings of isotropic piezoelectric actuators are and paved the way for the introduction of anisotropic actuators for shear actuation.

Chapter 2 provides a model for a single cell, composite beam with distributed, planar, anisotropic actuators. This model is representative of both aircraft wings and helicopter blades. The resulting force-deformation relations are used in the following chapters to determine system static displacement response.

Chapter 3 presents a parameter study of the variables which influence twist actuation of composite beams. PFC's and IDEPFC's are materials with tailorable actuation properties. It is thus necessary to determine how the different properties influence twist and what the optimum actuation properties are to maximize twist. Chapter three gives a clear explanation of the essence of shear actuation and the parameters which influence it.

Chapter 4 builds on the model presented in chapter two. An adaptive beam finite element, based on the model, is developed for system response simulation. The associated finite element code is used to validate the model and the beam element. Validation is completed by comparing simulation results with experimental results published for non-actuated box beams. The next step for the validation of the model and code is to compare the response of an anisotropic actuated, composite, box beam with the results given by a commercial Finite Element Analysis (FEA) code.

Chapter 5 presents the experimental work done for the study. The first part of the chapter describes tests done on non-actuated box beams and concludes with model comparisons. The second part of the chapter presents the design, manufacturing, and testing of a twist actuated, scale model helicopter blade.

Chapter 6 concludes the study with a summary of the work accomplished and gives direction for future work in this field.

Modeling of Actuated, Single Cell, Composite Beams

Chapter 2

The major driving factors for engineering systems are performance and cost. Depending on the complexity of a system, an analytical description of the system can be obtained from a mathematical model. By using adequate modeling techniques, it is possible to reduce development costs and to optimize the performance of a system prior to actual manufacturing or assembly. This chapter focuses on the formulation of a model of anisotropically actuated, single cell, composite beams for the prediction of the static displacement response such beams.

2.1 Introduction

Closed, single cell, composite beams are used in aircraft wings and helicopters blades for either primary load carrying or supplementary load carrying. In order to model these beams accurately, it is necessary to analyze the physical operation environment of composite beams used in aircraft and helicopter applications as well as the construction of these beams.

For aircraft, the major loading of the wing is the pressure distribution which produces the lifting forces. This loading primarily tends to bend and twist the wing. The bending is in the vertical spanwise plane. Therefore, aircraft wings can be adequately modeled as composite plates being loaded in bending and twist. Ehlers [Ehlers and Weisshaar, 1992] used this approach to model an adaptive wing. In this model the stiffness of the wing consisted of the bending stiffness, torsional stiffness and a coupling term to account for any coupling between the bending and torsional modes of deformation. The stiffnesses

were calculated using CLPT [Jones, 1975] which reflects the composite laminated construction nature of a composite wing.

Helicopter blades are exposed to very nonlinear, time-varying forcings during operation. The blades are not only loaded in vertical bending and torsion, but also loaded in horizontal bending and centripetal tension. This operating environment requires the usage of more complex models for helicopter blades. The large length to chord ratios of helicopter blades makes it appropriate to use one dimensional beam models [Hodges, 1988]. Furthermore, composite helicopter blades are generally single cell, beams which can exhibit numerous structural couplings depending on the beam shape and material ply angles in the beam walls. In order to model these non-classical effects, models were developed which account for the composite construction of helicopter blades. Rehfield [Rehfield, 1985] presented a high order beam model for a composite beam which allows for displacement and rotation in all directions as well as an cross-sectional out-of-plane torsional warping displacement. The inclusion of a single torsional warping mode was based on the work by Bauchau [Bauchau, 1985] in which it was shown that the torsional warping mode is the most significant mode. Rehfield's model has been used for both adaptive wings [Song et al., 1992] and helicopter blades [Hodges, 1990].

The objective of this chapter is to derive an analytical model for anisotropic actuated, single cell, composite beams based on the passive beam models which have already been developed. This model will be used for adaptive composite beam design. For the helicopter application, the actuated beam system is a completely dynamic problem, but for initial control mechanism design, a static model will suffice. Use of the model is the ability to predict the static response of the beam when actuated with distributed, anisotropic material inclusions.

2.2 Actuated Beam Description and Assumptions

The main spar of a helicopter blade can be approximated as a closed, single cell, thin-walled, composite beam. The beam wall is constructed from a composite laminate with material plies of different thicknesses and orientations. For the case where the blades are actuated with in-plane actuators, the actuator material plies can be included anywhere in the cross-section. A generic cross-section of a single cell, composite beam with the associated global and local coordinates is shown in Figure 2-1. The global cartesian coordinate

system (x, y, z) is situated at the root of the beam and is fixed in space. On the other hand the local cartesian coordinate system (x, t, n) is located at the mid-plane of the cross-section of the laminate beam wall and moves around the contour with the circumferential coordinate s . In the local coordinate system, t is the tangential coordinate and n is the outward normal coordinate (tangential and normal to the mid-plane contour of the beam wall).

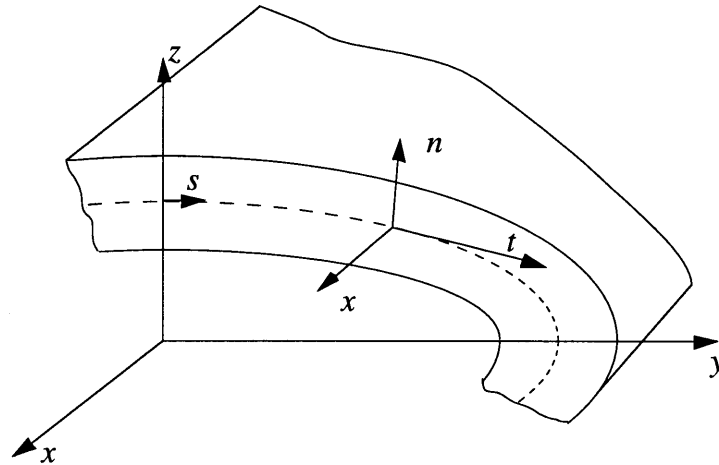


Figure 2-1. Global and Local Coordinate Systems (Quarter segment shown)

The model for the thin-walled, anisotropically actuated, single cell, composite beam is based on the following assumptions [Rehfield, 1985; Song et al., 1992]:

- Cross-sectional shape is maintained during deformation (no local twisting or transverse bending) but out-of-plane displacements are allowed.
- Wall thickness is small compared to other dimensions so that the problem can be treated as a thin-walled, plane stress problem.
- The transverse in-plane normal stresses are negligible (no internal pressure).
- Rate of twist can vary along the length of the beam and it acts as a measure of the torsional warping of the cross-section.
- Active material sections can be modeled with linear piezoelectric constitutive relations and are excited with electric field applied through the thickness of the actuator.
- Constant properties along the longitudinal axis (x-axis) of the beam.

There is no prior restriction on the cross-sectional shape of the beam. Active material inclusions can be located anywhere in the cross-section of the beam. This type of beam

model is general enough to model a composite helicopter blade as well as the general actuation of a closed, single cell, composite beam.

2.3 Strain-Displacement Relations

The strain at any point in the beam wall is a function of the displacement at that specific point. Therefore it is necessary to determine the displacement of any point in the beam wall as a function of the beam variables. For certain structural problems where specific displacements are more evident than others, a simplified displacement description can be used to describe the strain state. This section describes the strain-displacement relations used for the anisotropically actuated, single cell, composite beam.

2.3.1 Position Vector and Normal Projection

The location of any point within the beam wall can be described by the location of the point in the local coordinate system and the position of the local coordinate system relative to the global coordinate system (see Figure 2-2).

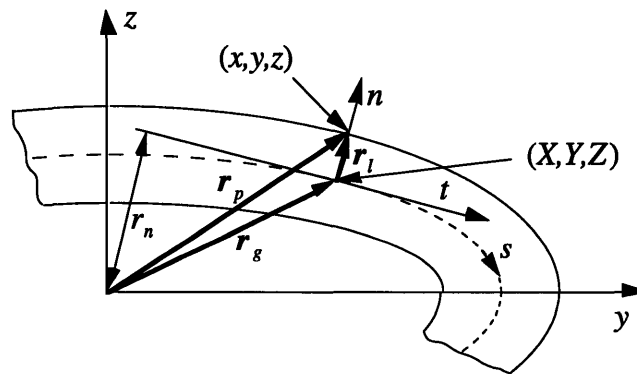


Figure 2-2. Position Vector of a Point in the Beam Wall

Coordinate x is the spanwise coordinate of a point, where as y and z represent the transverse coordinates of a point in the cross-section. X , Y and Z describes the mid-plane contour of the cross-section, in global coordinates. The origin location of the local coordinate system is given by $(X(x), Y(s), Z(s))$. Due to the assumed constant spanwise properties coordinates $Y(s)$ and $Z(s)$ are not functions of the spanwise coordinate x . The location of a point in the local coordinate system are only given by the normal coordinate n . With these descriptions the location of a point in the beam wall is completely defined.

$$\begin{aligned}
 \mathbf{r}_p &= x\hat{x} + y\hat{y} + z\hat{z} \\
 &= \mathbf{r}_g + \mathbf{r}_l \\
 &= X\hat{x} + Y\hat{y} + Z\hat{z} + n\hat{n}
 \end{aligned} \tag{2.1}$$

In Figure 2-2, \mathbf{r}_p is the point position vector, \mathbf{r}_g is the mid-plane position vector, and \mathbf{r}_l is the local position vector. Unit vectors of the coordinate systems are denoted with a ($\hat{\cdot}$). The unit tangential vector, \hat{t} , in the local coordinate system is given by the derivative of the mid-plane position vector with respect to the circumferential coordinate s :

$$\hat{t} = \frac{\mathbf{r}_{g,s}}{\|\mathbf{r}_{g,s}\|} = \frac{(Y_{,s}\hat{y} + Z_{,s}\hat{z})}{\sqrt{(Y_{,s})^2 + (Z_{,s})^2}} \tag{2.2}$$

where $(\cdot)_{,*}$ denote the derivative with respect to variable “*”. If the circumferential coordinate, s , is defined to represent actual mid-plane contour length from a specific point in the cross-section, the magnitude of the mid-plane derivative is equal to unity and the expression for the unit tangential vector reduce to the following expression:

$$\begin{aligned}
 \hat{t} &= Y_{,s}\hat{y} + Z_{,s}\hat{z} \\
 &= t_y\hat{y} + t_z\hat{z}
 \end{aligned} \tag{2.3}$$

where t_y and t_z are the components of the unit tangential vector in the global coordinate system. To obtain the unit outward normal vector in the local coordinate system, the cross product between the spanwise unit vector, \hat{x} , and the unit tangential vector, \hat{t} needs to be determined:

$$\begin{aligned}
 \hat{n} &= \hat{x} \times \hat{t} = -Z_{,s}\hat{y} + Y_{,s}\hat{z} \\
 &= -t_z\hat{y} + t_y\hat{z} \\
 &= n_y\hat{y} + n_z\hat{z}
 \end{aligned} \tag{2.4}$$

In equation (2.4), n_y and n_z are the components of the unit normal in the global coordinate system. For further use it is convenient to define the normal projection, r_n , of the mid-plane position vector, \mathbf{r}_g , on the unit normal vector, \hat{n} :

$$\begin{aligned}
 r_n &= \mathbf{r}_g \cdot \hat{n} \\
 &= -YZ_{,s} + ZY_{,s}
 \end{aligned} \tag{2.5}$$

2.3.2 Beam Cross-Section Kinematics

The displacement field of the beam is decomposed into a multi-axial, rigid rotation and translation of the beam cross-section, as well as a warping displacement normal to the plane of the cross-section. Global displacement variables used in the model are shown in Figure 2-3. $U(x)$, $V(x)$, and $W(x)$ are the global displacements of the cross-section along the spanwise coordinate, x . The rotation of the cross-section given by $\phi(x)$, $\beta_y(x)$, and $\beta_z(x)$ are defined positive in the direction given by the right-hand-rule. As stated earlier, the rate of twist, $\phi_{,x}$, acts as measure of the out-of-plane torsional warping displacement of the cross-section.

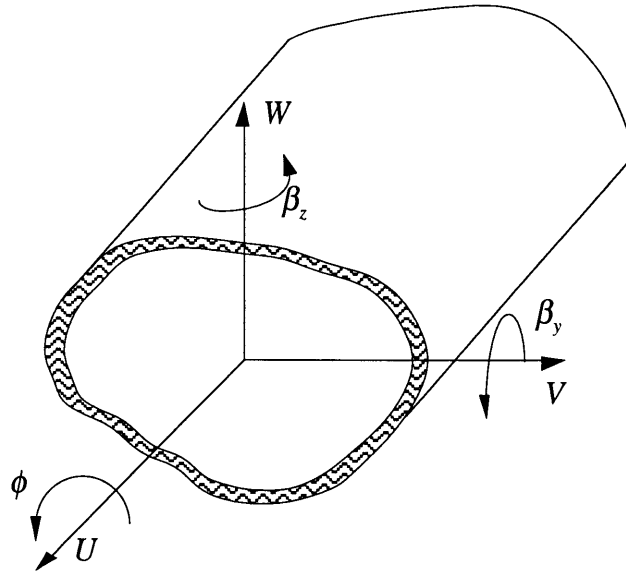


Figure 2-3. Global Displacement Variables

The global displacements, u , v , and w of any point in the beam wall can be given in terms of cross-sectional displacement values, $U(x)$, $V(x)$, $W(x)$, the cross-sectional rotation $\phi(x)$, $\beta_y(x)$, $\beta_z(x)$, and the beam twist rate, $\phi_{,x}$.

The normal displacement, u , consist of three parts:

- the cross-section displacement - U ,
- the out-of-plane rotation of the cross-section - u_{rot} , and
- the warping displacement - u_{warp} .

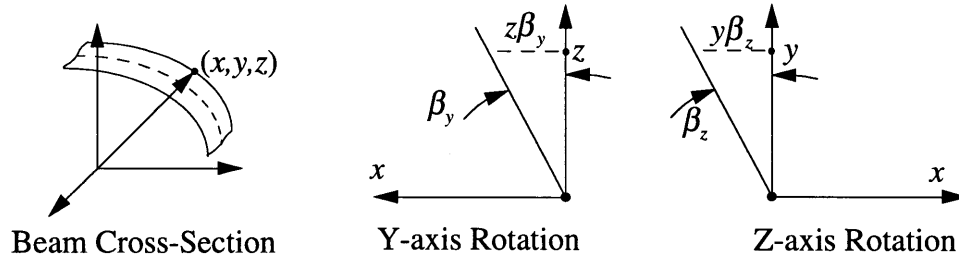


Figure 2-4. Normal Displacements Associated with Beam Out-of-Plane Rotation

The cross-sectional displacement, U , is shown in Figure 2-3. The out-of-plane normal displacement associated with the rotation (β_y, β_z) of the cross-section is shown in Figure 2-4. This rotational normal displacement can be expressed as (small angles assumed):

$$\begin{aligned}
 u_{rot} &= z\beta_y - y\beta_z \\
 &= (Z + nn_z)\beta_y - (Y - nn_y)\beta_z \\
 &= (Z + nY_{,s})\beta_y - (Y - nZ_{,s})\beta_z
 \end{aligned} \tag{2.6}$$

The warping displacement is the product of the rate of twist and the torsional warping function, $\psi(s)$, which will be determined in the next section. Thus the normal displacement can be expressed as:

$$\begin{aligned}
 u &= U + u_{rot} + u_{warp} \\
 &= U - (Y - nZ_{,s})\beta_z + (Z + nY_{,s})\beta_y + \psi\phi_{,x}
 \end{aligned} \tag{2.7}$$

The in-plane displacements, v and w , of any point in point of the beam wall are determined by the transverse cross-sectional displacements, V, W , and the in-plane rotation, ϕ , of the cross-section:

$$v = V - (Z + nY_{,s})\phi \tag{2.8}$$

and

$$w = W + (Y - nZ_{,s})\phi \tag{2.9}$$

To obtain the in-plane shear strain at any point in the beam wall it is convenient to define the in-plane tangential displacement, u_t :

$$\begin{aligned}
u_t &= (u\hat{x} + v\hat{y} + w\hat{z}) \cdot \hat{t} \\
&= (v\hat{y} + w\hat{z}) \cdot (Y_{,s}\hat{y} + Z_{,s}\hat{z}) \\
&= vY_{,s} + wZ_{,s}
\end{aligned} \tag{2.10}$$

2.3.3 Torsional Warping Function

To complete the kinematic description of the cross-sectional displacement it is necessary to construct an appropriate torsional warping function. When a closed, single cell beam is twisted, an out-of-plane displacement is observed. This out-of-plane displacement of the cross-section is called the warping of the beam. The warping consist of two parts: the mid-plane warping (primary warping) and the through-thickness warping (secondary warping) [Song et al., 1992]. In this study, the secondary warping is ignored under the thin-walled beam assumption.

The warping displacement is due to shear stresses in the beam wall. For thin-walled beam structures, the shear flow in the walls is constant around the cross-section when the beam is subjected to a pure torque [Megson, 1990]. The shear flow, q , is defined as the shear force per unit length in the beam wall:

$$q = \tau t \tag{2.11}$$

where t represent the wall thickness and τ represent the in-plane shear stress at the specific point in the beam wall. The shear flow can be expressed as a function of the “effective” wall shear stiffness, G_{eff} , and the in-plane shear strain, γ_{xs} . The effective wall shear stiffness is defined as the thickness averaged shear stiffness of the composite laminate wall for the plane stress problem [Smith and Chopra, 1990] (for isotropic materials the effective shear stiffness reduces to the shear modulus, G):

$$q = G_{eff} \gamma_{xs} t \tag{2.12}$$

The in-plane shear strain can be obtained from the normal displacement and the tangential in-plane displacement at any point:

$$\gamma_{xs} = u_{,s} + u_{t,x} \tag{2.13}$$

By substituting for the in-plane shear strain, the shear flow is:

$$\begin{aligned} q &= G_{eff}t(u_{,s} + u_{t,x}) \\ &= G_{eff}t(u_{,s} + v_{,x}Y_{,s} + w_{,x}Z_{,s}) \end{aligned} \quad (2.14)$$

The warping displacement is described by the rotational degree of freedom, ϕ . In the next step of constructing the warping function only the displacements associated with the rotational degree of freedom (equation (2.7 - 2.9)) are substituted into equation (2.14):

$$\begin{aligned} q &= G_{eff}t(\psi_{,s}\phi_{,x} + \phi_{,x}(YZ_{,s} - ZY_{,s} + n)) \\ &= G_{eff}t(\psi_{,s}\phi_{,x} - \phi_{,x}(r_n + n)) \end{aligned} \quad (2.15)$$

The torsional warping function, $\psi(s)$, is still undetermined and the goal is to obtain an expression for $\psi(s)$ from compatibility considerations. For thin-walled beams the shear flow is not a function of the normal coordinate because $r_n \gg n$. Thus the shear flow reduces to:

$$q = G_{eff}t(\psi_{,s}\phi_{,x} - \phi_{,x}r_n) \quad (2.16)$$

This equation can be integrated around the contour of the cross-section from any arbitrary point with the twist rate being constant at any specific span location:

$$\begin{aligned} \int_0^s \frac{q}{G_{eff}t} ds &= \int_0^s (\psi_{,s}\phi_{,x} - r_n\phi_{,x}) ds \\ &= \phi_{,x} \int_0^s \psi_{,s} ds - \phi_{,x} \int_0^s r_n ds \end{aligned} \quad (2.17)$$

From compatibility it holds that the warping displacement must be continuous around the contour:

$$\oint_{\Gamma} \psi_{,s} ds = 0 \quad (2.18)$$

When the mid-plane normal projection is integrated around a closed cross-section the following relation holds:

$$\oint_{\Gamma} r_n ds = 2A \quad (2.19)$$

where A represents the area of the mid-plane contour and Γ represents the cross-section contour as well as the actual mid-plane contour length. Equations (2.18) and (2.19) can be used to express the twist rate as:

$$\phi_{,x} = \frac{1}{-2A} \oint_{\Gamma} \frac{q}{G_{eff}t} ds \quad (2.20)$$

Equation (2.17) can be rewritten by substituting for the twist rate from equation (2.20):

$$\int_0^s \psi_{,s} ds = \frac{-2A \int_0^s \frac{q}{G_{eff}t} ds}{\oint_{\Gamma} \frac{q}{G_{eff}t} ds} + \int_0^s r_n ds \quad (2.21)$$

$$\psi(s) - \psi(0) = \frac{-2A \int_0^s \frac{q}{G_{eff}t} ds}{\oint_{\Gamma} \frac{q}{G_{eff}t} ds} + \int_0^s r_n ds$$

This function can be simplified by noting that the shear flow, q , is constant around the contour of the beam during twisting and that the warping function can be constructed from a point where the warping function is zero. The resulting warping function is the one that Rehfield [Rehfield and Atiligan, 1990] used for the single cell, composite beam model:

$$\psi(s) = \frac{-2A}{\Gamma} \alpha^*(s) + \int_0^s r_n ds \quad (2.22)$$

with

$$\alpha^*(s) = \int_0^s \alpha ds = \int_0^s \frac{\frac{\Gamma}{G_{eff}t}}{\oint_{\Gamma} \frac{1}{G_{eff}t} ds} ds \quad (2.23)$$

where Γ represents both contour and the actual mid-plane contour length. The warping parameter, α , describes the influence of laminate wall construction on the warping displacement. If the beam wall is constructed from isotropic material the warping parameter are equal to unity and the warping function is purely a geometric function.

2.3.4 Strain Relations

The displacement relations (equation (2.7 - 2.9)) are used to obtain the strains in the beam wall. The definitions for strains are according to small strain elasticity definitions [Boresi and Sidebottom, 1985]. Axial normal strain, ϵ_{xx} , can be decomposed into the mid-plane contour value, ϵ_{xx}^o , as well as the local bending curvature contribution, $n\kappa_{xx}$, at a specific point in the beam wall:

$$\begin{aligned}\epsilon_{xx} &= u_{,x} \\ &= U_{,x} - Y\beta_{z,x} + Z\beta_{y,x} + \psi\phi_{,xx} + n(Y_{,s}\beta_{y,x} + Z_{,s}\beta_{z,x}) \\ &= \epsilon_{xx}^o + n\kappa_{xx}\end{aligned}\quad (2.24)$$

with

$$\begin{aligned}\epsilon_{xx}^o &= U_{,x} - Y\beta_{z,x} + Z\beta_{y,x} + \psi\phi_{,xx} \\ \kappa_{xx} &= Y_{,s}\beta_{y,x} + Z_{,s}\beta_{z,x}\end{aligned}\quad (2.25)$$

The in-plane shear strain is assumed constant across the wall thickness and is not a function of the through-thickness coordinate, n :

$$\begin{aligned}\gamma_{xs} &= u_{,s} + u_{t,x} \\ &= (V_{,x} - \beta_z)Y_{,s} + (W_{,x} + \beta_y)Z_{,s} - \frac{2A\alpha\phi_{,x}}{\Gamma} + n(Z_{,ss}\beta_z + Y_{,ss}\beta_y - \phi_{,x}) \\ &= (V_{,x} - \beta_z)Y_{,s} + (W_{,x} + \beta_y)Z_{,s} - \frac{2A\alpha\phi_{,x}}{\Gamma} \\ &= \gamma_{xs}^o\end{aligned}\quad (2.26)$$

where γ_{xs}^o is the mid-plane, in-plane shear strain. In equation (2.24), the higher order thickness effects are neglected under the assumption that the shear strain is constant through the thickness for a thin-walled section. The transverse shear strains can be identified from equation (2.26) and are defined as follows (Timoshenko beam shear strain definition):

$$\begin{aligned}\gamma_{xy} &= V_{,x} - \beta_z \\ \gamma_{xz} &= W_{,x} + \beta_y\end{aligned}\quad (2.27)$$

Finally the in-plane shear strain can be expressed by substituting for the transverse shear strains in equation (2.26):

$$\gamma_{xs} = \gamma_{xy} Y_{,s} + \gamma_{xz} Z_{,s} - \frac{2A\alpha\phi_{,x}}{\Gamma} \quad (2.28)$$

Other strain components are removed from the analysis by the plane stress assumption and the assumption that the “hoop” stress is negligible ($\sigma_{ss} = 0$).

2.4 Constitutive Relations

Constitutive relations are relations which describe the material behavior in terms of some basic, independent, state variables. The behavior of a material can be linear or non-linear depending on the type of material and the range of the independent state variables. The simplest constitutive relations are linearized relations which are only valid for specific small ranges of the independent state variables.

2.4.1 Linear Piezoelectric Constitutive Relations

The walls of the active closed, single cell, composite beam are constructed from general composite materials which can be active or non-active. It is assumed that both passive and active materials used for beam construction can be modeled with the linear piezoelectric constitutive relationships. The main interests for the actuation of adaptive structures is the induced stresses and strains and not the electrical displacements. Therefore, the general constitutive relations given in equation (1.3) are reduced to the following relationship (in the 1-2-3 material coordinate system):

$$\begin{Bmatrix} T_1 \\ T_2 \\ \cdot \\ T_6 \end{Bmatrix} = \begin{bmatrix} C_{11} & C_{12} & \cdot & C_{16} \\ C_{21} & \cdot & \cdot & \cdot \\ \cdot & \cdot & \cdot & \cdot \\ C_{61} & \cdot & \cdot & C_{66} \end{bmatrix}^E \begin{Bmatrix} S_1 \\ S_2 \\ \cdot \\ S_6 \end{Bmatrix} - \begin{bmatrix} \left[\begin{matrix} d_{11} & d_{12} & \cdot & d_{16} \\ d_{21} & \cdot & \cdot & \cdot \\ d_{31} & \cdot & \cdot & d_{36} \end{matrix} \right] \begin{bmatrix} C_{11} & C_{12} & \cdot & C_{16} \\ C_{21} & \cdot & \cdot & \cdot \\ \cdot & \cdot & \cdot & \cdot \\ C_{61} & \cdot & \cdot & C_{66} \end{bmatrix}^E \right)^T \begin{Bmatrix} E_1 \\ E_2 \\ E_3 \end{Bmatrix} \end{bmatrix} \quad (2.29)$$

or

$$\begin{aligned} T &= c^E S - (dc^E)^T E \\ &= c^E S - (e)^T E \end{aligned} \quad (2.30)$$

In equation (2.30) the matrix transpose is denoted with $(\cdot)^T$. For the rest of the study, engineering notation will be used for the stress and strain (σ, ε) [Jones, 1975] instead of the notation used by the IEEE [IEEE, 1978], and the strain and electrical boundary condition superscripts will be dropped.

Carbon Fiber Reinforced Plastic (CFRP), and Glass Fiber Reinforced Plastic (GFRP) composites and PFC's (along fiber direction) are transversely isotropic materials. For transversely isotropic materials, there are only five independent stiffness coefficients. In the proposed actuator configuration it is assumed that actuation can be effectively modeled with through-thickness fields (effective values used to model IDEPFC's). For the rest of this section it is assumed that the material axis system coincide with the principal material property directions. For PFC's, with poling in the through-thickness direction, the free actuation strain constants present are d_{31} , d_{32} and d_{33} . Under these conditions equation (2.30) reduces to the following set of equations:

$$\begin{Bmatrix} \sigma_{11} \\ \sigma_{22} \\ \sigma_{33} \\ \tau_{23} \\ \tau_{31} \\ \tau_{12} \end{Bmatrix} = \begin{bmatrix} C_{11} & C_{12} & C_{12} & 0 & 0 & 0 \\ C_{12} & C_{22} & C_{23} & 0 & 0 & 0 \\ C_{12} & C_{23} & C_{22} & 0 & 0 & 0 \\ 0 & 0 & 0 & \frac{C_{22} - C_{23}}{2} & 0 & 0 \\ 0 & 0 & 0 & 0 & C_{66} & 0 \\ 0 & 0 & 0 & 0 & 0 & C_{66} \end{bmatrix} \begin{Bmatrix} \varepsilon_{11} \\ \varepsilon_{22} \\ \varepsilon_{33} \\ \gamma_{23} \\ \gamma_{31} \\ \gamma_{12} \end{Bmatrix} - \begin{Bmatrix} e_{31} \\ e_{32} \\ e_{33} \\ 0 \\ 0 \\ 0 \end{Bmatrix} E_3 \quad (2.31)$$

with

$$\begin{aligned} e_{31} &= C_{11}d_{31} + C_{12}d_{32} + C_{12}d_{33} \\ e_{32} &= C_{12}d_{31} + C_{22}d_{32} + C_{23}d_{33} \\ e_{33} &= C_{12}d_{31} + C_{23}d_{32} + C_{22}d_{33} \end{aligned} \quad (2.32)$$

In equation (2.31), e_{ij} is the stress actuation constants with applied electrical field in the i -direction and stress in the j -direction. These constitutive relations will be used in the next section to describe the stress in any ply in terms of the strain in that specific ply.

2.4.2 Plane Stress Problem

The important stresses for thin-walled composite beams are the normal stresses and the in-plane shear stress in the laminate walls. The stresses in the through-thickness direction does exist but are small. Therefore the problem can treated as a plane stress problem with:

$$\sigma_{33} = 0, \tau_{23} = 0, \text{ and } \tau_{31} = 0 \quad (2.33)$$

A static condensation process can be used in equation (2.31) to remove the effect of the stresses which are zero. The resulting ply elastic constants, Q_{ij} , [Jones, 1975] and induced stress constants, e_{ij} , [Bent et al., 1995] are specifically for the plane stress problem and differs from the constants used for a complete 3-D analysis (equation (2.31)). Plane stress actuation stress coefficients are denoted with an asterisks “*”. Note that these relations are for the 1-2-3 material coordinate system and still need to be related to the local beam wall coordinate system defined earlier.

$$\begin{Bmatrix} \sigma_{11} \\ \sigma_{22} \\ \tau_{12} \end{Bmatrix} = \begin{bmatrix} Q_{11} & Q_{12} & 0 \\ Q_{12} & Q_{22} & 0 \\ 0 & 0 & Q_{66} \end{bmatrix} \begin{Bmatrix} \varepsilon_{11} \\ \varepsilon_{22} \\ \gamma_{12} \end{Bmatrix} - \begin{bmatrix} e_{31} \\ e_{32} \\ 0 \end{bmatrix}^* E_3 \quad (2.34)$$

or

$$\sigma = Q\varepsilon - e^* E_3 \quad (2.35)$$

with

$$\begin{aligned} Q_{11} &= C_{11} - \frac{C_{12}^2}{C_{22}} \\ Q_{12} &= C_{12} - \frac{C_{12}C_{23}}{C_{22}} \\ Q_{22} &= C_{22} - \frac{C_{23}^2}{C_{22}} \\ Q_{66} &= C_{66} \end{aligned} \quad (2.36)$$

and

$$\begin{aligned} e_{31}^* &= e_{31} - \frac{C_{12}}{C_{22}} e_{33} \\ e_{32}^* &= e_{32} - \frac{C_{23}}{C_{22}} e_{33} \end{aligned} \tag{2.37}$$

2.4.3 Property Rotations

The plane stress properties of equation (2.34) are for a coordinate axis system which is aligned with the principal material property axis system. The composite plies in the walls can be aligned at an angle relative to the local structural coordinate system. To obtain the correct material properties in the structural coordinate system, the material properties must be rotated according to the tensor transformation laws [Jones, 1975]. The relative location of the structural axis and the material axis system are shown in Figure 2-5.

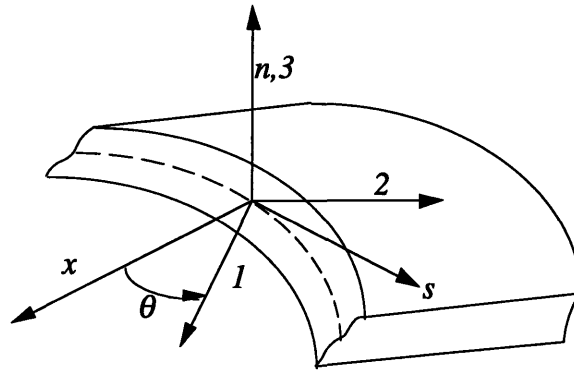


Figure 2-5. Structural and Material Coordinate Systems

The stress and strain transformation from the 1-2-3 material system to the x-s-n local coordinate system are:

$$\begin{Bmatrix} \sigma_{xx} \\ \sigma_{ss} \\ \tau_{xs} \end{Bmatrix} = \begin{bmatrix} \cos^2 \theta & \sin^2 \theta & -2 \sin \theta \cos \theta \\ \sin^2 \theta & \cos^2 \theta & 2 \sin \theta \cos \theta \\ \sin \theta \cos \theta & -\sin \theta \cos \theta & \cos^2 \theta - \sin^2 \theta \end{bmatrix} \begin{Bmatrix} \sigma_{11} \\ \sigma_{22} \\ \tau_{12} \end{Bmatrix} \tag{2.38}$$

or

$$\sigma_{xsn} = T^{-1} \sigma_{123} \tag{2.39}$$

where the subscripts refer to the coordinate system. The tensor strain transformation is:

$$\begin{Bmatrix} \varepsilon_{xx} \\ \varepsilon_{ss} \\ \gamma_{xs}/2 \end{Bmatrix} = T^{-1} \begin{Bmatrix} \varepsilon_{11} \\ \varepsilon_{22} \\ \gamma_{12}/2 \end{Bmatrix} \quad (2.40)$$

To transform the shear strain from tensor format to engineering format the following operation needs to be completed:

$$\varepsilon_{xsn} = \begin{Bmatrix} \varepsilon_{xx} \\ \varepsilon_{ss} \\ \gamma_{xs} \end{Bmatrix} = \begin{bmatrix} 1 & 0 & 0 \\ 0 & 1 & 0 \\ 0 & 0 & 2 \end{bmatrix} \begin{Bmatrix} \varepsilon_{xx} \\ \varepsilon_{ss} \\ \gamma_{xs}/2 \end{Bmatrix} = \mathbf{H} \begin{Bmatrix} \varepsilon_{xx} \\ \varepsilon_{ss} \\ \gamma_{xs}/2 \end{Bmatrix} \quad (2.41)$$

To obtain the final constitutive relations in the x - s - n coordinate system, the relations from the above equations are combined in the single transformation:

$$\sigma_{xsn} = T^{-1} \mathbf{Q} \mathbf{H} \mathbf{T}^{-1} \varepsilon_{xsn} - T^{-1} \mathbf{e}^* E_n \quad (2.42)$$

The stiffness and actuation stress coefficients can be redefined from equation (2.42) to obtain a relationship which can be manipulated more easily:

$$\begin{Bmatrix} \sigma_{xx} \\ \sigma_{ss} \\ \tau_{xs} \end{Bmatrix} = \begin{bmatrix} R_{11} & R_{12} & R_{16} \\ R_{12} & R_{22} & R_{26} \\ R_{16} & R_{26} & R_{66} \end{bmatrix} \begin{Bmatrix} \varepsilon_{xx} \\ \varepsilon_{ss} \\ \gamma_{xs} \end{Bmatrix} - \begin{bmatrix} P_{nxx} \\ P_{nss} \\ P_{nxs} \end{bmatrix} E_n \quad (2.43)$$

in which

$$\mathbf{R} = T^{-1} \mathbf{Q} \mathbf{H} \mathbf{T}^{-1} \quad (2.44)$$

with the rotated ply stiffness coefficients defined as:

$$\begin{aligned} R_{11} &= Q_{11} \cos^4 \theta + 2(Q_{12} + 2Q_{66}) \sin^2 \theta \cos^2 \theta + Q_{22} \sin^4 \theta \\ R_{12} &= (Q_{11} + Q_{22} - 4Q_{66}) \sin^2 \theta \cos^2 \theta + Q_{12} (\sin^4 \theta + \cos^4 \theta) \\ R_{22} &= Q_{11} \sin^4 \theta + 2(Q_{12} + 2Q_{66}) \sin^2 \theta \cos^2 \theta + Q_{22} \cos^4 \theta \\ R_{16} &= (Q_{11} - Q_{22} - 2Q_{66}) \sin \theta \cos^3 \theta + (Q_{11} - Q_{22} + 2Q_{66}) \sin^3 \theta \cos \theta \\ R_{26} &= (Q_{11} - Q_{22} - 2Q_{66}) \sin^3 \theta \cos \theta + (Q_{11} - Q_{22} + 2Q_{66}) \sin \theta \cos^3 \theta \\ R_{66} &= (Q_{11} + Q_{22} - 2Q_{12} - 2Q_{66}) \sin^2 \theta \cos^2 \theta + Q_{66} (\sin^4 \theta + \cos^4 \theta) \end{aligned} \quad (2.45)$$

The rotated actuation stress coefficients are given by:

$$\mathbf{p} = \mathbf{T}^{-1} \mathbf{e}^* \quad (2.46)$$

with

$$\begin{aligned} p_{nxx} &= e_{31}^* \cos^2 \theta + e_{32}^* \sin^2 \theta \\ p_{nss} &= e_{31}^* \sin^2 \theta + e_{32}^* \cos^2 \theta \\ p_{nxs} &= (e_{31}^* - e_{32}^*) \sin \theta \cos \theta \end{aligned} \quad (2.47)$$

For the rotated actuation stress coefficient, p_{ijk} , an electrical field applied in the i-direction results in a stress, σ_{jk} . Rotated plane stress properties will be assumed available henceforth.

2.4.4 Plate Formulation

It is convenient for further modeling to make use of the CLPT to model the response of the beam wall. In plate theory the strain assumption is that the strain at any point within the plate is a combination of the mid-plane strains, ϵ_{ij}^o , and the curvature strains, κ_{ij} [Jones, 1975]:

$$\begin{Bmatrix} \epsilon_{xx} \\ \epsilon_{ss} \\ \gamma_{xs} \end{Bmatrix} = \begin{Bmatrix} \epsilon_{xx}^o \\ \epsilon_{ss}^o \\ \gamma_{xs}^o \end{Bmatrix} + n \begin{Bmatrix} \kappa_{xx} \\ \kappa_{ss} \\ \kappa_{xs} \end{Bmatrix} \quad (2.48)$$

This strain description are substituted into the constitutive relations (equation.(2.43)) to obtain the stresses as a function of the mid-plane strains and the local curvature of the plate. The stresses are integrated over the thickness of the plate to obtain the stress resultants for the plate. This method removes the thickness variable from the problem which simplifies the analysis. The stress resultants are defined as follows:

$$\text{Force resultants: } N_{xx} = \int_{-\frac{t}{2}}^{\frac{t}{2}} \sigma_{xx} dn, N_{ss} = \int_{-\frac{t}{2}}^{\frac{t}{2}} \sigma_{ss} dn, \text{ and } N_{xs} = \int_{-\frac{t}{2}}^{\frac{t}{2}} \tau_{xs} dn \quad (2.49)$$

$$\text{Moment resultants: } M_{xx} = \int_{-\frac{t}{2}}^{\frac{t}{2}} n \sigma_{xx} dn, M_{ss} = \int_{-\frac{t}{2}}^{\frac{t}{2}} n \sigma_{ss} dn, \text{ and } M_{xs} = \int_{-\frac{t}{2}}^{\frac{t}{2}} n \tau_{xs} dn \quad (2.50)$$

The stresses are then substituted into the stress resultants to obtain the reduced constitutive relations:

$$\begin{Bmatrix} N_{xx} \\ N_{ss} \\ N_{xs} \\ M_{xx} \\ M_{ss} \\ M_{xs} \end{Bmatrix} = \begin{bmatrix} \mathbf{A} & \mathbf{B} \\ \mathbf{B} & \mathbf{D} \end{bmatrix} \begin{Bmatrix} \varepsilon_{xx}^o \\ \varepsilon_{ss}^o \\ \gamma_{xs}^o \\ \kappa_{xx} \\ \kappa_{ss} \\ \kappa_{xs} \end{Bmatrix} - \begin{Bmatrix} N_{xx}^a \\ N_{ss}^a \\ N_{xs}^a \\ M_{xx}^a \\ M_{ss}^a \\ M_{xs}^a \end{Bmatrix} \quad (2.51)$$

with

$$A_{ij} = \int_{-\frac{t}{2}}^{\frac{t}{2}} R_{ij} dn \quad B_{ij} = \int_{-\frac{t}{2}}^{\frac{t}{2}} n R_{ij} dn \quad D_{ij} = \int_{-\frac{t}{2}}^{\frac{t}{2}} n^2 R_{ij} dn \quad (2.52)$$

and

$$\begin{aligned} N_{xx}^a &= \int_{-\frac{t}{2}}^{\frac{t}{2}} p_{nxx} E_n dn & N_{ss}^a &= \int_{-\frac{t}{2}}^{\frac{t}{2}} p_{nss} E_n dn & N_{xs}^a &= \int_{-\frac{t}{2}}^{\frac{t}{2}} p_{nxs} E_n dn \\ M_{xx}^a &= \int_{-\frac{t}{2}}^{\frac{t}{2}} n p_{nxx} E_n dn & M_{ss}^a &= \int_{-\frac{t}{2}}^{\frac{t}{2}} n p_{nss} E_n dn & M_{xs}^a &= \int_{-\frac{t}{2}}^{\frac{t}{2}} n p_{nxs} E_n dn \end{aligned} \quad (2.53)$$

\mathbf{A} , \mathbf{B} , and \mathbf{D} are the plate stiffness coefficients and N_{ij}^a , M_{ij}^a are the actuation force and moment stress resultants. An original assumption made for the model was the negligible transverse normal stresses (no internal pressure) which can be enforced by setting N_{ss} to zero. Another assumption made was that the cross-section is infinitely rigid in its own plane which results in zero transverse and twisting curvature ($\kappa_{ss}, \kappa_{xs} = 0$). The influence of ε_{ss} can be removed through static condensation. The resulting reduced constitutive relationship is:

$$\begin{Bmatrix} N_{xx} \\ N_{xs} \\ M_{xx} \end{Bmatrix} = \begin{bmatrix} L_{11} & L_{12} & L_{13} \\ L_{12} & L_{22} & L_{23} \\ L_{13} & L_{23} & L_{33} \end{bmatrix} \begin{Bmatrix} \varepsilon_{xx}^o \\ \gamma_{xs}^o \\ \kappa_{xx} \end{Bmatrix} - \begin{Bmatrix} N_{xx}^a \\ N_{xs}^a \\ M_{xx}^a \end{Bmatrix}^* \quad (2.54)$$

with

$$\begin{aligned} L_{11} &= A_{11} - \frac{A_{12}^2}{A_{22}} & L_{12} &= A_{16} - \frac{A_{12}A_{26}}{A_{22}} & L_{13} &= B_{11} - \frac{A_{12}B_{12}}{A_{22}} \\ L_{22} &= A_{66} - \frac{A_{26}^2}{A_{22}} & L_{23} &= B_{16} - \frac{A_{26}B_{12}}{A_{22}} & L_{33} &= D_{11} - \frac{B_{12}^2}{A_{22}} \end{aligned} \quad (2.55)$$

Stress resultants with the superscript “a” represent the actuation stress resultants which are given by the following expressions:

$$\left(N_{xx}^a\right)^* = N_{xx}^a - \frac{A_{12}}{A_{22}} N_{ss}^a, \quad \left(N_{xs}^a\right)^* = N_{xs}^a - \frac{A_{26}}{A_{22}} N_{ss}^a, \quad \text{and} \quad \left(M_{xx}^a\right)^* = M_{xx}^a - \frac{B_{12}}{A_{22}} N_{ss}^a \quad (2.56)$$

The asterisks “*” in the above equations denote reduced actuation stress resultants and will implicitly assumed henceforth. The plate constitutive relations (equation (2.54)) can be written in matrix format as:

$$N = L\varepsilon - N^a \quad (2.57)$$

where N and N^a are reduced plate and plate actuation stress resultants.

2.5 Equations of Motion

The principle of minimum potential energy is used to obtain the equations of equilibrium [Meirovitch, 1986], [Boresi and Sidebottom, 1985]. The equations and associated boundary conditions are obtained by applying calculus of variations to the system energy expression:

$$\delta U - \delta W_{ext} = 0 \quad (2.58)$$

with U the internal strain energy and W_{ext} the external work done on the system.

2.5.1 Internal Strain Energy

The variational internal strain energy for the composite beam is:

$$\delta U = \int_0^l \int_{\Gamma} \left(N_{xx} \delta \varepsilon_{xx}^o + N_{xs} \delta \gamma_{xs} + M_{xx} \delta \kappa_{xx} \right) ds dx \quad (2.59)$$

By substituting for the strains from equations (2.24) and (2.24) the internal strain energy can be expressed in terms of the global displacement variables:

$$\begin{aligned} \delta U = & \int_0^l \oint_{\Gamma} N_{xx} (\delta U_{,x} - Y \delta \beta_{z,x} + Z \delta \beta_{y,x} + \psi \delta \phi_{,xx}) ds dx \\ & + \int_0^l \oint_{\Gamma} N_{xs} \left(\delta \gamma_{xy} Y_{,s} + \delta \gamma_{xz} Z_{,s} - \frac{2A\alpha}{\Gamma} \delta \phi_{,x} \right) ds dx \\ & + \int_0^l \oint_{\Gamma} M_{xx} (Y_{,s} \delta \beta_{y,x} + Z_{,s} \delta \beta_{z,x}) ds dx \end{aligned} \quad (2.60)$$

The variation of the global displacement variables are zero around the circumference, therefore the integrals can be evaluated around the contour before applying calculus of variations to the system. These contour integrals represent internal reaction forces in the beam:

$$\text{- Normal force:} \quad N = \oint_{\Gamma} N_{xx} ds \quad (2.61)$$

$$\text{- Shear force along y-axis:} \quad Q_y = \oint_{\Gamma} N_{xs} Y_{,s} ds \quad (2.62)$$

$$\text{- Shear force along z-axis:} \quad Q_z = \oint_{\Gamma} N_{xs} Z_{,s} ds \quad (2.63)$$

$$\text{- Twisting moment:} \quad M_x = \oint_{\Gamma} N_{xs} \left(\frac{-2A\alpha}{\Gamma} \right) ds \quad (2.64)$$

$$\text{- Bending moment:} \quad M_y = \oint_{\Gamma} (N_{xx} Z + M_{xx} Y_{,s}) ds \quad (2.65)$$

$$\text{- Bending moment:} \quad M_z = \oint_{\Gamma} (N_{xx} (-Y) + M_{xx} Z_{,s}) ds \quad (2.66)$$

and the

$$\text{- Bimoment:} \quad Q_w = \oint_{\Gamma} N_{xx} \psi ds \quad (2.67)$$

The vector of internal beam forces, \mathbf{F} , is defined as:

$$\mathbf{F} = [N \quad Q_y \quad Q_z \quad M_x \quad M_y \quad M_z \quad Q_w]^T \quad (2.68)$$

All the internal forces are typical of beam problems except for the internal bimoment. The internal bimoment is the counterpart of the external bimoment which results in pure warping displacement of the beam when loaded. A simple bimoment loading for a rectangular beam would be tension point loads at two opposite corners of the beam and compressive point loads at the other two corners. By substituting for the internal forces the internal strain energy expression can be greatly simplified:

$$\delta U = \int_0^l \left(N\delta U_{,x} + Q_y\delta\gamma_{xy} + Q_z\delta\gamma_{xz} + M_x\delta\phi_{,x} \right. \\ \left. + M_y\delta\beta_{y,x} + M_z\delta\beta_{z,x} + Q_w\delta\phi_{,xx} \right) dx \quad (2.69)$$

2.5.2 External Work

To determine the variational external work it is necessary to specify a specific loading condition. For the typical wing and helicopter blade, the beam is cantilevered at the one end and free at the other end. Typical loadings would be distributed loadings in the spanwise direction and point loads at the free end of the beam. The external point loads, at the end of the beam, corresponding to the internal beam forces are:

- Normal force at the free end: \bar{N} ,
- Shear force in the y-direction: \bar{Q}_y ,
- Shear force in the z-direction: \bar{Q}_z ,
- Twisting moment: \bar{M}_x ,
- Bending moment around the y-axis: \bar{M}_y ,
- Bending moment around the z-axis: \bar{M}_z , and
- Bimoment applied at the tip: \bar{Q}_w .

These externally applied point loads at the free end of the beam can be expressed in vector format as:

$$\bar{F}(l) = [\bar{N} \quad \bar{Q}_y \quad \bar{Q}_z \quad \bar{M}_x \quad \bar{M}_y \quad \bar{M}_z \quad \bar{Q}_w]^T \quad (2.70)$$

In equation (2.70) the over bar, ($\bar{\cdot}$), denote a point load and \bar{F} is the vector of beam point loads. The spanwise distributed loadings are of the same types as the point loadings. These distributed loadings are:

- Normal force: n_x ,
- Shear force in the y-direction: q_y ,
- Shear force in the z-direction: q_z ,

- Twisting moment: m_x ,
- Bending moment around the y-axis: m_y ,
- Bending moment around the z-axis: m_z , and
- Distributed applied bimoment: q_w .

The variational external work can be written as:

$$\begin{aligned} \delta W_{ext} = & \bar{N}\delta U(l) + \bar{Q}_y\delta V(l) + \bar{Q}_z\delta W(l) + \bar{M}_x\delta\phi(l) \\ & + \bar{M}_y\delta\beta_y(l) + \bar{M}_z\delta\beta_z(l) + \bar{Q}_w\delta\phi_{,x}(l) \\ & + \int_0^l (n_x\delta U + q_y\delta V + q_z\delta W + m_x\delta\phi + m_y\delta\beta_y + m_z\delta\beta_z + q_w\delta\phi_{,x})dx \end{aligned} \quad (2.71)$$

2.5.3 Equilibrium Equations and Boundary Conditions

The equations of equilibrium and associated boundary conditions are obtained by applying the calculus of variations to equation (2.58). The expressions for the internal strain energy and the external work are substituted into equation (2.58). The next step is to complete the integration by parts of the equations such that the displacement variations occur only in the first order. The equilibrium equations are obtained by the fact that within the beam the different displacement variations are undetermined and therefore the integrands must be zero. This leads to the following equilibrium equations:

$$N_{,x} + n_x = 0 \quad (2.72)$$

$$Q_{y,x} + q_y = 0 \quad (2.73)$$

$$Q_{z,x} + q_z = 0 \quad (2.74)$$

$$M_{x,x} - Q_{w,xx} + m_x - q_{w,x} = 0 \quad (2.75)$$

$$M_{y,x} - Q_z + m_y = 0 \quad (2.76)$$

$$M_{z,x} + Q_y + m_z = 0 \quad (2.77)$$

Boundary conditions for the system are obtained from the requirement that the end point values of the integration factors must be zero. The geometric boundary conditions are :

$$\begin{aligned}
 U(0) &= 0 \\
 V(0) &= 0 \\
 W(0) &= 0 \\
 \phi(0) &= 0 \\
 \beta_y(0) &= 0 \\
 \beta_z(0) &= 0 \\
 \phi_{,x}(0) &= 0
 \end{aligned} \tag{2.78}$$

The natural boundary conditions at the free end of the beam are:

$$\begin{aligned}
 N(l) &= \bar{N} \\
 Q_y(l) &= \bar{Q}_y \\
 Q_z(l) &= \bar{Q}_z \\
 M_x(l) - Q_{w,x}(l) &= \bar{M}_x + q_w(l) \\
 M_y(l) &= \bar{M}_y \\
 M_z(l) &= \bar{M}_z \\
 Q_w(l) &= \bar{Q}_w
 \end{aligned} \tag{2.79}$$

The system of equilibrium equations are a system of 14th order differential equations. Associated with the 14th order system are 14 boundary conditions, seven at each end. To obtain the internal forces at any point in the beam, a solution to the system of equations must be obtained. Although it might be helpful to know the internal forces the ultimate goal is the determination of the displacement of the actuated composite box beam. The final part of the modeling are the force-displacement relations which describe the relation between the internal forces and the global displacements.

2.5.4 Force-Displacement Relations

To determine the displacement of the beam a set of equations are needed which relate the internal forces to the global displacements. These equations are obtained by substituting the strain-displacement relations, equations (2.24) and (2.26), into the constitutive relations (equation (2.54)). These augmented constitutive relations are finally substituted into the internal force definitions (equations.(2.61) to (2.67)) to obtain the force-displacement relations. The displacement variables used for the force-displacement relations are a combination of the global displacement variables and can be expressed in matrix notation as:

$$\mathbf{u} = [U_{,x} \quad \gamma_{xy} \quad \gamma_{xz} \quad \phi_{,x} \quad \beta_{y,x} \quad \beta_{z,x} \quad \phi_{,xx}]^T \quad (2.80)$$

In equation (2.80) the superscript “ T ” denote the matrix transpose. As an example, the normal internal force, N , is considered:

$$\begin{aligned} N &= \oint_{\Gamma} N_{xx} ds \\ &= \oint_{\Gamma} L_{11} \epsilon_{xx}^o ds + \oint_{\Gamma} L_{12} \gamma_{xs} ds + \oint_{\Gamma} L_{13} \kappa_{xx} ds - \oint_{\Gamma} N_{xx}^a ds \end{aligned} \quad (2.81)$$

When the strain displacement relations are substituted into equation (2.81), the internal normal force can be expressed as:

$$\begin{aligned} N &= \oint_{\Gamma} \left(L_{11} (U_{,x} - Y\beta_{z,x} + Z\beta_{y,x} + \psi\phi_{,xx}) \right) ds \\ &\quad + \oint_{\Gamma} \left(L_{12} \left(\gamma_{xy} Y_{,s} + \gamma_{xz} Z_{,s} - \frac{2A\alpha}{\Gamma} \phi_{,x} \right) \right) ds \\ &\quad + \oint_{\Gamma} \left(L_{13} (Y_{,s}\beta_{y,x} + Z_{,s}\beta_{z,x}) \right) ds - \oint_{\Gamma} N_{xx}^a ds \end{aligned} \quad (2.82)$$

The normal force expression of equation (2.82) can be written in matrix form with the introduction of the beam stiffness coefficients:

$$N = [K_{11} \quad K_{12} \quad K_{13} \quad K_{14} \quad K_{15} \quad K_{16} \quad K_{17}] \mathbf{u} - N^a \quad (2.83)$$

where the beam stiffness coefficients and actuation forcing are defined from equation (2.82) as follows:

$$\begin{aligned} K_{11} &= \oint_{\Gamma} L_{11} ds & K_{12} &= \oint_{\Gamma} L_{12} Y_{,s} ds \\ K_{13} &= \oint_{\Gamma} L_{12} Z_{,s} ds & K_{14} &= \oint_{\Gamma} L_{12} \left(-\frac{2A\alpha}{\Gamma} \right) ds \\ K_{15} &= \oint_{\Gamma} (L_{11} Z + L_{13} Y_{,s}) ds & K_{16} &= \oint_{\Gamma} (-L_{11} Y + L_{13} Z_{,s}) ds \\ K_{17} &= \oint_{\Gamma} L_{11} \psi ds \end{aligned} \quad (2.84)$$

This substitution and simplification process can be applied to all the internal forces and the resulting force-displacements relations are:

$$\begin{bmatrix} N \\ Q_y \\ Q_z \\ M_x \\ M_y \\ M_z \\ Q_w \end{bmatrix} = \begin{bmatrix} K_{11} & K_{12} & \cdot & \cdot & \cdot & \cdot & \cdot \\ K_{12} & K_{22} & & & & & \\ \cdot & & \cdot & & & & \\ \cdot & & & \cdot & & & \\ \cdot & & & & \cdot & & \\ \cdot & & & & & K_{67} & \\ \cdot & \cdot & \cdot & \cdot & \cdot & K_{67} & K_{77} \end{bmatrix} \begin{bmatrix} U_{,x} \\ \gamma_{xy} \\ \gamma_{xz} \\ \phi_{,x} \\ \beta_{y,x} \\ \beta_{z,x} \\ \phi_{,xx} \end{bmatrix} - \begin{bmatrix} N \\ Q_y \\ Q_z \\ M_x \\ M_y \\ M_z \\ Q_w \end{bmatrix}^a \quad (2.85)$$

or

$$\mathbf{F} = \mathbf{K}\mathbf{u} - \mathbf{F}^a \quad (2.86)$$

where \mathbf{K} is the beam stiffness matrix and \mathbf{F}^a is the vector of internal actuation forces. The definitions for the other beam stiffness coefficients are:

$$\begin{aligned} K_{22} &= \oint_{\Gamma} L_{22} (Y_{,s})^2 ds & K_{23} &= \oint_{\Gamma} L_{22} Z_{,s} Y_{,s} ds \\ K_{24} &= \oint_{\Gamma} L_{22} \left(\frac{-2A}{\Gamma} \alpha \right) Y_{,s} ds & K_{25} &= \oint_{\Gamma} (L_{12} Z + L_{23} Y_{,s}) Y_{,s} ds \\ K_{26} &= \oint_{\Gamma} (-L_{12} Y + L_{23} Z_{,s}) Y_{,s} ds & K_{27} &= \oint_{\Gamma} L_{12} \psi Y_{,s} ds \end{aligned} \quad (2.87)$$

$$\begin{aligned} K_{33} &= \oint_{\Gamma} L_{22} (Z_{,s})^2 ds & K_{34} &= \oint_{\Gamma} L_{22} \left(-\frac{2A\alpha}{\Gamma} \right) Z_{,s} ds \\ K_{35} &= \oint_{\Gamma} (L_{12} Z + L_{23} Y_{,s}) Z_{,s} ds & K_{36} &= \oint_{\Gamma} (-L_{12} Y + L_{23} Z_{,s}) Z_{,s} ds \\ K_{37} &= \oint_{\Gamma} L_{12} \psi Z_{,s} ds & Q_z^a &= \oint_{\Gamma} N_{xs}^a Z_{,s} ds \end{aligned} \quad (2.88)$$

$$\begin{aligned} K_{44} &= \oint_{\Gamma} L_{22} \left(-\frac{2A\alpha}{\Gamma} \right)^2 ds & K_{45} &= \oint_{\Gamma} (L_{12} Z + L_{23} Y_{,s}) \left(-\frac{2A\alpha}{\Gamma} \right) ds \\ K_{46} &= \oint_{\Gamma} (-L_{12} Y + L_{23} Z_{,s}) \left(-\frac{2A\alpha}{\Gamma} \right) ds & K_{47} &= \oint_{\Gamma} L_{12} \psi \left(-\frac{2A\alpha}{\Gamma} \right) ds \end{aligned} \quad (2.89)$$

$$K_{55} = \oint_{\Gamma} \begin{bmatrix} (L_{11} Z + L_{13} Y_{,s}) Z \\ + (L_{13} Z + L_{33} Y_{,s}) Y_{,s} \end{bmatrix} ds \quad K_{56} = \oint_{\Gamma} \begin{bmatrix} (-L_{11} Y + L_{13} Z_{,s}) Z \\ + (-L_{13} Y + L_{33} Z_{,s}) Y_{,s} \end{bmatrix} ds \quad (2.90)$$

$$K_{57} = \oint_{\Gamma} [L_{11} Z \psi + L_{13} Y_{,s} \psi] ds$$

$$K_{66} = \oint_{\Gamma} \begin{bmatrix} (-L_{11} Y + L_{13} Z_{,s}) (-Y) \\ + (-L_{13} Y + L_{33} Z_{,s}) Z_{,s} \end{bmatrix} ds \quad K_{67} = \oint_{\Gamma} [L_{11} \psi (-Y) + L_{13} \psi Z_{,s}] ds \quad (2.91)$$

$$K_{77} = \oint_{\Gamma} L_{11} \psi^2 ds \quad (2.92)$$

and the actuation forcings are:

$$\begin{aligned} N^a &= \oint_{\Gamma} N_{xx}^a ds & Q_y^a &= \oint_{\Gamma} N_{xs}^a Y_{,s} ds \\ Q_z^a &= \oint_{\Gamma} N_{xs}^a Z_{,s} ds & M_x^a &= \oint_{\Gamma} N_{xs}^a \left(-\frac{2A\alpha}{\Gamma} \right) ds \\ M_y^a &= \oint_{\Gamma} (N_{xx}^a Z + M_{xx}^a Y_{,s}) ds & M_z^a &= \oint_{\Gamma} (N_{xx}^a (-Y) + M_{xx}^a Z_{,s}) ds \\ Q_w^a &= \oint_{\Gamma} N_{xx}^a \psi ds \end{aligned} \quad (2.93)$$

This analysis is similar to analysis given by Rehfield [Rehfield, 1985], but with the added feature that the actuator force term F^a accounts for general actuation by active material.

2.5.5 Structural Coupling

The off-diagonal beam stiffness coefficients describe any structural couplings which might be present in a composite beam. From the definition of the beam stiffness coefficients it can be seen that beam structural couplings have two different origins. The first of the coupling origins is the geometrical shape of the cross-section of the beam. The second origin of beam coupling lies with beam wall construction. If the beam is constructed from a composite laminate which exhibits coupling then the beam itself will also exhibit structural coupling.

For simple sections, like rectangles and tubes, made from isotropic materials the stiffness matrix is diagonal and the equations of equilibrium are uncoupled. For more complicated cross-sections, the off-diagonal stiffness terms do not vanish. By moving, and rotating the global coordinate system it is possible to get some off-diagonal terms to vanish. This is effectively obtaining the cross-section's shear center and principal axes.

Except for very simple cross-sections and uncoupled wall laminates, composite beams normally exhibit structural couplings. Rehfield [Rehfield et al., 1988] investigated the effect of structural coupling in a beam which was designed with extension-twist coupling. With their model they showed that secondary bending-shear coupling accompanies extension-twist coupling and that the beam is more flexible in bending than described by standard beam theory. Smith [Smith and Chopra, 1990] constructed box beams from composite laminates with various structural couplings. Experimental loading of these

beams in bending and twisting proved the importance of including structural couplings in helicopter blade models. In the cases where structural couplings are present the equilibrium equations are coupled through the stiffness coefficients and the solution of the system of equations becomes very difficult.

2.5.6 Solution of the Governing Equations

It is very difficult, if not impossible, to obtain analytical solutions for the complete, coupled systems of governing equations. For beams without any coupling or with coupling between only a few modes of deformation it is possible to obtain analytical solutions. An example of such an analytical solution is given by Rehfield [Rehfield et al., 1988] for a beam with extension-twist coupling being subjected to an external torque.

One possible method to obtain the solution for the complete coupled system is the finite difference method. Ehlers [Ehlers, 1994] employed this solution method for his study of actuated, closed, single cell, composite beams. The problem with the finite difference method is that an intricate matrix manipulation must be performed on the original system of equations to obtain equations which are solvable with the finite difference method. Without the matrix manipulation, the need arises to apply mixed boundary conditions in the solution which is very difficult to accomplish with the finite difference method.

Another solution technique which can be used is the finite element method. This method requires the derivation of the system of equations for a high order finite element based on the model derived in this chapter. The advantage of this method is the ease of boundary condition application and ability to obtain approximate solutions for beams with spanwise varying properties. These advantages justify the use of the finite element method and it will be used for the rest of this study.

2.6 Summary

In the first section of this chapter an introduction to composite beams was given with specific reference to the helicopter blade application and the modeling techniques which are used to model helicopter blades. The next section gave a general description of an actuated, closed, single cell, composite beam and the assumptions which are made for the model presented in this chapter. Section three described the kinematic assumptions for the displacement of the beam and resulting strain state in the beam wall. Through the usage of

seven global displacement variables, the complete three-dimensional beam problem was reduced a high order one-dimensional problem. In the fourth section, a systematic derivation of the laminate constitutive relations was presented from the basic ply constitutive relations. The last section in this chapter was used to present the derivation of the equations of equilibrium and the force-displacement relations. The beam stiffness coefficients were defined from the force-displacement relations which are used to transform wall laminate properties into equivalent beam properties.

The objective of the inclusion of active materials in the composite beam is to obtain twist deformations. Twist can be obtained by the following actuation configurations:

- Direct twist actuation,
- Warping actuation of the beam,
- Extension actuation with an extension-twist coupled beam, and
- Bending actuation with a bending-twist coupled beam.

Ehlers [Ehlers, 1994] showed that it is possible to induce twist in the beam through warping actuation. The effectiveness of this method of actuation has not yet been confirmed. Twist obtained through structural couplings is a possibility, but helicopter blades in current use do not exhibit these structural coupling characteristics due to high centripetal force fields present during operation. Therefore this study is restricted to direct twist actuation through inducing shear stresses in the beam walls.

Shear inducing actuator systems are characterized by their stiffness anisotropies, as well as their free strain anisotropies. In this chapter, the goal is to determine how the different actuator's anisotropies (stiffness and actuation) influence the twist of a rectangular, composite, box beam and to establish the characteristics of an optimal twist actuator for composite, box beams. Finally, existing shear inducing actuator materials are compared based on actuator anisotropies to determine which actuator material system performs the best as a twist actuator.

3.1 Composite Box Beam Description

The first step in any parameter study is to describe the physical system by some mathematical model. The requirement on the model used for a parameter study is that it should be realistic but simple enough that the influence of the most important parameters can be examined.

The main load carrying member in helicopter blades is the spar structure. These spars normally have rectangular or D-shaped cross-sections. Typical helicopter blade spars are constructed from isotropic material, 0° and $\pm\theta^\circ$ composite material plies. Angled plies will cause structural couplings in the spar but this does not happen very often in practice. Helicopter blades can not exhibit structural couplings because the centripetal loading will result in undesirable displacements during operation. The same argument holds for aircraft wings where structurally coupled wings are only used in special cases. An example of such a special case is the usage of structural coupling in a composite forward swept aircraft wing to prevent divergence [Weisshaar, 1980].

It is assumed that helicopter spar structures can be modeled with rectangular composite box beams. The general form of the beam is shown in Figure 3-1. This geometric approximation simplifies the modeling considerably but maintains the important characteristics.

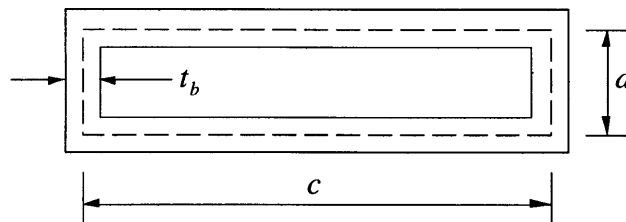


Figure 3-1. General Box Beam for Parameter Study

In Figure 3-1, c is the mid-plane cross-sectional chord, d is the mid-plane cross-sectional height, and t_b is the blade wall thickness. The next step in establishing a model for the parameter study is to look at the construction of the beam. For the parameter study it is assumed that the beam is made from a composite laminate, constructed from a combination of :

- Isotropic layers,
- 0° composite material layers, and

- $\pm\theta^\circ$ composite material layers of equal thickness.

It is assumed that the laminate used for construction is the same around the contour of the rectangular box beam. This assumption simplifies the determination of the beam stiffness coefficients but does not change the accuracy of the model.

To simplify the analysis it is assumed that only the membrane response of the beam wall is important. This implies that strains in the beam walls are not strong functions of the wall thickness and all curvatures can be set to zero in the relevant equations. This approximation holds for thin-walled structures but breaks down as the wall thickness increases. In the next section, the laminate membrane stiffnesses (equation (2.51)) are examined as these stiffnesses determine the overall beam stiffnesses.

3.1.1 Laminate Membrane Stiffness

To determine the beam stiffness coefficients it is necessary to calculate the laminate membrane stiffness coefficients. This calculation can be simplified by examining the contributions from the different construction plies to the membrane stiffness coefficients. For a single isotropic layer the plane stress constitutive relation looks as follows [Jones, 1975]:

$$\begin{Bmatrix} \sigma_{11} \\ \sigma_{22} \\ \tau_{12} \end{Bmatrix} = \begin{bmatrix} Q_{11} & Q_{12} & 0 \\ Q_{12} & Q_{11} & 0 \\ 0 & 0 & Q_{66} \end{bmatrix} \begin{Bmatrix} \varepsilon_{11} \\ \varepsilon_{22} \\ \gamma_{12} \end{Bmatrix} \quad (3.1)$$

where

$$\begin{aligned} Q_{11} &= \frac{E}{1-\nu^2} \\ Q_{12} &= \frac{\nu E}{1-\nu^2} \\ Q_{66} &= G = \frac{E}{2(1+\nu)} \end{aligned} \quad (3.2)$$

In equation (3.2), E is the material extensional (Young's) modulus and ν is the poisson's ratio. The stiffness coefficients for an isotropic layer are independent of angle, thus for an isotropic layer the laminate membrane constitutive relations reduce to the following equations:

$$\begin{Bmatrix} N_{xx} \\ N_{ss} \\ N_{xs} \end{Bmatrix} = \begin{bmatrix} A_{11} & A_{12} & 0 \\ A_{12} & A_{11} & 0 \\ 0 & 0 & A_{66} \end{bmatrix}_{iso} \begin{Bmatrix} \varepsilon_{xx}^o \\ \varepsilon_{ss}^o \\ \gamma_{xs}^o \end{Bmatrix} \quad (3.3)$$

This relationship is obtained by ignoring the moment stress resultants of equation (2.51) and setting the bending curvatures to zero. For any 0° transversely isotropic layers, the membrane constitutive relations are:

$$\begin{Bmatrix} N_{xx} \\ N_{ss} \\ N_{xs} \end{Bmatrix} = \begin{bmatrix} A_{11} & A_{12} & 0 \\ A_{12} & A_{22} & 0 \\ 0 & 0 & A_{66} \end{bmatrix}_0 \begin{Bmatrix} \varepsilon_{xx}^o \\ \varepsilon_{ss}^o \\ \gamma_{xs}^o \end{Bmatrix} \quad (3.4)$$

The combined $\pm\theta^\circ$ composite material layers, of equal thickness, are considered as a single combined laminate which are used in the construction of the beam wall. For the negative angled plies the rotated ply stiffness coefficients are of the same magnitude but opposite sign as for the positive angled plies:

$$\begin{aligned} (R_{16})_\theta &= -(R_{16})_{-\theta} \\ (R_{26})_\theta &= -(R_{26})_{-\theta} \end{aligned} \quad (3.5)$$

and the extensional-shear coupling stiffnesses are zero:

$$\begin{aligned} (A_{16})_{\pm\theta} &= (R_{16})_\theta t + (R_{16})_{-\theta} t = 0 \\ (A_{26})_{\pm\theta} &= (R_{26})_\theta t + (R_{26})_{-\theta} t = 0 \end{aligned} \quad (3.6)$$

Thus for a laminate constructed from $\pm\theta^\circ$ composite material layers of equal thickness, the membrane stiffness matrix is:

$$A_{\pm\theta} = \begin{bmatrix} A_{11} & A_{12} & 0 \\ A_{12} & A_{22} & 0 \\ 0 & 0 & A_{66} \end{bmatrix}_{\pm\theta} \quad (3.7)$$

For the complete beam wall laminate, the membrane stiffness matrix is the sum all the constituent laminate membrane stiffnesses. With the assumed type of construction the complete membrane stiffness coefficient matrix reduces to:

$$A = \begin{bmatrix} A_{11} & A_{12} & 0 \\ A_{12} & A_{22} & 0 \\ 0 & 0 & A_{66} \end{bmatrix} \quad (3.8)$$

The constitutive relationship used for the model in Chapter 2 (equation (2.54)) reduces with the membrane response assumption to:

$$\begin{Bmatrix} N_{xx} \\ N_{xs} \end{Bmatrix} = \begin{bmatrix} L_{11} & 0 \\ 0 & L_{22} \end{bmatrix} \begin{Bmatrix} \epsilon_{xx}^o \\ \gamma_{xs} \end{Bmatrix} - \begin{Bmatrix} N_{xx}^a \\ N_{xs}^a \end{Bmatrix}^* \quad (3.9)$$

This reduced constitutive relationship and the beam cross-sectional geometry determine the force-displacement relationship for the beam (equation (2.85)).

3.1.2 Box Beam Stiffnesses for Parameter Study

The doubly symmetric, rectangular cross-section of the box beam with circumferentially constant laminate wall construction and the membrane response assumption leads to a composite beam stiffness matrix which is diagonal:

$$\begin{Bmatrix} N \\ Q_y \\ Q_z \\ M_x \\ M_y \\ M_z \\ Q_w \end{Bmatrix} = \begin{bmatrix} K_{11} & 0 & 0 & 0 & 0 & 0 & 0 \\ 0 & K_{22} & 0 & 0 & 0 & 0 & 0 \\ 0 & 0 & K_{33} & 0 & 0 & 0 & 0 \\ 0 & 0 & 0 & K_{44} & 0 & 0 & 0 \\ 0 & 0 & 0 & 0 & K_{55} & 0 & 0 \\ 0 & 0 & 0 & 0 & 0 & K_{66} & 0 \\ 0 & 0 & 0 & 0 & 0 & 0 & K_{77} \end{bmatrix} \begin{Bmatrix} U_{,x} \\ \gamma_{xy} \\ \gamma_{xz} \\ \phi_{,x} \\ \beta_{y,x} \\ \beta_{z,x} \\ \phi_{,xx} \end{Bmatrix} - \begin{Bmatrix} N \\ Q_y \\ Q_z \\ M_x \\ M_y \\ M_z \\ Q_w \end{Bmatrix}^a \quad (3.10)$$

This type of stiffness matrix represents a beam without any structural couplings. The next step in the actuation parameter study is the description and analysis of the twist actuation of the beam.

3.2 Actuator Description

The proposed twist actuator, used for the parameter study, consists of two actuator plies made from anisotropic actuation material. This two ply actuator “package”, or “single” actuation ply, can be included in a composite box beam anywhere along the contour of the cross-section. The two plies in the package are placed at angles of $\pm\theta^\circ$ and are of equal

thickness. For the rest of the parameter study the actuator package is treated single actuation ply. This actuator package is consistent with the construction scheme assumed in the previous section for the beam and thus do not introduce any structural coupling in the beam. Figure 3-2 shows the general form of the actuator package.

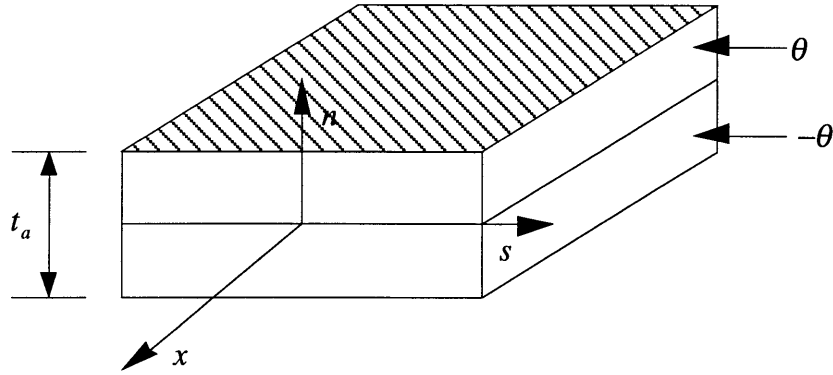


Figure 3-2. Twist Actuator Package (Consisting of Two Actuation Plies at $\pm\theta^\circ$)

3.2.1 Actuator Package Induced Stress Resultants

The actuator's ability to induce stresses is described by the plate actuation stress resultants (equation (2.56)). Only the membrane actuation stress resultants need be considered under the membrane response assumption. For the actuator package the induced stress resultants are:

$$\begin{aligned}
 (N_{xx}^a)^* &= N_{xx}^a - \frac{A_{12}}{A_{22}} N_{ss}^a \\
 &= \left(\frac{t_a}{2} P_{nxx(\theta)} E_{n(\theta)} + \frac{t_a}{2} P_{nxx(-\theta)} E_{n(-\theta)} \right) \\
 &\quad - \frac{A_{12}}{A_{22}} \left(\frac{t_a}{2} P_{nss(\theta)} E_{n(\theta)} + \frac{t_a}{2} P_{nss(-\theta)} E_{n(-\theta)} \right)
 \end{aligned} \tag{3.11}$$

and

$$\begin{aligned}
 (N_{xs}^a)^* &= N_{xs}^a - \frac{A_{26}}{A_{22}} N_{ss}^a \\
 &= \left(\frac{t_a}{2} P_{nxs(\theta)} E_{n(\theta)} + \frac{t_a}{2} P_{nxs(-\theta)} E_{n(-\theta)} \right) \\
 &\quad - \frac{A_{26}}{A_{22}} \left(\frac{t_a}{2} P_{nss(\theta)} E_{n(\theta)} + \frac{t_a}{2} P_{nss(-\theta)} E_{n(-\theta)} \right)
 \end{aligned} \tag{3.12}$$

To simplify these stress resultant equations, the rotated induced stress actuation constants ($p_{nxx}, p_{nss}, p_{nxs}$) are expressed in terms of the material ply angle and the properties of a single actuator material ply (equation (2.46)):

$$\begin{Bmatrix} p_{nxx} \\ p_{nss} \\ p_{nxs} \end{Bmatrix}_\theta = \begin{Bmatrix} e_{31}^* \cos^2(\theta) + e_{32}^* \sin^2(\theta) \\ e_{31}^* \sin^2(\theta) + e_{32}^* \cos^2(\theta) \\ \cos(\theta)\sin(\theta)(e_{31}^* - e_{32}^*) \end{Bmatrix} \quad (3.13)$$

which result in the following expressions for the induced stress resultants for the actuator package:

$$\begin{aligned} (N_{xx}^a)^* &= \frac{t_a}{2} (e_{31}^* \cos^2(\theta) + e_{32}^* \sin^2(\theta)) (E_{n(\theta)} + E_{n(-\theta)}) \\ &\quad - \frac{A_{12}}{A_{22}} \frac{t_a}{2} (e_{31}^* \sin^2(\theta) + e_{32}^* \cos^2(\theta)) (E_{n(\theta)} + E_{n(-\theta)}) \end{aligned} \quad (3.14)$$

and

$$\begin{aligned} (N_{xs}^a)^* &= \frac{t_a}{2} (\cos \theta \sin \theta (e_{31}^* - e_{32}^*)) (E_{n(\theta)} - E_{n(-\theta)}) \\ &\quad - \frac{A_{26}}{A_{22}} \frac{t_a}{2} (e_{31}^* \sin^2(\theta) + e_{32}^* \cos^2(\theta)) (E_{n(\theta)} + E_{n(-\theta)}) \\ &= \frac{t_a}{2} (\cos \theta \sin \theta (e_{31}^* - e_{32}^*)) (E_{n(\theta)} - E_{n(-\theta)}) \end{aligned} \quad (3.15)$$

In equation (3.15) the second term of the expression is equal to zero because $A_{26} = 0$ for the actuated box beam (see the previous section).

3.2.2 Maximized Induced Shear Stress Resultants

The interest for this study lies with the capability of the twist actuator to induce twist in a composite box beam. The induced moment of any actuator is directly proportional to the amount of shear stress which can be induced by an actuator. It is therefore necessary to maximize the induced shear stress resultant (equation (3.15)) for the actuator package. This maximization is to be completed given that the orientation angle, θ , can be varied and that the through-thickness field in the different plies of the actuator package can be varied. For this study it is assumed that the applied fields in the different plies have the same

magnitude, but that the sign may be varied. From equation (3.15) it can be seen that the induced shear stress resultant is maximized when:

$$E_{n(-\theta)} = -E_{n(\theta)} \quad (3.16)$$

and

$$\theta = 45^\circ \quad (3.17)$$

With the application of the field and angle to maximize twist, the actuation stress resultants reduce to:

$$(N_{xx}^a)^* = 0 \quad (3.18)$$

and

$$\begin{aligned} (N_{xy}^a)^* &= \frac{t_a}{2} (\cos \theta \sin \theta (e_{31}^* - e_{32}^*)) (E_{n(\theta)} - E_{n(-\theta)}) \\ &= \frac{t_a}{2} (e_{31}^* - e_{32}^*) E_{n(\theta)} \end{aligned} \quad (3.19)$$

The superscript “*” indicates that the induced shear stress resultant are a reduced stress resultant (see equation (2.56)) and it will be assumed implicitly henceforth. The orientation angle subscript “ θ ” will also be dropped. The total shear stress resultant can be expressed in terms of the full 3-D material properties as:

$$\begin{aligned} N_{xy}^a &= \frac{t_a}{2} \left(\left(e_{31} - \frac{C_{12}}{C_{22}} e_{33} \right) - \left(e_{32} - \frac{C_{23}}{C_{22}} e_{33} \right) \right) E_n \\ &= \frac{t_a}{2} \left(\begin{array}{l} \left(C_{11} - \frac{C_{12}^2}{C_{22}} \right) d_{31} + \left(C_{12} - \frac{C_{12} C_{23}}{C_{22}} \right) d_{32} \\ - \left(C_{22} - \frac{C_{23}^2}{C_{22}} \right) d_{32} - \left(C_{12} - \frac{C_{12} C_{23}}{C_{22}} \right) d_{31} \end{array} \right) E_n \end{aligned} \quad (3.20)$$

and by substituting for the plane stress ply stiffness coefficients (equation (2.36)), the induced shear stress resultant for the actuator package can be expressed in terms of the properties of a single actuator ply as:

$$\begin{aligned}
N_{xs}^a &= \frac{t_a}{2} \left(\left(C_{11} - \frac{C_{12}^2}{C_{22}} \right) d_{31} + \left(C_{12} - \frac{C_{12}C_{23}}{C_{22}} \right) (d_{32} - d_{31}) - \left(C_{22} - \frac{C_{23}^2}{C_{22}} \right) d_{32} \right) E_n \\
&= \frac{t_a}{2} (Q_{11}d_{31} + Q_{12}(d_{32} - d_{31}) - Q_{22}d_{32}) E_n
\end{aligned} \tag{3.21}$$

3.3 Non-Dimensional Actuated Box Beam Twist

The model for the beam used in the actuator parameter study assumes constant laminate construction around the contour of the beam. Consistent with this assumption, actuator material is present all around the contour of the beam. The beam cross-section with actuation included is shown in Figure 3-3. t_a and t_s is the actuator package thickness and the thickness of the passive structural plies.

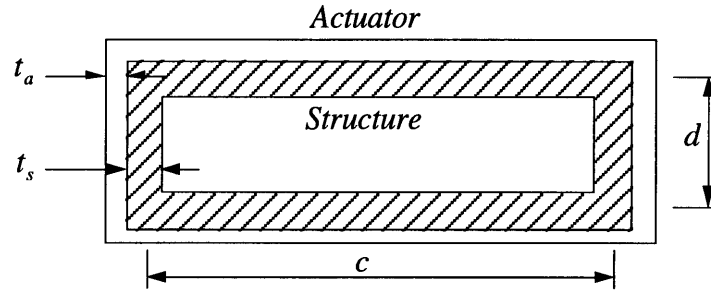


Figure 3-3. Beam Cross-Section with Actuator Package Included

3.3.1 Induced Torque and Beam Torsional Stiffness

The amount of twist of the actuated beam is a function of the actuator induced twisting moment and the beam torsional and warping stiffnesses. The induced twisting moment can be obtained by integrating the shear stress resultant (equation (3.19)) around the contour of the beam (equation (2.88)):

$$\begin{aligned}
M_x^a &= \oint_{\Gamma} N_{xs}^a \left(-\frac{2A\alpha}{\Gamma} \right) ds \\
&= \oint_{\Gamma} \frac{t_a}{2} (Q_{11}d_{31} + Q_{12}(d_{32} - d_{31}) - Q_{22}d_{32}) \left(-\frac{2A\alpha}{\Gamma} \right) E_n ds
\end{aligned} \tag{3.22}$$

The beam torsional and warping stiffness coefficients were defined in the previous chapter as (equation (2.88) and (2.90)):

$$K_{44} = \oint_{\Gamma} L_{22} \left(-\frac{2A\alpha}{\Gamma} \right)^2 ds, \quad (3.23)$$

and

$$K_{77} = \oint_{\Gamma} L_{11} \psi^2 ds \quad (3.24)$$

It is convenient to write the reduced plate membrane stiffness coefficients, (L_{11}, L_{22}) , in terms of the contributions from the base structure and the actuator package:

$$\begin{aligned} L_{11} &= \int_{-\frac{t}{2}}^{\frac{t}{2}} \left(R_{11} - \frac{R_{12}^2}{R_{22}} \right) dn \\ &= \int_0^{t_s} \left(R_{11} - \frac{R_{12}^2}{R_{22}} \right) dn + \int_0^{t_a} \left(R_{11} - \frac{R_{12}^2}{R_{22}} \right) dn \end{aligned} \quad (3.25)$$

and

$$\begin{aligned} L_{22} &= \int_{-\frac{t}{2}}^{\frac{t}{2}} \left(R_{66} - \frac{R_{26}^2}{R_{22}} \right) dn \\ &= \int_0^{t_s} \left(R_{66} - \frac{R_{26}^2}{R_{22}} \right) dn + \int_0^{t_a} \left(R_{66} - \frac{R_{26}^2}{R_{22}} \right) dn \end{aligned} \quad (3.26)$$

In equations (3.25) and (3.26) the superscripts “a” and “s” refer to the actuator and base structure respectively. To simplify the analysis, the concept of smeared properties are introduced for both the structure and the actuator. The smeared stiffnesses are the thickness averaged stiffnesses for the base structure as well as the actuator package :

$$A_{ij}^s = t_s R_{ij}^s = \int_0^{t_s} R_{ij} dn, \text{ and } A_{ij}^a = t_a R_{ij}^a = \int_0^{t_a} R_{ij} dn \quad (3.27)$$

Expressed in smeared stiffness values, the reduced stiffness coefficients are:

$$L_{11} = t_s \left(R_{11} - \frac{R_{12}^2}{R_{22}} \right)^s + t_a \left(R_{11} - \frac{R_{12}^2}{R_{22}} \right)^a \quad (3.28)$$

and

$$L_{22} = t_s R_{66}^s + t_a R_{66}^a \quad (3.29)$$

Due to the assumed laminate wall construction R_{26}^s and R_{26}^a are zero and thus do not enter equation (3.29). This type of “smearing” reduces the number of stiffness coefficients that need be considered in the analysis but does not reduce the accuracy of the analysis. Substituting the smeared properties into equation (3.24) leads to the following expressions for the torsional and warping stiffnesses:

$$K_{44} = \oint_{\Gamma} (t_s R_{66}^s + t_a R_{66}^a) \left(-\frac{2A\alpha}{\Gamma}\right)^2 ds \quad (3.30)$$

and

$$K_{77} = \oint_{\Gamma} \left(t_s \left(R_{11}^s - \frac{(R_{12}^s)^2}{R_{22}^s} \right) + t_a \left(R_{11}^a - \frac{(R_{12}^a)^2}{R_{22}^a} \right) \right) \psi^2 ds \quad (3.31)$$

The major considerations for the parameter study are the properties of the actuator material. Therefore the torsional stiffness of the beam should be written as a function of the actuator ply properties. The easiest starting point is the smeared shear stiffness of the actuator package:

$$R_{66}^a = \frac{1}{t_a} \left(\frac{t_a}{2} R_{66(45^\circ)} + \frac{t_a}{2} R_{66(-45^\circ)} \right) \quad (3.32)$$

with

$$\begin{aligned} R_{66(45^\circ)} &= (Q_{11} + Q_{22} - 2Q_{12}) \sin^2(45) \cos^2(45) \\ &\quad + Q_{66} (\sin^4(45) + \cos^4(45)) \\ &= \frac{1}{4} (Q_{11} + Q_{22} - 2Q_{12}) \end{aligned} \quad (3.33)$$

and similarly

$$R_{66(-45^\circ)} = \frac{1}{4} (Q_{11} + Q_{22} - 2Q_{12}) \quad (3.34)$$

therefore the effective actuator shear stiffness reduces to:

$$R_{66}^a = \frac{1}{4}(Q_{11} + Q_{22} - 2Q_{12}) \quad (3.35)$$

The beam torsional stiffness can also be expressed in terms of the plane stress stiffness coefficients by substituting equation (3.32) into equation (3.30):

$$K_{44} = \oint_{\Gamma} \left(t_s R_{66}^s + t_a \frac{1}{4}(Q_{11} + Q_{22} - 2Q_{12}) \right) \left(-\frac{2A\alpha}{\Gamma} \right)^2 ds \quad (3.36)$$

3.3.2 Beam Tip Twist

The actuated beam is modeled as a cantilevered beam with no applied forces or moments except for the moment internally applied by the actuator package. The equation of equilibrium which relates the internal twisting moment and bimoment is (equation (2.74)):

$$M_{x,x} - Q_{w,xx} = 0 \quad (3.37)$$

The geometric boundary conditions are:

$$\begin{aligned} \phi &= 0 & @ x &= 0 \\ \phi_{,x} &= 0 & @ x &= 0 \end{aligned} \quad (3.38)$$

and the natural boundary conditions are (see Chapter 2):

$$\begin{aligned} M_x(l) - Q_{w,x}(l) &= 0 \\ Q_w(l) &= 0 \end{aligned} \quad (3.39)$$

The governing equation is obtained by integrating the twist equilibrium equation with respect to the spanwise coordinate, x .

$$\begin{aligned} \int M_{x,x} dx - \int Q_{w,xx} dx &= \int 0 dx \\ M_x - Q_{w,x} &= Const \end{aligned} \quad (3.40)$$

By evaluating equation (3.40) at the free end ($x = l$) of the twist actuated beam, it can be concluded that the integration constant's value is zero.

$$M_x(l) - Q_{w,x}(l) = Const = 0 \quad (3.41)$$

Therefore the twist governing equation reduces to:

$$M_x - Q_{w,x} = 0 \quad (3.42)$$

By applying the actuated beam assumptions, the beam stiffness matrix (equation (3.10)) becomes diagonal and the internal twisting moment and bimoment can be expressed as:

$$M_x = K_{44}\phi_{,x} - M_x^a \quad (3.43)$$

and

$$Q_w = K_{77}\phi_{,xx} \quad (3.44)$$

Equations (3.43) and (3.44) can be substituted into equation (3.42) to express the governing equation in terms of the twist deformation variable, ϕ :

$$K_{44}\phi_{,x} - K_{77}\phi_{,xxx} = M_x^a \quad (3.45)$$

which is solved subject to following boundary conditions:

$$\begin{aligned} \phi &= 0 & @ x &= 0 \\ \phi_{,x} &= 0 & @ x &= 0 \\ \phi_{,xx} &= 0 & @ x &= l \quad (Q_w(l) = 0) \end{aligned} \quad (3.46)$$

The solution to the equilibrium equation consists of the homogeneous solution and the particular solution [Rehfield et al., 1988]. It is convenient to complete the solution in terms of the normalized spanwise coordinate:

$$\xi = \frac{x}{l} \quad (3.47)$$

For the homogenous solution it is assumed that the solution takes the general exponential form:

$$\phi_{\text{hom}} = \Phi e^{r\xi} \quad (3.48)$$

where Φ is the twist amplitude. The assumed homogeneous solution is substituted into the homogeneous governing differential equation to obtain an expression for the unknown parameter, r :

$$\begin{aligned}\phi_{,xxx} - \frac{K_{44}}{K_{77}} \phi_{,x} &= 0 \\ \frac{r^3}{l^3} \Phi e^{r\xi} - \frac{K_{44}}{K_{77}} \frac{r}{l} \Phi e^{r\xi} &= 0 \\ \frac{r^3}{l^3} - \frac{K_{44}}{K_{77}} \frac{r}{l} &= 0\end{aligned}\quad (3.49)$$

The roots of the polynomial in equation (3.49) are:

$$r_1 = 0, r_2 = \sqrt{\frac{K_{44}}{K_{77}}} l, r_3 = -\sqrt{\frac{K_{44}}{K_{77}}} l \quad (3.50)$$

and the general homogeneous solution is:

$$\begin{aligned}\phi_{\text{hom}} &= Ae^{r_2\xi} + Be^{r_3\xi} + Ce^{r_1\xi} \\ &= Ae^{\lambda\xi} + Be^{-\lambda\xi} + C\end{aligned}\quad (3.51)$$

with

$$\lambda^2 = \frac{K_{44}}{K_{77}} l^2 \quad (3.52)$$

The particular solution to the differential equation is:

$$\phi_{\text{part}}(x) = \frac{M_x^a x}{K_{44}} \quad (3.53)$$

or expressed in terms of the normalized coordinate the particular solution is:

$$\phi_{\text{part}}(\xi) = \frac{M_x^a l}{K_{44}} \xi \quad (3.54)$$

The complete solution is the sum of the homogeneous and particular solutions:

$$\begin{aligned}\phi &= \phi_{\text{hom}} + \phi_{\text{part}} \\ &= Ae^{\lambda\xi} + Be^{-\lambda\xi} + C + \frac{M_x^a l}{K_{44}} \xi\end{aligned}\quad (3.55)$$

The constants in equation (3.55) can be evaluated with the application of the boundary conditions (equation (3.44)):

$$\begin{aligned}\phi(0) &= 0 = A + B + C \\ \phi_{,\xi}(0) &= 0 = \lambda A - \lambda B + \frac{M_x^a l}{K_{44}} \\ \phi_{,\xi\xi}(1) &= 0 = \lambda^2 A e^\lambda + \lambda^2 B e^{-\lambda}\end{aligned}\quad (3.56)$$

Solution of equation (3.56) gives the expressions for the constants:

$$\begin{aligned}A &= -\frac{M_x^a l}{K_{44}} \left(\frac{e^{-2\lambda}}{\lambda(1+e^{-2\lambda})} \right) \\ B &= \frac{M_x^a l}{K_{44}} \left(\frac{1}{\lambda(1+e^{-2\lambda})} \right) \\ C &= \frac{M_x^a l}{K_{44}} \left(\frac{e^{-2\lambda} - 1}{\lambda(1+e^{-2\lambda})} \right)\end{aligned}\quad (3.57)$$

By substituting the expressions for the unknown constants into equation (3.55) yields the beam twist expression in terms of the normalized spanwise coordinate:

$$\phi(\xi) = \frac{M_x^a l}{K_{44}} \left\{ \frac{[e^{-\lambda\xi} + e^{-2\lambda} - e^{-\lambda(2-\xi)} - 1]}{\lambda(1+e^{-2\lambda})} + \xi \right\} \quad (3.58)$$

The factor λ accounts for influence of warping on the twist of the beam. This factor is very important and needs to be examined more closely. The warping factor can be expressed as a function of the plate stiffness coefficients:

$$\begin{aligned}\lambda^2 &= \frac{K_{44}}{K_{77}} l^2 \\ &= \frac{\oint_{\Gamma} L_{22} \left(-\frac{2A\alpha}{\Gamma}\right)^2 ds}{\oint_{\Gamma} L_{11} \psi^2 ds}\end{aligned}\quad (3.59)$$

For the case where the laminate construction is constant around the contour, the warping parameter reduces to the following expression:

$$\alpha = \frac{\frac{\Gamma}{Gt}}{\oint \frac{1}{Gt} ds} = 1 \quad (3.60)$$

Then for the rectangular cross-section (Figure 3-1) the beam stiffness coefficients reduce to:

$$K_{44} = L_{22} \frac{4A^2}{\Gamma} = L_{22} \frac{2(cd)^2}{(c+d)} \quad (3.61)$$

and

$$K_{77} = L_{11} \frac{c^2 d^2 (c-d)^2}{24(c+d)} \quad (3.62)$$

with c and d the beam chord and height as defined in Figure 3-1. Thus for a rectangular, circumferentially constant stiffness box beam, the warping constant λ^2 becomes:

$$\begin{aligned} \lambda^2 &= \frac{48L_{22}l^2}{L_{11}(c-d)^2} \\ &= \frac{48L_{22}\eta^2}{L_{11}(1-\zeta)^2} \end{aligned} \quad (3.63)$$

with

$$\eta = \frac{l}{c}, \text{ and } \zeta = \frac{d}{c} \quad (3.64)$$

When the beam is square ($c = d$) the warping constant goes to infinity and the section does exhibit any warping during twisting. If it is assumed that the laminate behaves quasi-isotropically, the plate shear stiffness reduces to:

$$L_{22} \approx \frac{L_{11}}{2(1+\nu)} = \frac{L_{11}}{2.3} \quad (3.65)$$

For a typical helicopter blade $\eta > 10$ and $\zeta \approx 1/4$ [Sandford, 1978]. With these bounds on the parameters, the warping constant are bounded by $\lambda > 60$. Thus $e^{-\lambda} \ll 1$ and the beam twist (equation (3.58)) reduces to:

$$\phi(\xi) = \frac{M_x^a l}{K_{44}} \left\{ \frac{1}{\lambda} (e^{-\lambda \xi} - 1) + \xi \right\} \quad (3.66)$$

At the beam tip, the twist is:

$$\phi(1) = \frac{M_x^a l}{K_{44}} \left(1 - \frac{1}{\lambda} \right) \quad (3.67)$$

or

$$\phi(l) = \frac{M_x^a l}{K_{44}} \left(1 - \frac{1}{\lambda} \right) \quad (3.68)$$

Equation (3.68) is a simplified expression for actuated beam tip twist, but it shows that warping of the beam can have a significant effect on beam tip twist. For values of $\lambda > 60$, the influence of warping on the twist is negligible, and in this case, the beam tip twist is:

$$\phi(l) = \frac{M_x^a}{K_{44}} l \quad (3.69)$$

Equation (3.69) will be used in the parameter study as it adequately describes the actuated twist response of helicopter blades.

3.3.3 Non-Dimensional Tip Twist Parameter

For any parameter study it is necessary to express the relevant equations, which describe the system, in terms of non-dimensional system parameters. With the assumption that all properties are constant around the contour, that the applied electrical field is also constant around the contour, and produces positive twist, the blade tip twist reduces to:

$$\begin{aligned}
\phi_{tip} &= \frac{M_x^a l}{K_{44}} \\
&= \frac{\oint_{\Gamma} \frac{t_a}{2} (Q_{11} d_{31} + Q_{12} (d_{32} - d_{31}) - Q_{22} d_{32}) \left(-\frac{2A\alpha}{\Gamma} \right) E_n ds}{\oint_{\Gamma} \left(t_s R_{66}^s + t_a \frac{1}{4} (Q_{11} + Q_{22} - 2Q_{12}) \right) \left(-\frac{2A\alpha}{\Gamma} \right)^2 ds} l \\
&= \frac{-t_a c d (Q_{11} d_{31} + Q_{12} (d_{32} - d_{31}) - Q_{22} d_{32}) E_n}{\left(\frac{4c^2 d^2 \left(t_s R_{66}^s + t_a \frac{1}{4} (Q_{11} + Q_{22} - 2Q_{12}) \right)}{2c + 2d} \right)} l \quad (3.70)
\end{aligned}$$

Equation (3.70) can be rearranged in such that the equation are a function of non-dimensional ratios:

$$\begin{aligned}
\phi_{tip} &= \frac{-t_a (Q_{11} d_{31} + Q_{12} (d_{32} - d_{31}) - Q_{22} d_{32}) E_n (c + d) l}{2cd \left(t_s R_{66}^s + t_a \frac{1}{4} (Q_{11} + Q_{22} - 2Q_{12}) \right)} \\
&= \frac{\frac{l}{c} \left(1 + \frac{d}{c} \right) \left(1 + \frac{Q_{12} d_{32}}{Q_{11} d_{31}} - \frac{Q_{12}}{Q_{11}} - \frac{Q_{22} d_{32}}{Q_{11} d_{31}} \right) (-d_{31} E_n) \frac{t_a Q_{11}}{t_s R_{66}^s}}{2 \frac{d}{c} \left(1 + \frac{t_a Q_{11}}{t_s R_{66}^s} \left(\frac{1}{4} - \frac{Q_{12}}{2Q_{11}} + \frac{Q_{22}}{4Q_{11}} \right) \right)} \quad (3.71)
\end{aligned}$$

Expressed in terms of the non-dimensional ratios, the tip twist (equation (3.71)) is:

$$\phi_{tip} = \frac{R_s^s R_{lc} (1 + R_{dc}) (1 + R_{Q12} R_d - R_{Q12} - R_{Q22} R_d) \Lambda_{act}}{2R_{dc} \left\{ 1 + R_s \left(\frac{1}{4} - \frac{1}{2} R_{Q12} + \frac{1}{4} R_{Q22} \right) \right\}} \quad (3.72)$$

where the non-dimensional system ratios are defined as follows:

$$\text{Geometric Ratios: } R_{lc} = \frac{l}{c}, R_{dc} = \frac{d}{c} \quad (3.73)$$

$$\text{Free Strain Anisotropy Ratio: } R_d = \frac{d_{32}}{d_{31}} \quad (3.74)$$

$$\text{Principal Actuation Strain: } \Lambda_{act} = -d_{31} E_n \quad (3.75)$$

$$\text{Stiffness Anisotropy's: } R_{Q12} = \frac{Q_{12}}{Q_{11}}, R_{Q22} = \frac{Q_{22}}{Q_{11}} \quad (3.76)$$

and

$$\text{Structural Stiffness Ratio: } R_s = \frac{t_a Q_{11}}{t_s R_{66}^s} \quad (3.77)$$

To complete the parameter study, it is necessary to express the beam tip twist as a parameter which is independent of induced actuation strain. In this way the twist inducing capability of different materials can be compared based on actuator anisotropies. The non-dimensional twist parameter, expresses the beam tip twist relative to some reference strain value. This reference strain value is the free strain developed in the 1-direction when a single actuator ply is actuated:

$$P_\phi = \frac{\phi_{tip}}{\Lambda_{act}} = \frac{R_{1c}(1+R_{dc})(1+R_{Q12}R_d - R_{Q12} - R_{Q22}R_d)R_s}{2R_{dc}\left\{1+R_s\left(\frac{1}{4}-\frac{1}{2}R_{Q12}+\frac{1}{4}R_{Q22}\right)\right\}} \quad (3.78)$$

The non-dimensionalized twist parameter, P_ϕ , represents the twist per unit induced principal actuation strain. It is used in the next section in an parameter study to determine how actuator anisotropies influence the beam twist.

3.4 Parameter Study

Equation (3.78) can be used for parameter studies on twist actuation by keeping all of the non-dimensional parameters fixed and varying one of the parameters with respect to one independent variable. The independent variable in this study is the structural stiffness ratio, R_s . The structural stiffness ratio represents not only the stiffness of the actuator relative to the structure but also the amount of actuator material present in the beam. By considering only small values of R_s , the possibility of a beam constructed purely from active material is excluded.

3.4.1 Influence of the Actuator Stiffness Anisotropy on Twist

The parameters that determine the performance of any actuator are the free strain anisotropy ratio, R_d , and the stiffness anisotropy ratios, R_{Q12} and R_{Q22} . The stiffness anisotropy ratio R_{Q12} is the equivalent plane stress poisson's ratio for the active material ply. For the parameter study it is assumed that R_{Q12} stays fairly constant and thus can be excluded from the study. Values for the parameters which are invariant during the study are given in Table 3-1. These values were obtained from Chinook CH-47D blade dimensions [Sandford, 1978].

TABLE 3-1. INVARIANT SYSTEM PARAMETERS FOR TWIST PARAMETER STUDY

R_{lc}	R_{dc}	R_{C12}
25	0.3	0.3

In the first part of the parameter study, the influence of the transverse stiffness anisotropy ratio, R_{Q22} , on twist is evaluated for different values of free strain anisotropy, R_d . Results of the study are shown in Figure 3-4.

To explain the results, it is convenient to consider the twist response when there is no transverse induced strain, i.e. R_d is equal to zero. In this case the induced moment is independent of the stiffness anisotropy, R_{Q22} . For small values of the structural stiffness ratio, R_s , the torsional stiffness of the beam stays fairly constant. Thus the resulting non-dimensional twist parameter is a linear function of the structural stiffness ratio, R_s .

To explain the other results, the response can be divided up into two categories. The first category is the response when there is transverse contraction when the actuator expands in the normal direction ($R_d < 0$). In this case, the twist parameter value is maximized by an actuator with stiffness isotropy. Stiffness in the transverse direction increases the induced shear and as a result, the induced twisting moment. Category two is the response when the actuator expands in both directions when actuated ($R_d > 0$). In this case, any stiffness in the transverse direction reduces the induced shear; thus the best actuator is the one with the smallest stiffness anisotropy ratio R_{Q22} . A secondary effect is the increase in the torsional stiffness of the beam. When the transverse stiffness is large, the effective shear modulus of the actuator package is large. R_{Q22} is large which results in high torsional stiffness. The worst case for category two response is the actuator with both stiffness and actuator isotropy which can not produce any twist.

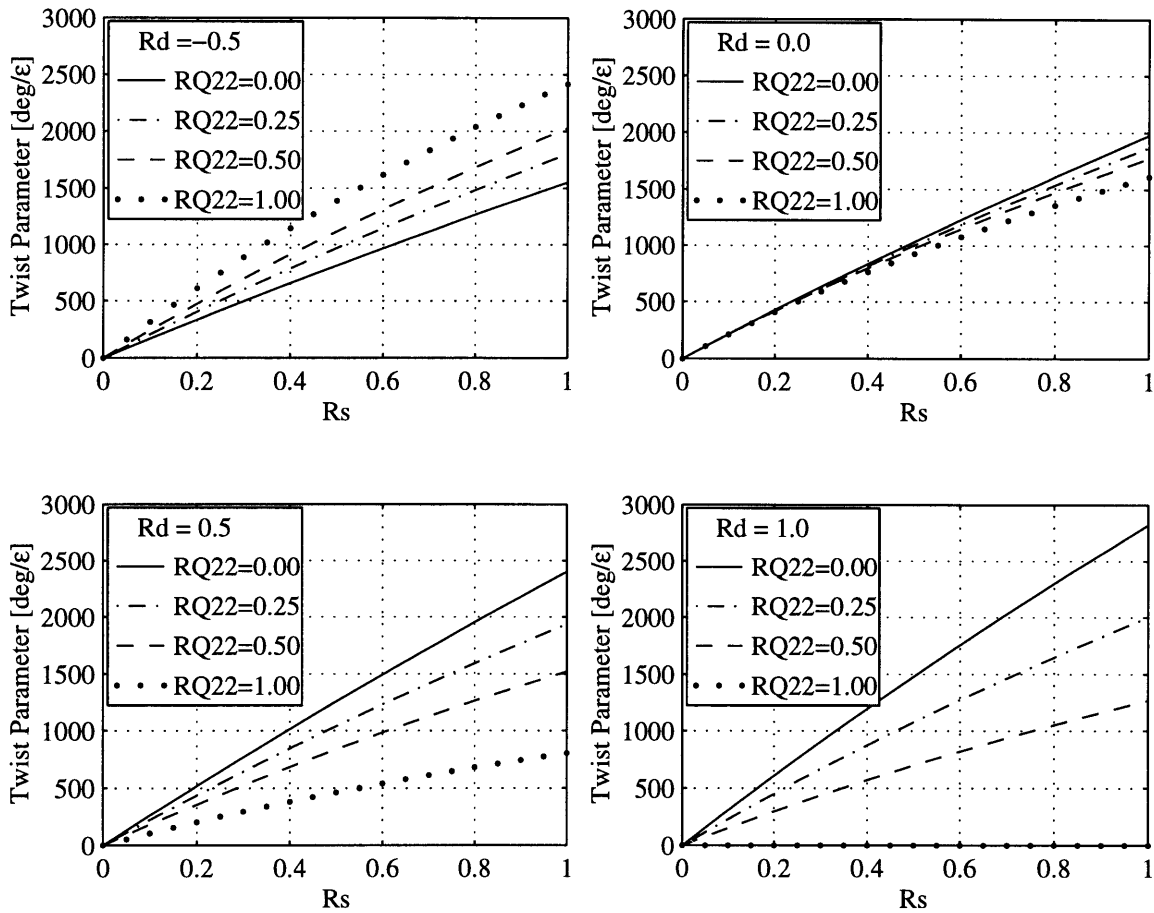


Figure 3-4. Influence of Actuator Stiffness Anisotropy, R_{Q22} , on the Twist Parameter

3.4.2 Influence of the Actuator Free Strain Anisotropy on Twist

To conclude the parameter study, the influence of the free strain anisotropy ratio, R_d , is evaluated for different values of the stiffness anisotropy ratio, R_{Q22} . Results from this study are shown in Figure 3-5.

For the case where the influence of R_d is considered, a phenomenon similar to that described in the previous section occurs. When R_{Q22} is equal to R_{Q12} , the induced shear is independent of the transverse induced strain and the response are the same for different values of R_d .

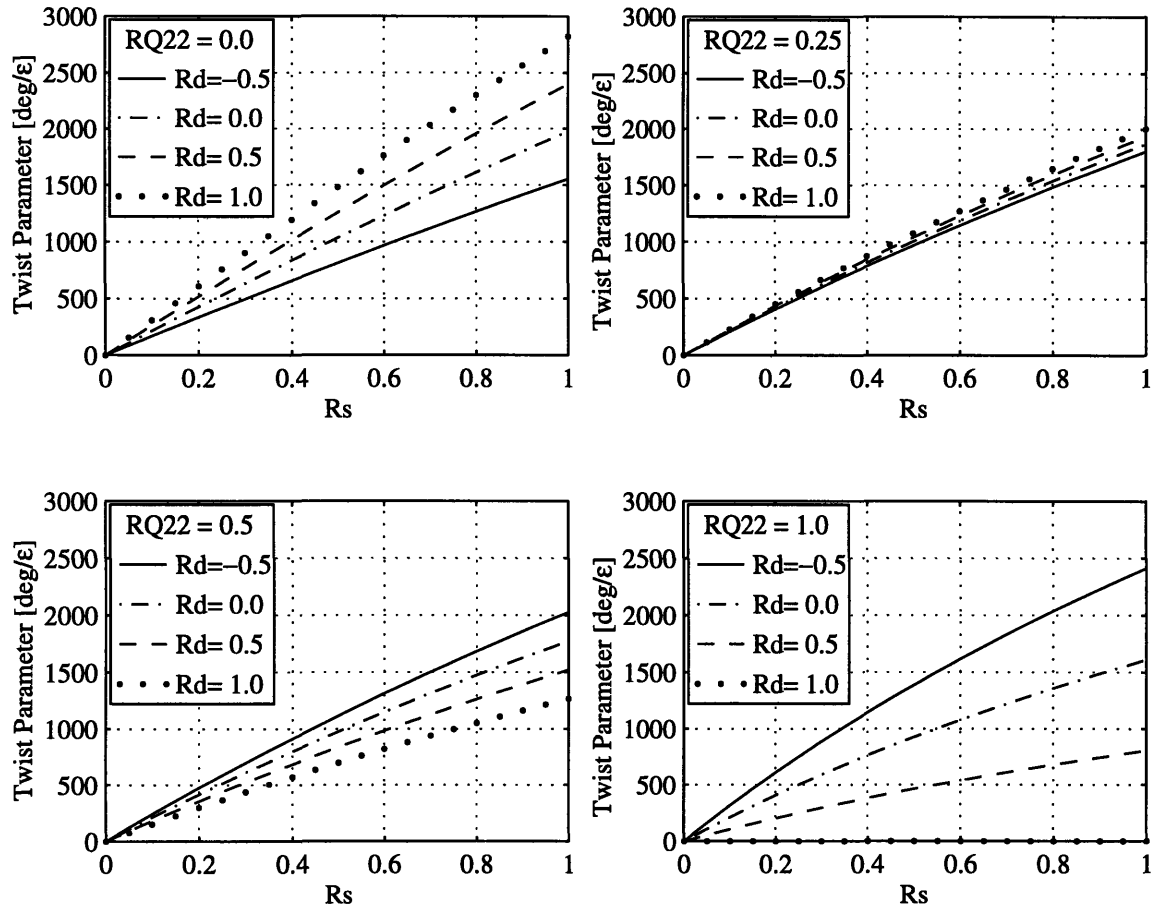


Figure 3-5. Influence of Free Strain Actuation Anisotropy, R_d , on the Twist Parameter

3.4.3 Twist Parameter Contour Plots

The results from the parameter study can be illustrated on contour plots of the twist parameter vs. the free strain anisotropy ratio, R_d , and the transverse stiffness anisotropy ratio, R_{Q22} , for specific values of R_s . In Figure 3-6, the contour plots for four different values of R_s are shown. The normalized twist parameter shows a saddle response. The saddle points are defined by R_d equal to zero (no transverse induced strain), and R_{Q22} equal to R_{Q12} (the induced shear stress resultant is independent of transverse induced strain, as shown in equation (3.75)).

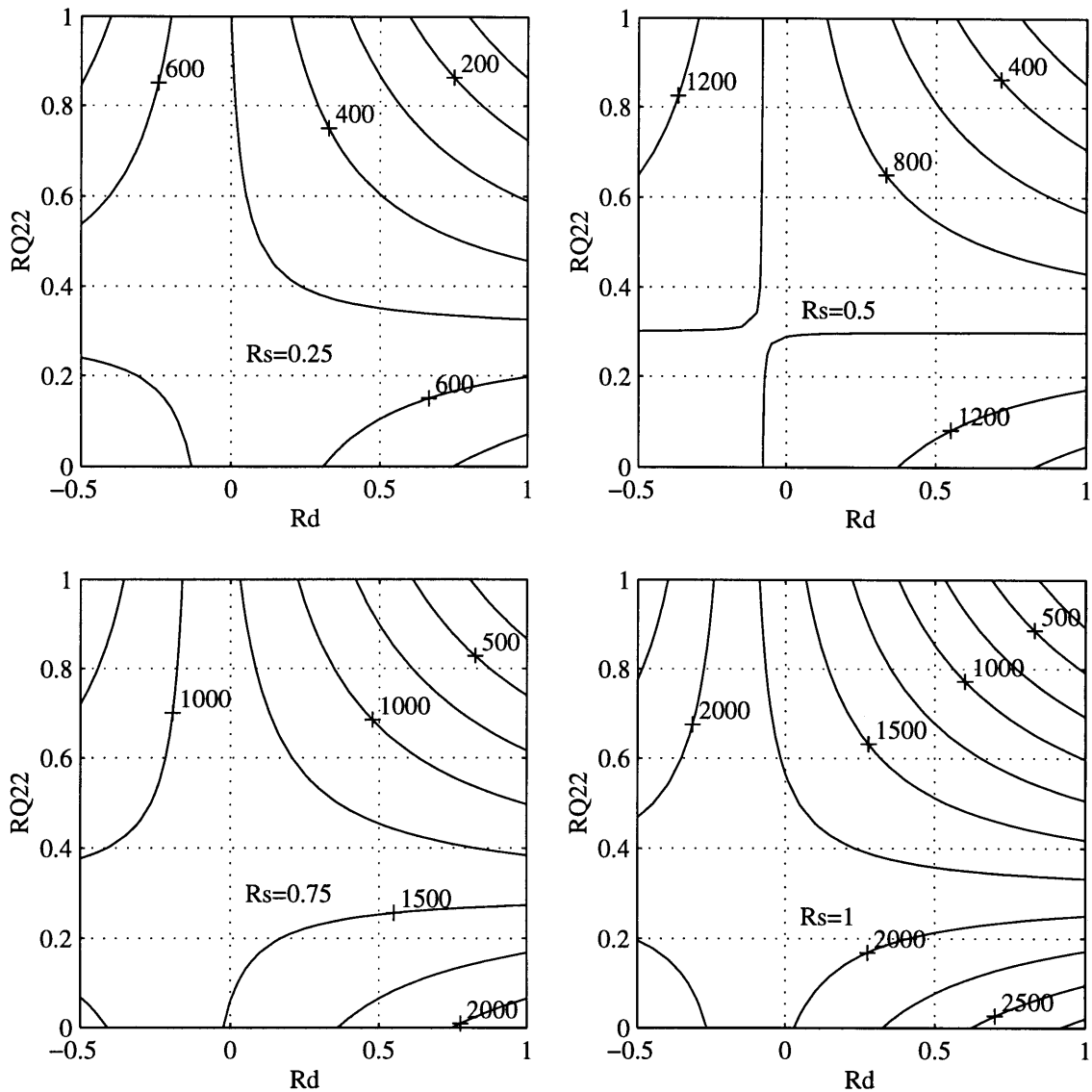


Figure 3-6. Non-Dimensionalized Twist Parameter Contour Plots

When the actuator expands in one direction and contracts in the other direction during actuation, the free strain anisotropy ratio is less than zero ($R_d < 0$). In this case, the normalized twist parameter is maximized by an actuator with stiffness isotropy ($R_{Q22} = 1$). This response is due to the fact that as the actuator becomes more isotropic (stiffness isotropy), the induced moment increases faster than the beam torsional stiffness.

For the case where the actuator expands in both directions, the free strain anisotropy ratio is greater than zero ($R_d > 0$). In this case, the twist parameter is maximized by an actuator with no transverse stiffness ($R_{Q12} = 0$). For $R_{Q22} = 0$, the twist parameter increases as R_d

increases (transverse induced strain increases) due to the fact that the gain in induced twist is larger than the increase in torsional stiffness.

From the parameter study results, it can be concluded that there are certain combinations of actuator properties which result in high levels of beam twist. For actuator systems where the designer can tailor the actuator properties, it is possible to design a good twist actuator. For instance, PFC's inherently have positive actuation strain in both directions ($R_d > 0$) and thus the goal would be to make R_{Q22} as small as possible. The opposite argument holds for IDEPFC's where transverse contraction occurs during actuation ($R_d < 0$) and the goal would be to design an actuator with stiffness isotropy ($R_{Q22} = 1$).

3.5 Actuator Comparison

Four different actuator types exist which are capable of inducing shear stresses in composite helicopter blade walls. To design an active blade it is necessary to determine which of the actuators is the most effective for inducing twist in the blade. In this section, the different actuator systems are compared based on the twist actuation capability due to actuator anisotropies. The measure used for the comparison is the non-dimensionalized twist parameter defined in the previous section. This comparison metric only takes the levels of stiffness and actuation anisotropies into account. Normal stiffness, normal in-plane strain, strength, fatigue, manufacturing procedures, material conformability, and reliability are not accounted for in the analysis. The mechanism of actuator operation is not relevant to this study and the reader is referred to the references for a description of actuator operation. Actuator systems considered for twist actuation are:

- Piezoelectric Fiber Composites (PFC) [Bent et al., 1995; Rodgers and Hagood, 1995],
- Directionally Applied Piezoelectrics (DAP) [Barrett, 1993],
- Interdigitated Electrode Monolithic Piezoelectric Actuators (IDEMON) [Hagood et al, 1993], and
- Interdigitated Electrode Piezoelectric Fiber Composites (IDEPFC) [Bent and Hagood, 1995].

Properties of the various actuator systems used for the comparison, are given in Table 3-2. PFC and IDEPFC actuator properties are model values for actuators with a ceramic fiber volume fraction of 0.56. This fiber volume fraction is based on a transverse line fiber

fraction [Rodgers and Hagood, 1995] of 0.8 for the IDEPFC actuators which were used in the twist actuated, scale model helicopter blade (see Chapter 5). The properties for the PFC and IDEPFC actuators include the effects of the electrodes which are attached to both sides of the fiber-matrix layer.

TABLE 3-2. TWIST ACTUATOR MATERIAL PROPERTIES

	PFC	DAP	IDEMON	IDEPFC
Q_{11}^a (GPa)	40.2	66.2	66.2	44.5
R_{Q12}	0.19	0.29	0.29	0.15
R_{Q22}	0.43	0.14	1	0.42
R_d	0.81	1	-0.5	-0.42
ρ_a (kg/m ³)	4810	7500	7500	4810
Λ_{act} ($\pm\mu\epsilon$)	250	250	450	450

The actuator comparison is done by comparing the twist parameter as a function of the structural stiffness ratio, R_s . The range for the comparison is for R_s varying between zero and unity. Results of the actuator comparison are shown in Figure 3-7.

From Figure 3-7 it is evident that the IDEMON, IDEPFC and DAP actuator systems have properties which produce comparable levels of the normalized twist parameter. It should be noted that the high free strain capability of IDE actuation systems will produce twist levels higher than equivalent systems using DAP actuators. On the other hand, PFC actuators do not perform very well. For PFC's, R_d is positive, and the goal would be to have R_{Q22} equal to zero. However, this is unattainable which results in the poor performance of PFC. The comparison of the materials is not an ultimate comparison, but the comparison does indicate that the IDE technology has good inherent capability to induce twist in a beam.

3.6 Summary

There is a wide array of actuator properties which can be realized with PFC actuator technology. The first part of this chapter was used to present a simple model of twist actuated, single cell, composite beams. By making realistic assumptions as to the construction of the composite beams and the twist actuation used in the beams, an expression for beam tip twist was obtained which effectively shows the influence of actuator properties.

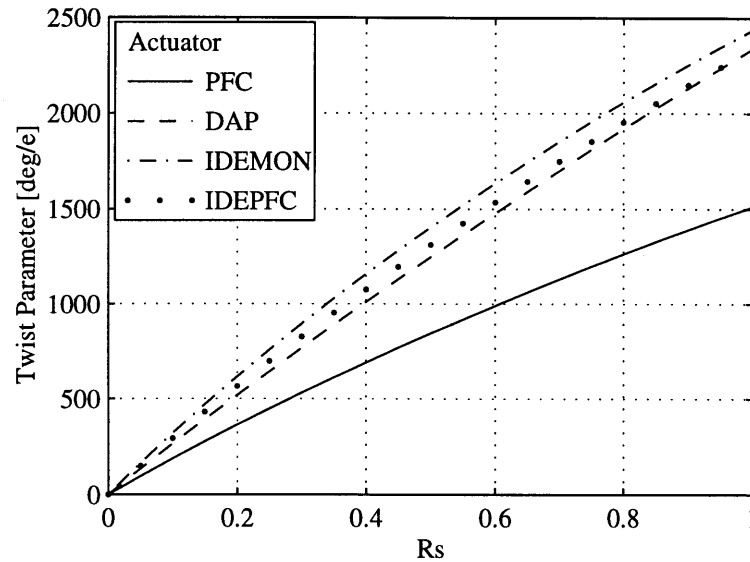


Figure 3-7. Actuator Comparison based on Actuator Anisotropies

The beam tip twist was non-dimensionalized to explore the influence of the different actuator anisotropies (stiffness and actuation) as related to the twist actuation of closed cell beams. The study indicated that there are two combinations of actuator properties which will induce high levels of twist. When the in-plane actuation strains are both positive or negative (the free strain anisotropy ratio R_d is positive), there should be a large difference in the longitudinal and transverse stiffness of the material (the stiffness anisotropy ratio, R_{Q22} , should be low). On the other hand, when the longitudinal and transverse in-plane actuation strains are of opposite sign (the free strain anisotropy ratio, R_d , is negative), the material should have isotropic passive stiffness properties for maximum twist (the stiffness anisotropy ratio, R_{Q22} , should be as close to one as possible). This result gives direction for future actuator development. The parameter study was also extended to comparing currently available anisotropic actuation systems for twist inducing capabilities. IDEMON and IDEPFC actuators have favorable actuation properties for twist actuation. DAP elements have completely different properties but the combination of properties are also inherently good for twist actuation. PFC actuators are capable of twist actuation but not very effectively.

Chapter 4 *Finite Element Displacement Simulation*

The Finite Element Method (FEM) is a very powerful method for obtaining approximate solutions to complex boundary value problems which are unsolvable by classical analytical methods. This method is typically used to analyze static and dynamic structural systems, buckling problems, thermal systems, heat transfer problems, electrical systems, magnetic systems, and coupled field system problems. In this chapter a displacement based finite element will be formulated for anisotropically actuated, single cell, composite beams. This element is used in the latter part of the chapter for displacement predictions of both passive and adaptive, single cell, composite beams.

In the FEM, the required solution domain is discretized into sets of smaller components or finite elements with similar geometry and physical descriptions. The different finite elements are joined in the solution domain by nodes. Associated with each of the element nodes are nodal degrees of freedom which represent physical unknowns in the problem. The objective of the method is to obtain approximate solutions to the nodal degrees of freedom. The physical unknowns (degrees of freedom) depend on the problem and can be forces, displacements, stresses, temperatures, pressures, voltages or any combination of unknowns. For this study displacement based finite elements will be used because the study objective is to predict the adaptive beam static displacements. Within each of the elements, interpolation functions are used to approximate the physical unknowns at any point in the element based on the nodal values of the unknowns. The nodal degrees of freedom are then used to describe the energy in the system. For structural systems, the approximate solution is obtained by applying the principle of minimum stationary potential energy (Hamilton's principle) [Zienkiewicz, 1971]. The result from this minimization is a

set of equations with the nodal degrees of freedom as the variables. Once the set of equations is obtained it is easy to apply the boundary conditions. The solution to the set of equations approximately satisfies equilibrium. Thus the FEM minimizes the system potential energy within the constraint of the assumed displacement field. By using more elements or higher order interpolation functions, the accuracy of the solution can be improved.

The set of governing differential equations derived in Section 2.5 is a set of 14th order coupled differential equations. It is very difficult to obtain an analytical solution to this set of equations for the general anisotropically actuated, single cell, composite beam. An approximate solution to this problem can be obtained with the FEM. The first objective of this chapter is to construct an adaptive beam finite element which can be used to simulate the static displacement response of actuated, single cell, composite beams. The second objective of this chapter is to validate the displacement solution obtained with the adaptive beam element (ABE) by comparison with previously published box beam experimental results and analytical results obtained from a commercial FEM package.

4.1 Adaptive High Order Beam Element

The basic building block for the FEM is the finite element. There are two major considerations for the adaptive beam element (ABE). The first consideration is the structural modeling of the single cell, composite beam and the second consideration is the electro-mechanical coupled fields problem which exist for the actuated beam. In this section an ABE is formulated which addresses both these considerations.

Two approaches exist for structural modeling of single cell beams [Boswell, 1990]. The first approach is to use combinations of shell elements to model the beam and the second approach is to use special beam elements. A high order single cell beam element reduces the overall cost of the analysis because fewer elements are needed to model the beam. Conventional beam finite elements do not represent the response of single cell beam accurately. Boswell [Boswell, 1990] describes an one-dimensional high order beam element, with three spanwise nodes, to model isotropic box beams. The nodal degrees of freedom are the node displacements, u, v, w , rotations, ϕ, β_y, β_z , and three distortion variables to describe warping (of which one is the twist rate, $\phi_{,x}$). This element construction is used as basis for the construction of an ABE based on the beam theory presented in Chapter 2.

The second consideration for the ABE is the coupled fields in the problem. Simple models approximate the straining effect of active materials with directional thermal expansion coefficients and an applied temperature to the structure. A more rigorous treatment of the electro-mechanical fields problem was presented by Allik [Allik and Hughes, 1970]. In this work, a general method for electro-elastic analysis is developed with the incorporation of the piezoelectric effect in a finite element formulation. The generalized displacement variables are the nodal displacements and electrical potentials. Generalized forcing consists of the mechanical forcing and the charge density. Hamilton's variational principle (principle of minimum potential energy) is extended to include the piezoelectric effect with the application of the principle of virtual displacements for both electrical and mechanical forcings. The coupled electro-mechanical system of equations is derived with the application of the variational principle to the system potential energy. Treatment of the adaptive nature for the ABE formulated in this study, is based on this extended principle of minimum potential energy as given by Allik [Allik and Hughes, 1970]. In the next section, the proposed adaptive, single cell, composite beam element is described and element formulation is given in the sections thereafter.

4.1.1 Adaptive Single Cell Composite Beam Element Description

The representative actuated single cell, composite beam element is based on the beam model presented in Chapter 2. A description of the beam geometry and construction was given in Section 2.3.2. There are no prior restriction on the cross-sectional shape of the element. The walls of the element are constructed from planar composite material plies which can be either passive or active and the wall construction can vary around the contour of the cross-section. It is assumed that the adaptive nature of the active plies can be modeled with linear piezoelectric constitutive relations with through-thickness applied electrical fields. Actuation of the active plies is completed by applying a differential voltage across the thickness of the ply. While this is not strictly true for general case of integrally actuated systems it will suffice for the system under consideration.

To describe the adaptive nature of the element, two adaptive nodes are assigned to the element. These nodes can be thought of as voltage nodes which represent the top and bottom of all the discrete ply areas. Associated with each of the nodes are voltage degrees of freedom. These voltage degrees of freedom represent the voltage at the top and the bottom of every ply and are used to determine the electrical field in every ply of the beam. For the k^{th} ply, the nodal voltage vector, \bar{v}^k is:

$$\bar{v}^k = \begin{bmatrix} v_{top}^k & v_{bottom}^k \end{bmatrix}^T \quad (4.1)$$

where v_{top}^k and v_{bottom}^k are the voltages at the top and the bottom of the k^{th} ply, in the i^{th} element. Therefore the complete voltage vector for the i^{th} element, with m discrete ply sections, is:

$$\bar{v} = \begin{bmatrix} v_{top}^1 & v_{bottom}^1 & v_{top}^2 & v_{bottom}^2 & \dots & v_{top}^m & v_{bottom}^m \end{bmatrix}^T \quad (4.2)$$

The deformation of the element is described by two displacement nodes one at each end of the element. Each of these nodes has seven degrees of displacement freedom which correspond to the global displacement variables defined in Section 2.3.2. These displacement degrees of freedom are the three cross-sectional translations, U, V, W , the three rotations, ϕ, β_y, β_z , and the rate of twist, $\phi_{,x}$ at the node. The complete adaptive, single cell, composite beam element is shown in Figure 4-1. Coordinate systems are the same as used for the model in Chapter 2.

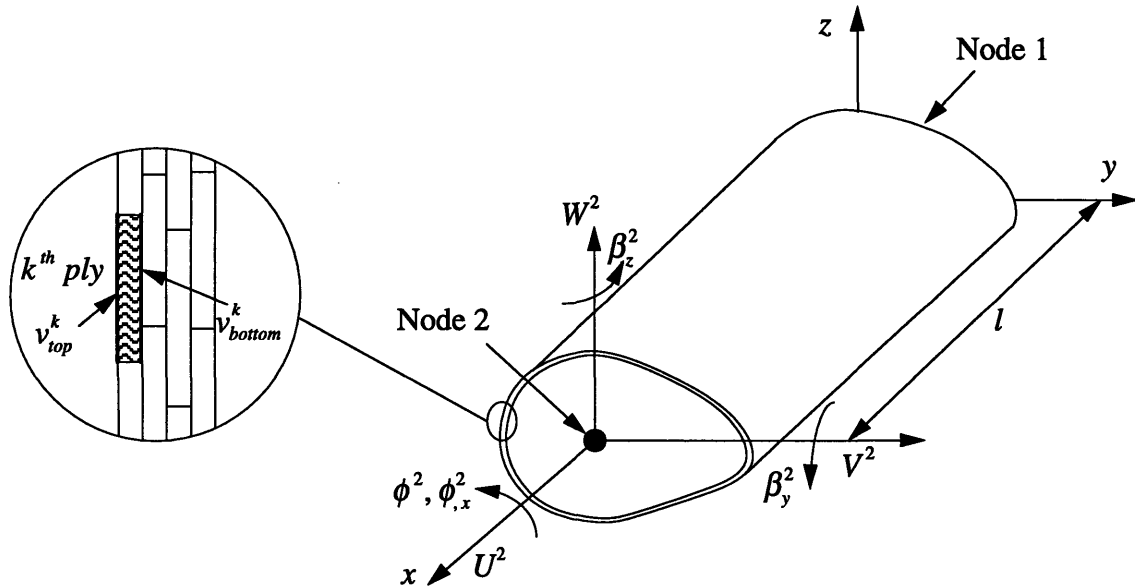


Figure 4-1. Adaptive Single Cell Composite Beam Element

The nodal displacement vector, \bar{u} , for element is:

$$\bar{u} = \begin{bmatrix} U^1 & V^1 & W^1 & \phi^1 & \beta_y^1 & \beta_z^1 & \phi_{,x}^1 & U^2 & V^2 & W^2 & \phi^2 & \beta_y^2 & \beta_z^2 & \phi_{,x}^2 \end{bmatrix}^T \quad (4.3)$$

where the superscripts 1 and 2 refer to the nodes at the each end of the element and the overbar denote displacement values at nodal points. These nodal degrees of freedom are used to describe the displacement and voltages anywhere in the wall of the element.

4.1.2 Displacement and Voltage Interpolation

In the FEM it is necessary to describe the field variable values inside the element in terms of the nodal values. Interpolation functions are used to approximate the solution to the unknown variables in the element. Thus the displacement, u , at any point in the beam can be given as:

$$u = N_u \bar{u} \quad (4.4)$$

where the unknown displacements in the beam are:

$$u = [U \ V \ W \ \phi \ \beta_y \ \beta_z \ \phi_{,x}]^T \quad (4.5)$$

Matrix N_u is the displacement interpolation matrix which contains the different displacement interpolation functions. With these displacement interpolation functions equation (4.4) can be expressed as:

$$u = \begin{bmatrix} N_1 & 0 & 0 & 0 & 0 & 0 & 0 & N_2 & 0 & 0 & 0 & 0 & 0 & 0 \\ 0 & N_1 & 0 & 0 & 0 & 0 & 0 & 0 & N_2 & 0 & 0 & 0 & 0 & 0 \\ 0 & 0 & N_1 & 0 & 0 & 0 & 0 & 0 & 0 & N_2 & 0 & 0 & 0 & 0 \\ 0 & 0 & 0 & N_3 & 0 & 0 & N_4 & 0 & 0 & 0 & N_5 & 0 & 0 & N_6 \\ 0 & 0 & 0 & 0 & N_1 & 0 & 0 & 0 & 0 & 0 & 0 & N_2 & 0 & 0 \\ 0 & 0 & 0 & 0 & 0 & N_1 & 0 & 0 & 0 & 0 & 0 & 0 & N_2 & 0 \\ 0 & 0 & 0 & N_7 & 0 & 0 & N_8 & 0 & 0 & 0 & N_9 & 0 & 0 & N_{10} \end{bmatrix} u_i \quad (4.6)$$

where N_1, N_2, \dots, N_{10} are the displacement interpolation functions. For the translations, U, V, W , and the rotations, β_y, β_z , linear interpolation functions are used. These interpolation functions are:

$$N_1 = 1 - \frac{x}{l} \quad (4.7)$$

and

$$N_2 = \frac{x}{l} \quad (4.8)$$

where x is the spanwise coordinate for the beam element, l is the element length, and N_i is the i^{th} interpolation function used in the analysis. The beam twist should be continuous to the first order and therefore hermitian interpolation functions are used [Cook et al., 1989]:

$$N_3 = 1 - \frac{3x^2}{l^2} + \frac{2x^3}{l^3} \quad (4.9)$$

$$N_4 = x - \frac{2x^2}{l} + \frac{x^3}{l^2} \quad (4.10)$$

$$N_5 = \frac{3x^2}{l^2} - \frac{2x^3}{l^3} \quad (4.11)$$

and

$$N_6 = \frac{-x^2}{l} + \frac{x^3}{l^2} \quad (4.12)$$

The interpolation functions for the twist rate are the derivatives of the twist interpolation functions:

$$N_7 = \frac{dN_3}{dx}, N_8 = \frac{dN_4}{dx}, N_9 = \frac{dN_5}{dx}, \text{ and } N_{10} = \frac{dN_6}{dx} \quad (4.13)$$

In a similar fashion the voltage at any point within the k^{th} ply can be expressed as:

$$v^k = N_v^k \bar{v}^k \quad (4.14)$$

where v^k is the voltage at a specific thickness location in the k^{th} ply and N_v^k is the voltage interpolation matrix. The resulting voltage interpolation is:

$$v^k = [N_{11} \quad N_{12}] \bar{v}^k \quad (4.15)$$

where N_{11} and N_{12} are the voltage interpolation functions. It is assumed that the voltage varies linearly with the thickness of the material ply. Thus the interpolation functions for the voltage interpolation are:

$$N_{11} = \frac{n}{t_k} \quad (4.16)$$

and

$$N_{12} = 1 - \frac{n}{t_k} \quad (4.17)$$

The variable n is the through-thickness variable and t_k is the k^{th} ply thickness. In the next sections the displacement and voltage interpolations are used to determine the strains and the fields in the beam.

4.1.3 Element Strains and Electrical Fields

The strain assumptions for the beam finite element are the same strain assumptions used for the analytical beam model of Chapter 2. The reader is referred to the first sections of Chapter 2 for coordinate system and strain assumption description. By differentiating the displacements, the strains in the element can be obtained according to the strain relations given in Section 2.3.4. Strains in the element are obtained from the displacements at the nodes through the following matrix operation:

$$\begin{aligned} \varepsilon &= L_u \mathbf{u} \\ &= L_u N_u \bar{\mathbf{u}} \end{aligned} \quad (4.18)$$

with L_u the matrix differential operator for this problem is:

$$L_u = \begin{bmatrix} \frac{d}{dx} & 0 & 0 & 0 & Z \frac{d}{dx} & -Y \frac{d}{dx} & \psi \frac{d^2}{dx^2} \\ 0 & Y_{,s} \frac{d}{dx} & Z_{,s} \frac{d}{dx} & -\frac{2A\alpha}{\Gamma} \frac{d}{dx} & Z_{,s} & -Y_{,s} & 0 \\ 0 & 0 & 0 & 0 & Y_{,s} \frac{d}{dx} & Z_{,s} \frac{d}{dx} & 0 \end{bmatrix} \quad (4.19)$$

Equation (4.18) can be rewritten as a single matrix multiplication which combines the effects of the differentiating as well as the displacement interpolation (which will be called the strain interpolation matrix, B_u):

$$\begin{aligned} \varepsilon &= L_u N_u \mathbf{u} \\ &= B_u \bar{\mathbf{u}} \end{aligned} \quad (4.20)$$

The strain, ε , is the reduced strain for the beam problem as defined in Section 2.3.4 and is not the engineering strain tensor. This strain expression will be used with the reduced plate constitutive relations to obtain internal mechanical strain energy of the beam.

The through-thickness applied field in any of the plies is the negative of the voltage gradient in the ply. This relationship can be expressed as:

$$\begin{aligned} E_n^k &= L_v v^k \\ &= L_v N_v \bar{v}^k \end{aligned} \quad (4.21)$$

with

$$L_v = -\frac{d}{dn} \quad (4.22)$$

Equation (4.21) can be written in terms of the field interpolation matrix, \mathbf{B}_v^k :

$$\begin{aligned} E_n^k &= L_v N_v^k \bar{v}^k \\ &= \mathbf{B}_v^k \bar{v}^k \end{aligned} \quad (4.23)$$

where E_n^k is the field in the k^{th} ply. For the ABE, the electrical field in all the plies can be expressed as:

$$\mathbf{E}_n = \begin{Bmatrix} E_n^1 \\ \cdot \\ \cdot \\ \cdot \\ \cdot \\ E_n^m \end{Bmatrix}_{m \times 1} = \begin{bmatrix} \mathbf{B}_v^1 & 0 & \cdot & \cdot & 0 & 0 \\ 0 & \cdot & \cdot & \cdot & 0 & 0 \\ 0 & 0 & \cdot & \cdot & 0 & 0 \\ 0 & 0 & \cdot & \cdot & 0 & 0 \\ 0 & 0 & \cdot & \cdot & \cdot & 0 \\ 0 & 0 & \cdot & \cdot & 0 & \mathbf{B}_v^m \end{bmatrix}_{m \times 2m} \begin{Bmatrix} v_i^1 \\ \cdot \\ \cdot \\ \cdot \\ \cdot \\ v_i^m \end{Bmatrix}_{2m \times 1} = \mathbf{B}_v \bar{v} \quad (4.24)$$

where m is the total number of individual ply segments in the beam. The electrical field will be used in the next section to determine the plate stress resultants when the beam is actuated.

4.1.5 Constitutive Relations

Constitutive relations are the mathematical model of the material from which a structure is made. In the beam element, CLPT is used to obtain the constitutive relations for the beam

wall (see Section 2.4.4). For the beam element, the electrical field may vary from ply to ply and the constitutive relations must reflect this possible variation. Expressed in matrix format, the equations looks as follows for a specific section of the beam wall:

$$\begin{Bmatrix} N_{xx} \\ N_{ss} \\ N_{xs} \\ M_{xx} \\ M_{ss} \\ M_{xs} \end{Bmatrix} = \begin{bmatrix} A & B \\ B & D \end{bmatrix} \begin{Bmatrix} \epsilon_{xx}^o \\ \epsilon_{ss}^o \\ \gamma_{xs}^o \\ \kappa_{xx} \\ \kappa_{ss} \\ \kappa_{xs} \end{Bmatrix} - \begin{bmatrix} \Sigma_{xx}^1 & \cdot & \cdot & \cdot & \cdot & \Sigma_{xx}^m \\ \Sigma_{ss}^1 & & & & & \Sigma_{ss}^m \\ \Sigma_{xs}^1 & & & & & \Sigma_{xs}^m \\ \Pi_{xx}^1 & & & & & \Pi_{xx}^m \\ \Pi_{ss}^1 & & & & & \Pi_{ss}^m \\ \Pi_{xs}^1 & \cdot & \cdot & \cdot & \cdot & \Pi_{xs}^m \end{bmatrix} \begin{Bmatrix} E_n^1 \\ \cdot \\ \cdot \\ \cdot \\ \cdot \\ E_n^m \end{Bmatrix} \quad (4.25)$$

where Σ_{ij}^k and Π_{ij}^k are the induced stress resultant coefficients for the k^{th} ply which are defined as follows (see Section 2.4.4):

$$\Sigma_{ij}^k = \int_{(t_k)_l}^{(t_k)_u} p_{nij} dn, \text{ and } \Pi_{ij}^k = \int_{(t_k)_l}^{(t_k)_u} p_{nij} n dn \quad (4.26)$$

with $(t_k)_u$ and $(t_k)_l$, the upper and lower thickness coordinates of the k^{th} ply. A static condensation can be performed on the equations to remove the influence of σ_{ss} which is assumed to be small (as in Section 2.4.4). The transverse and twisting curvatures are also ignored as was previously done. Under these assumptions, equation (4.25) reduces to:

$$\begin{Bmatrix} N_{xx} \\ N_{xs} \\ M_{xx} \end{Bmatrix} = \begin{bmatrix} L_{11} & L_{12} & L_{13} \\ L_{12} & L_{22} & L_{23} \\ L_{13} & L_{23} & L_{33} \end{bmatrix} \begin{Bmatrix} \epsilon_{xx}^o \\ \gamma_{xs}^o \\ \kappa_{xx} \end{Bmatrix} - \begin{bmatrix} \Sigma_{xx}^1 - \frac{A_{12}}{A_{22}} \Sigma_{ss}^1 & \cdot & \cdot & \Sigma_{xx}^m - \frac{A_{12}}{A_{22}} \Sigma_{ss}^m \\ \Sigma_{xs}^1 - \frac{A_{26}}{A_{22}} \Sigma_{ss}^1 & \cdot & \cdot & \Sigma_{xs}^m - \frac{A_{26}}{A_{22}} \Sigma_{ss}^m \\ \Pi_{xx}^1 - \frac{B_{12}}{A_{22}} \Sigma_{ss}^1 & \cdot & \cdot & \Pi_{xx}^m - \frac{B_{12}}{A_{22}} \Sigma_{ss}^m \end{bmatrix} \begin{Bmatrix} E_n^1 \\ \cdot \\ \cdot \\ E_n^m \end{Bmatrix} \quad (4.27)$$

For convenience, the above matrices are redefined as:

$$\mathbf{L} = \begin{bmatrix} L_{11} & L_{12} & L_{13} \\ L_{12} & L_{22} & L_{23} \\ L_{13} & L_{23} & L_{33} \end{bmatrix} \quad (4.28)$$

and

$$P = \begin{bmatrix} P_{11} & \cdot & \cdot & P_{1m} \\ P_{21} & \cdot & \cdot & P_{2m} \\ P_{31} & \cdot & \cdot & P_{3m} \end{bmatrix} = \begin{bmatrix} \Sigma_{xx}^1 - \frac{A_{12}}{A_{22}} \Sigma_{ss}^1 & \cdot & \cdot & \Sigma_{xx}^m - \frac{A_{12}}{A_{22}} \Sigma_{ss}^m \\ \Sigma_{xs}^1 - \frac{A_{26}}{A_{22}} \Sigma_{ss}^1 & \cdot & \cdot & \Sigma_{xs}^m - \frac{A_{26}}{A_{22}} \Sigma_{ss}^m \\ \Pi_{xx}^1 - \frac{B_{12}}{A_{22}} \Sigma_{ss}^1 & \cdot & \cdot & \Pi_{xx}^m - \frac{B_{12}}{A_{22}} \Sigma_{ss}^m \end{bmatrix} \quad (4.29)$$

The constitutive relations are used to write the potential energy of the beam in terms of the reduced wall properties and the nodal degrees of freedom of the ABE. In the next section, the equilibrium equations for the system are derived by applying the principle of minimum system potential energy.

4.1.6 Governing Equations

The complete finite element formulation for piezoelectric media was presented by Allik [Allik and Hughes, 1970]. In this work, the governing equations were obtained from the principle of minimum system potential energy. This formulation is used as a basis to obtain the equilibrium equations for the ABE.

In general terms, the principle of minimum potential energy can be stated as (equation (2.57)):

$$\delta U - \delta W_{ext} = 0 \quad (4.30)$$

where U is the internal energy associated with the system and W_{ext} is the external energy. For the actuated single cell composite beam the variation of the internal energy is :

$$\begin{aligned} \delta U &= \iiint_V \{ \delta \epsilon^T \sigma - \delta E^T D \} dndsdx \\ &= \iiint_V \delta \epsilon^T \sigma dndsdx \end{aligned} \quad (4.31)$$

In the actuated beam case it is assumed that the electrical fields are prescribed and thus the variation of the second term in equation (4.31) are equal to zero.

The variational internal energy can be rewritten in terms of the adaptive beam geometry and associated deformation variables as:

$$\begin{aligned}
\delta U &= \int_0^l \oint_{\Gamma} \delta \boldsymbol{\varepsilon}^T \{ \mathbf{L} \boldsymbol{\varepsilon} - \mathbf{P} \mathbf{E}_n \} ds dx \\
&= \int_0^l \oint_{\Gamma} \delta (\mathbf{B}_u \bar{\mathbf{u}})^T \{ \mathbf{L} \mathbf{B}_u \bar{\mathbf{u}} - \mathbf{P} \mathbf{B}_v \bar{\mathbf{v}} \} ds dx \\
&= \int_0^l \oint_{\Gamma} \{ \delta \bar{\mathbf{u}}^T [\mathbf{B}_u^T \mathbf{L} \mathbf{B}_u \bar{\mathbf{u}}] - \delta \bar{\mathbf{u}}^T [\mathbf{B}_u^T \mathbf{P} \mathbf{B}_v \bar{\mathbf{v}}] \} ds dx
\end{aligned} \tag{4.32}$$

For the external work we only consider the spanwise distributed forcing and concentrated end forces described in Chapter 2. For a more rigorous treatment of general external forcing the reader is referred to Allik [Allik and Hughes, 1970] as well as Hagood [Hagood et al., 1990]. Therefore, the variation of the external work is:

$$\begin{aligned}
\delta W_{ext} &= \int_0^l \delta \mathbf{u}^T \mathbf{q} dx + \delta \mathbf{u}^T \bar{\mathbf{F}} \\
&= \int_0^l \delta \bar{\mathbf{u}}^T \mathbf{N}_u^T \mathbf{q} dx + \delta \bar{\mathbf{u}}^T [\mathbf{N}_u^T]_{\Theta \bar{\mathbf{F}}} \bar{\mathbf{F}}
\end{aligned} \tag{4.33}$$

In equation (4.33) the displacement interpolation matrix is evaluated at the point where the concentrated forces act. Equations (4.32) and (4.33) can be substituted into the variational energy principle. By allowing the displacement variations to be arbitrary, the following set of equilibrium equations are obtained:

$$\mathbf{K} \bar{\mathbf{u}} - \Theta \bar{\mathbf{v}} = \mathbf{F} \tag{4.34}$$

with

$$\mathbf{K} = \int_0^l \oint_{\Gamma} \mathbf{B}_u^T \mathbf{L} \mathbf{B}_u ds dx \tag{4.35}$$

$$\Theta = \int_0^l \oint_{\Gamma} \mathbf{B}_u^T \mathbf{P} \mathbf{B}_v ds dx \tag{4.36}$$

and

$$\mathbf{F} = \int_0^l \mathbf{N}_u^T \mathbf{q} dx + [\mathbf{N}_u^T]_{\Theta \bar{\mathbf{F}}} \bar{\mathbf{F}} \tag{4.37}$$

Equation (4.34) is the set of governing equations for the adaptive single cell composite beam element. K is the beam element stiffness matrix, Θ is the electro-mechanical coupling matrix, and F is the element forcing matrix. These equations are solved subject to the boundary conditions which apply to a specific beam element. The following section of this chapter describes the displacement simulation for a general actuated beam modeled with the formulated ABE. The final sections of this chapter are used to verify the accuracy of the element and the validity of the analytical model (of Chapter 2), from which the ABE was formulated.

4.1.7 Actuated Beam Displacement Simulation

The first step in solving for the static response of a general actuated, single cell, composite beam is to discretize the beam into a number of ABE's. For each of the elements in the beam, the element equilibrium equation (equation (4.34)) needs to be determined. Force boundary conditions are applied at the element level but geometric boundary conditions are applied at the system level. The next step in the solution procedure is the assembly of the global beam equilibrium equations. Equations are assembled on a element by element basis according to standard finite element assembly procedures [Cook et al., 1989], [Zienkiewicz, 1971].

Once the set of global equations has been constructed, the geometric boundary conditions are applied to the system of equations. The final step in the displacement simulation is the solution of the reduced set of beam equilibrium equations to obtain the nodal displacements. If required, the continuous displacement solution can be obtained from the displacement interpolation relations.

The simulation procedure, outlined above, was implemented for an actuated, single cell, composite beam which was cantilevered at one end, with concentrated forces at the free end. Numerical simulation was done with MATLAB¹ Code. The Code is confined to Appendix A. An outline of the displacement simulation is given in Figure 4-2. The function "Beam.m" defines the adaptive beam in terms of the different ABE's which is used to construct the complete beam model. The relevant element equations are calculated before hand by the function "Elem.m" and stored in an element library for later use by "Beam.m".

¹MATLAB 4.2, The MathWorks, Inc., Natick, MA.

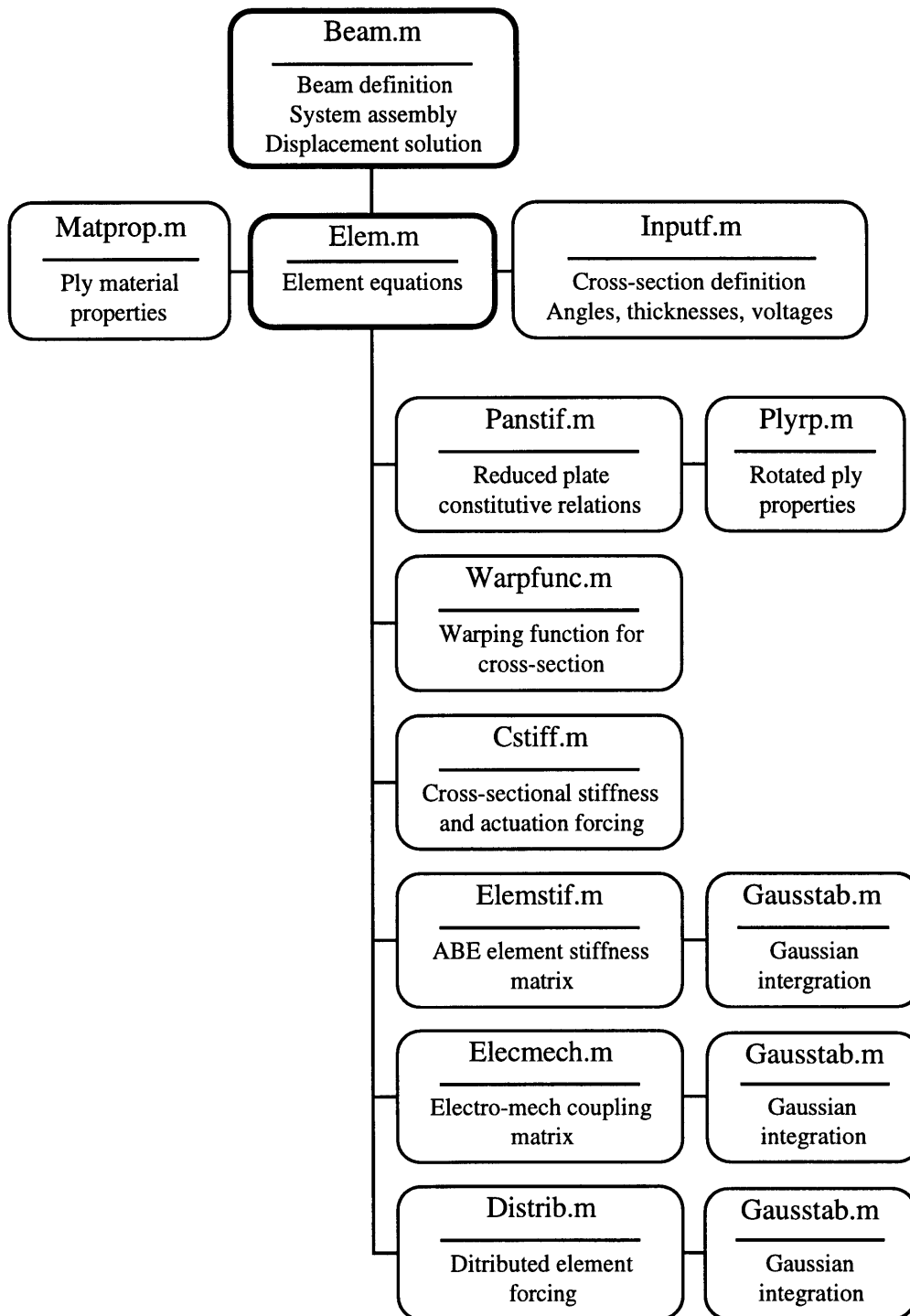


Figure 4-2. Displacement Simulation Code Outline

The input to the element function is “Matprop.m” which defines the ply material properties and “Inputf.m” which defines the adaptive beam element in terms of beam cross-sectional shape, construction, and applied actuation voltages. The minor functions shown in Figure 4-2 are used by “Elem.m” to determine element equations. It should be noted that “Cstiff.m” and “Elemstif.m” both calculate the adaptive beam element stiffness matrices but according to different formulations. “Cstiff.m” produces the beam model cross-sectional stiffness matrix as defined in equation (2.85) where as “Elemstif.m” produces the finite element stiffness matrix as defined in equation (4.35). The beam model cross-sectional stiffness matrix is used to produce an output of beam stiffnesses in terms of standard engineering terms (EI , GJ). These values are used for comparing beam model stiffnesses with published helicopter blade stiffnesses.

In the next section of this chapter, the simulation code is used to simulate the static response of passive and adaptive, single cell, composite beams. The finite element code and modeling are verified by comparing displacement predictions with previously published experimental results and results obtained with a commercial FEM package.

4.2 Non-Actuated Beam Model Verification

The purpose of the actuated, single cell, composite beam model and the associated ABE is to be used as a tool in the design of anisotropic actuated, single cell, composite beams for helicopter blade control. Before the model can be used for design, it needs to be verified for accuracy in modeling actuated, single cell, composite beams. The verification process should ideally be completed by comparing model simulation results with experimental results. In this section previously published, experimental, passive box beam displacement results are used to validate the non-actuated capabilities of the model and code.

4.2.1 Previous Experimental Work

Smith [Smith and Chopra, 1990] formulated and evaluated an analytical model for composite, box beams. The model evaluation was done by testing of a large number of passive, composite, box beams with different wall constructions. These experimental results were used to verify the model and code developed in this study. The experimental, passive, box beam geometry is shown in Figure 4-3.

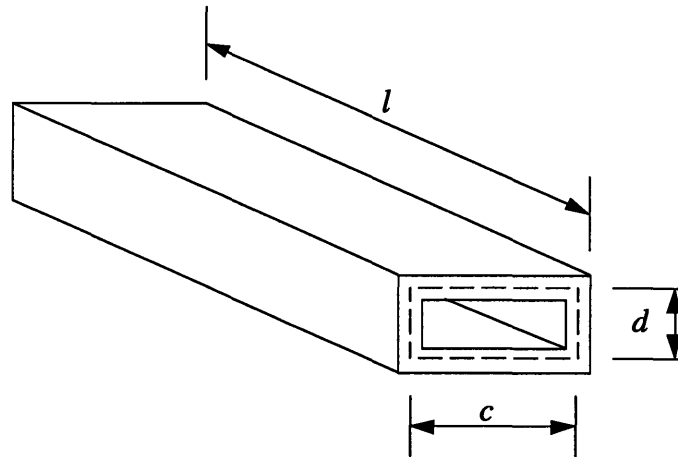


Figure 4-3. Experimental Passive Box Beam Geometry [Smith and Chopra, 1990]

An autoclave process was used to manufacture the composite, box beams from unidirectional, graphite/epoxy, pre-preg plies. The material used for the beams was the Hercules AS4/3501-6 material system with cured plane stress properties as given in Table 4-1 (values used by Smith [Smith and Chopra, 1990]).

TABLE 4-1. AS4/3506-1 MATERIAL PROPERTIES

Ply Thickness, t	0.127 mm
Normal Modulus, E_1	142 GPa
Transverse Modulus, E_2	9.8 GPa
Poisson's Ratio, ν	0.42
Shear Modulus, G	6 GPa

Three classes of box beams were designed, manufactured, and tested by Smith [Smith and Chopra, 1990] for the model validation. These classes were:

- Cross-ply layup beams,
- Symmetric layup beams, and
- Anti-symmetric layup beams.

In this case, layup refers to the laminate layups used to construct the beam walls. For this study the experimental results published by Smith are used to validate the model and code developed earlier in this study. More detailed descriptions of the different classes of beams will be given in the next sections together with the presentation of experimental (Smith's results) and model results (displacement predictions using the MATLAB code developed for this study).

4.2.2 Cross-Ply Beam Results

Cross-ply layup beams were constructed from alternating composite plies at 0° and 90° . This class of beams does not display any structural couplings. Cross-ply beam dimensions and layups are given in Table 4-2. The finite element model of this beam had 120 elements to ensure sufficient convergence of the simulation results.

TABLE 4-2. CROSS-PLY BOX BEAM DIMENSIONS AND LAYUPS

Length l	Chord c	Height d	Layup: Top&Bottom	Layup: Sides
762 mm (30 in)	51.6 mm (2.03 in)	25.3 mm (0.995in)	$[0/90]_3$	$[0/90]_3$

Cross-ply beam bending slope results are shown in Figure 4-4. For this test, a unit shear force was applied at the tip of the box beam in the z -direction. Figure 4-5 shows the twist for a cross-ply beam twist for a unit torque applied at the tip of the beam. For this study the correlation between the model and experimental results are determined by the maximum error between the model and experimental results, expressed as a percentage of the beam tip deflection or twist, as predicted by the beam model. Another measure of correlation is the level to which the model correctly predicts the spanwise distribution of twist and displacement.

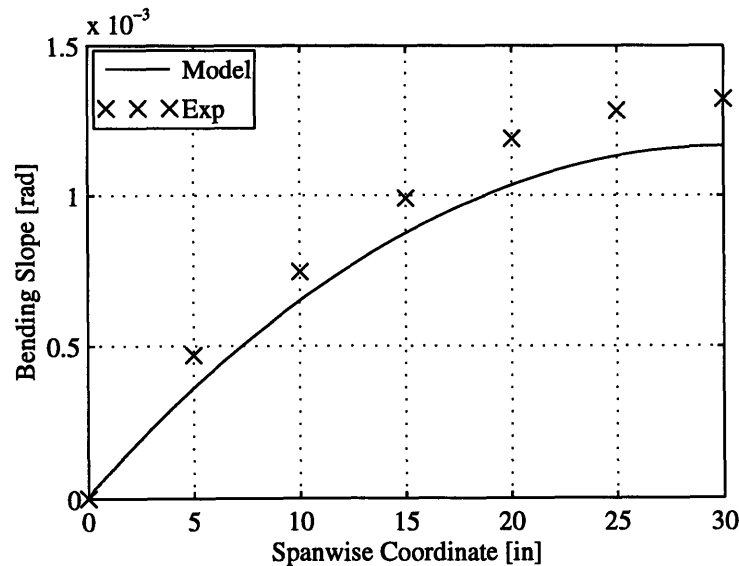


Figure 4-4. Cross-Ply Beam Bending Slope, $W_{,x}$, for a Unit Tip Shear Force, \bar{Q}_z

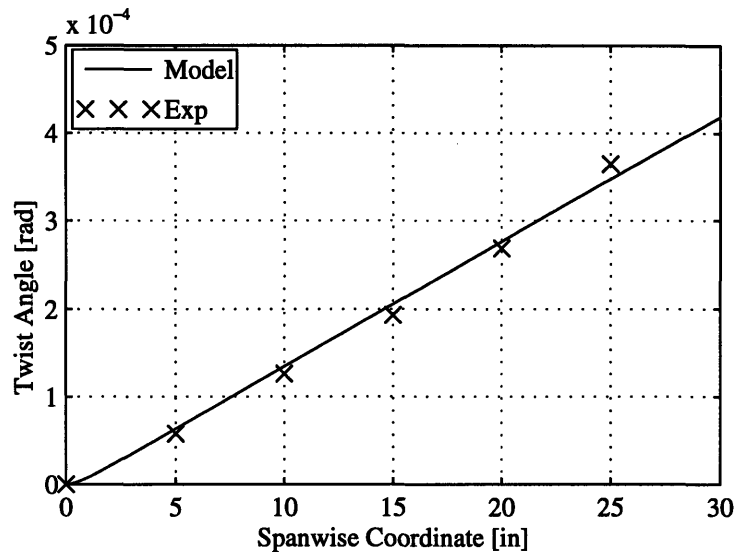


Figure 4-5. Cross-Ply Beam Twist , ϕ , for a Unit Tip Torque, \bar{M}_x

There is a slight discrepancy between model bending slope predictions and the experimental results but the spanwise distribution of the bending slope is accurately modeled. The maximum error between the model and experimental bending slope results is 13% (% of model tip bending slope). There is no explanation for the discrepancy, but the same trends were observed for the analytical model predictions by Smith and Chopra [Smith, 1990]. There is very close agreement between the model and the experimental twist results. The maximum error for the twist results is 5% (percentage of the model tip twist).

4.2.3 Symmetric Beam

Symmetric beams were constructed with the top and bottom panels of the beam being mirror images relative to the chord of the beam. These types of beams exhibit bending-torsion coupling as well as extension-shear coupling. Bending-torsion coupling is the primary coupling effect and was examined in the experimental testing. A schematic of the symmetric beam is shown in Figure 4-6. Symmetric beam dimensions and layups are given in Table 4-3. Three different beams were tested. Each of the beams had a different level of bending-torsion coupling resulting from varying ply orientation angles. The finite element model had 120 ABE's to ensure sufficient convergence of the simulation results.

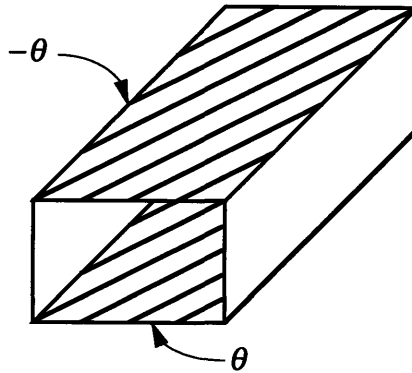


Figure 4-6. Symmetric Box Beam Schematic

TABLE 4-3. SYMMETRIC BOX BEAM DIMENSIONS AND LAYUPS

Length l	Chord c	Height d	Layup: Top&Bottom	Layup: Sides
762 mm (30 in)	23.4 mm (0.923 in)	12.8 mm (0.507 in)	Top: $[-15]_6$ Bottom: $[15]_6$	$[15 / -15]_3$
762 mm (30 in)	23.4 mm (0.923 in)	12.8 mm (0.507 in)	Top: $[-30]_6$ Bottom: $[30]_6$	$[30 / -30]_3$
762 mm (30 in)	23.4 mm (0.923 in)	12.8 mm (0.507 in)	Top: $[-45]_6$ Bottom: $[45]_6$	$[45 / -45]_3$

For each of the symmetric beams, a unit shear force, \bar{Q}_z , was applied at the tip of the beam. Due to the bending-torsion coupling both the bending slope, $W_{,x}$, and twist angle, ϕ , were measured during the testing of these symmetric beams. The displacement results ($W_{,x}$ and ϕ) for the each of the beams are shown in Figure 4-7 - 4-9.

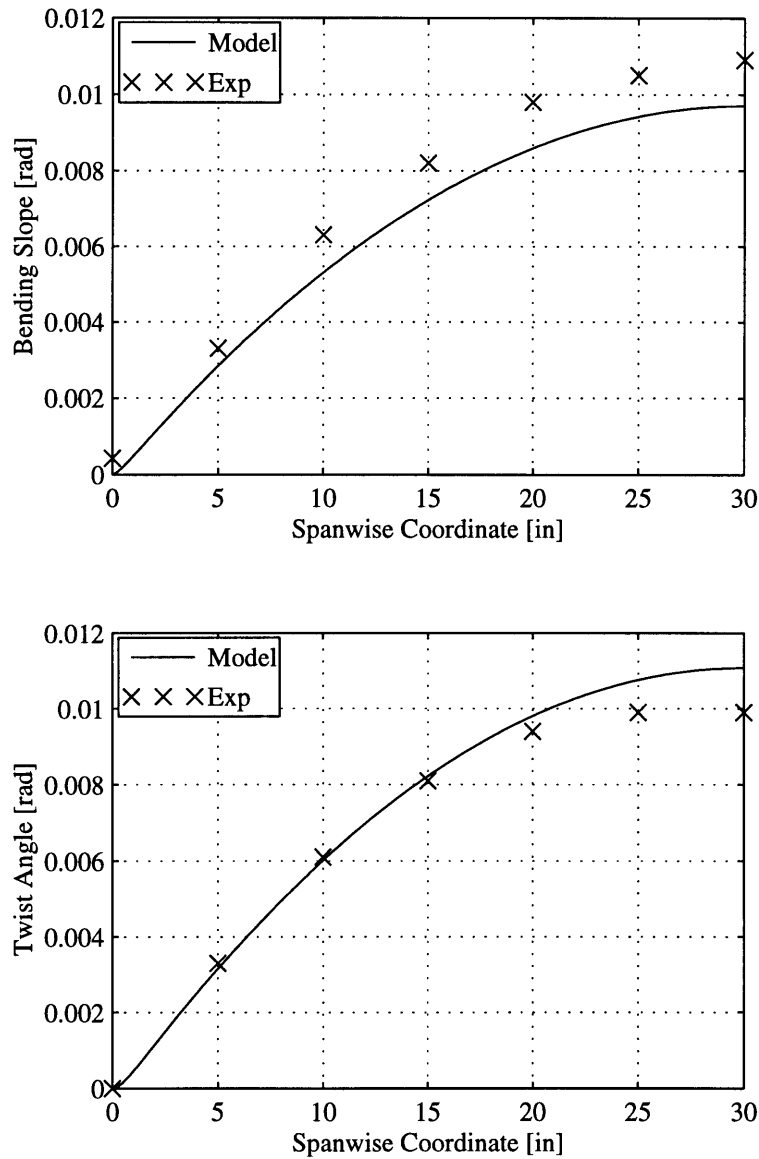


Figure 4-7. Symmetric Layup Beam - Bending Slope and Twist for a Unit Tip Shear Load, \bar{Q}_z (Top $[-15]_6$ & Bottom $[15]_6$)

The results show definite bending-torsion coupling for the symmetric beam. Model bending slope predictions are in slight error (12% maximum error) but the correct spanwise distribution was predicted. There is close agreement between the model and experimental results for the twist angle up to a spanwise beam coordinate of 20 inches. The maximum error between model and experimental results is 10%.

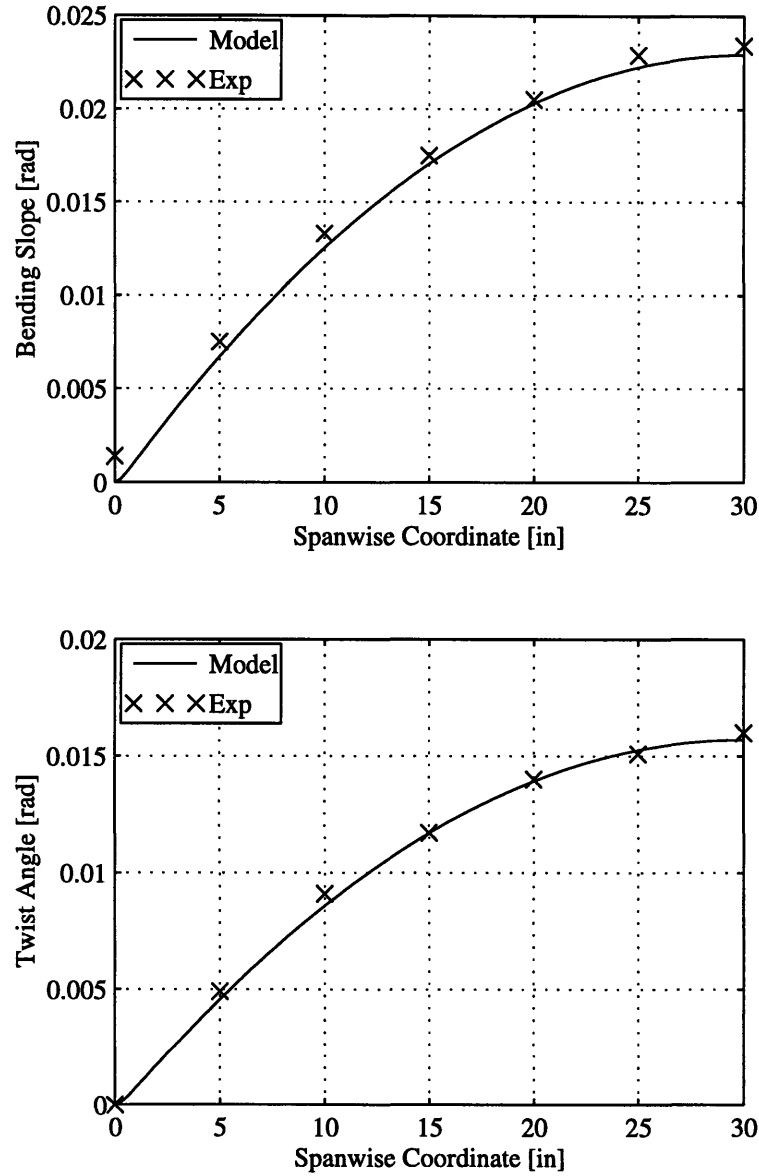


Figure 4-8. Symmetric Layup Beam - Bending Slope and Twist for a Unit Tip Shear Load, \bar{Q}_z (Top $[-30]_6$ & Bottom $[30]_6$)

Model predictions and experimental results closely agree for the shear loading of the $[30]_6$ -symmetric beam. The maximum error for the bending slope predictions is 6% and only 3% for the twist results. As stated before the level of twist increases as level of bending-torsion coupling increases with the orientation angle increasing from 15 to 30 degrees.

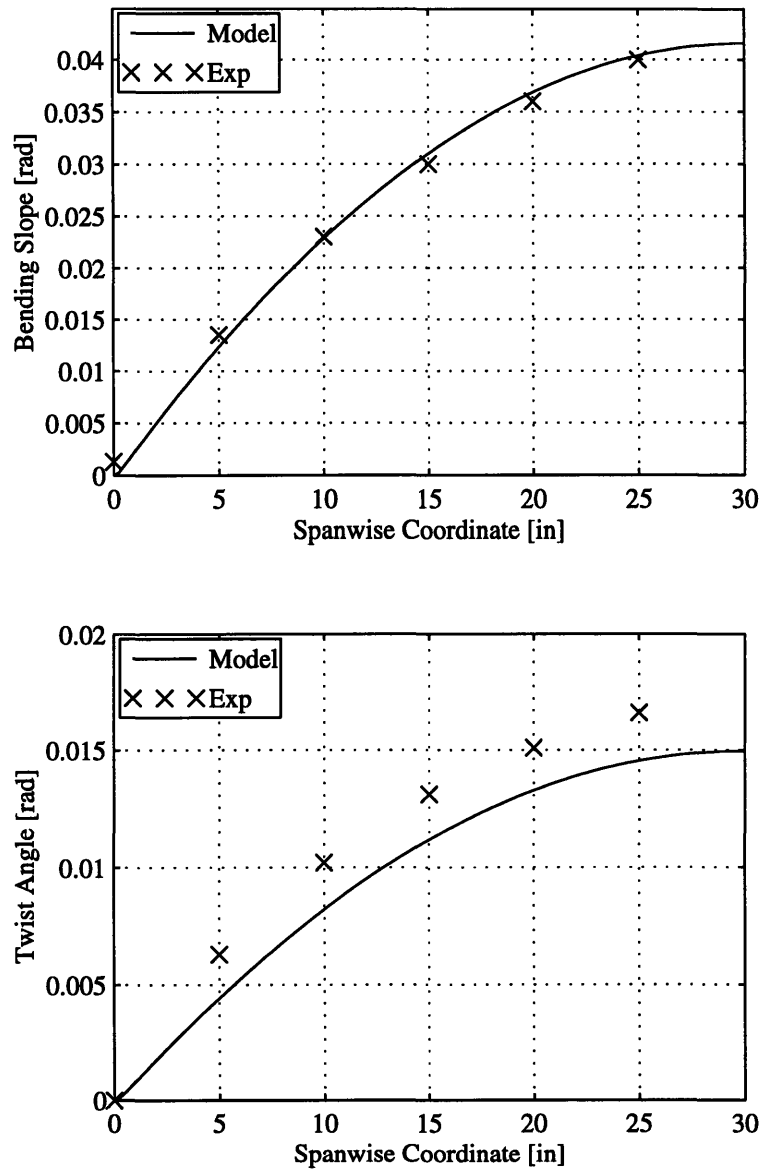


Figure 4-9. Symmetric Layup Beam - Bending Slope and Twist for a Unit Tip Shear Load, \bar{Q}_z (Top $[-45]_6$ & Bottom $[45]_6$)

Model bending slope predictions and experimental results agree for the shear loading of the $[45]_6$ -symmetric beam. The bending slope prediction maximum error is 3%. There is a slight error in the twist predictions (14% maximum error) but the spanwise distribution of model predicted twist is correct. This correlation is satisfactory for model validation.

4.2.4 Anti-Symmetric Beam Results

Anti-symmetric beams were constructed with the top and bottom panels of the beam being of opposite orientation relative to the chord of the beam. These types of beams exhibit extension-torsion coupling as well as bending-shear coupling. Extension-torsion coupling is the primary coupling effect but this coupling effect was either not examined by Smith [Smith and Chopra, 1990] or the results were not published. A schematic of the anti-symmetric beam is shown in Figure 4-10. Anti-symmetric beam dimensions and layups are given in Table 7.4. Three different anti-symmetric beams were tested (see Table 7-4) by applying a unit tip shear load in the z-direction. The finite element model (from Section 4.1) had 120 ABE's to ensure sufficient convergence of the simulation results.

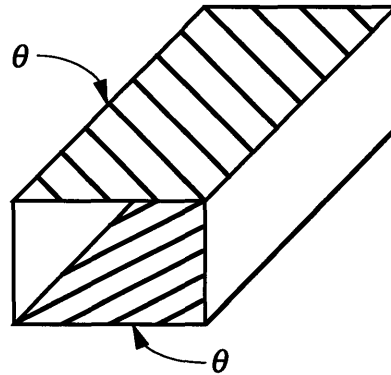


Figure 4-10. Anti-symmetric Box Beam Schematic

TABLE 4-4. ANTI-SYMMETRIC BOX BEAM DIMENSIONS AND LAYUPS

Length l	Chord c	Height d	Layup: Top&Bottom	Layup: Sides
762 mm (30 in)	23.4 mm (0.923 in)	12.8 mm (0.507 in)	Top: $[15]_6$ Bottom: $[15]_6$	$[15]_6$
762 mm (30 in)	23.4 mm (0.923 in)	12.8 mm (0.507 in)	Top: $[0/30]_3$ Bottom: $[0/30]_6$	$[0/30]_3$
762 mm (30 in)	23.4 mm (0.923 in)	12.8 mm (0.507 in)	Top: $[0/45]_3$ Bottom: $[0/45]_3$	$[0/45]_3$

For each of the anti-symmetric beams, a unit shear force, \bar{Q}_z , was applied at the tip of the beam. The bending slope results, $W_{,x}$, for the different anti-symmetric beams are shown in Figure 4-11 - 4-13.

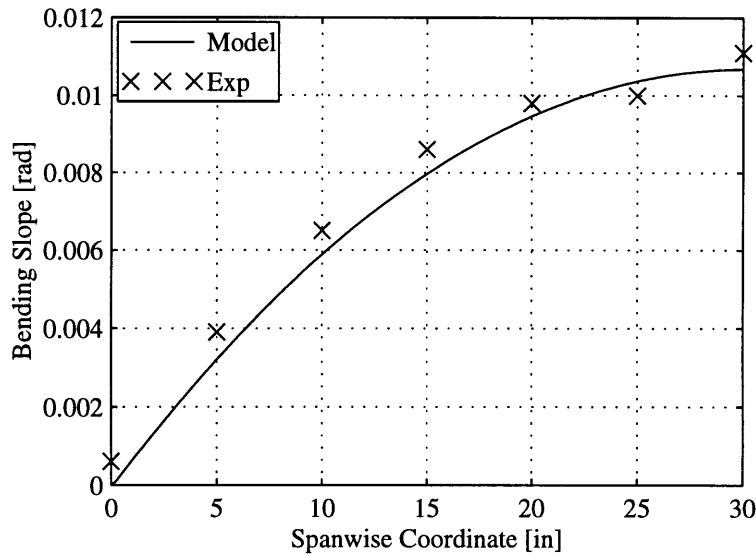


Figure 4-11. Anti-Symmetric Layup Beam - Bending Slope for a Unit Tip Shear Load, \bar{Q}_z (Top [15]₆ & Bottom [15]₆)

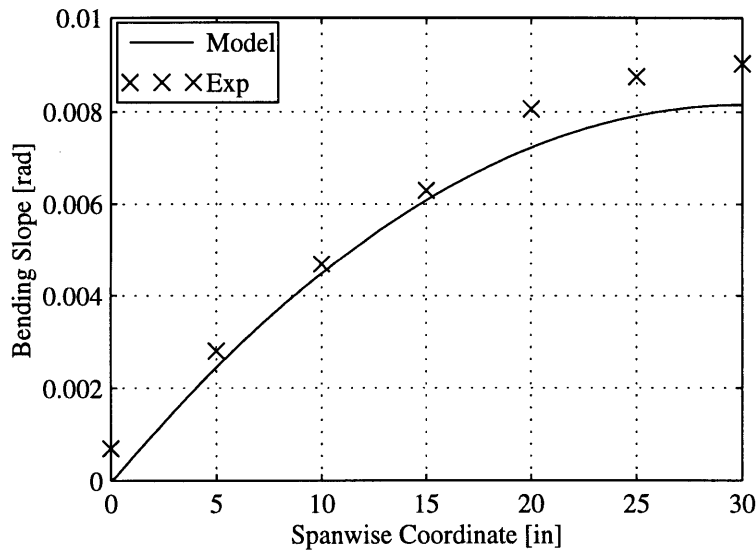


Figure 4-12. Anti-Symmetric Layup Beam - Bending Slope for a Unit Tip Shear Load, \bar{Q}_z (Top [0/30]₃ & Bottom [0/30]₃)

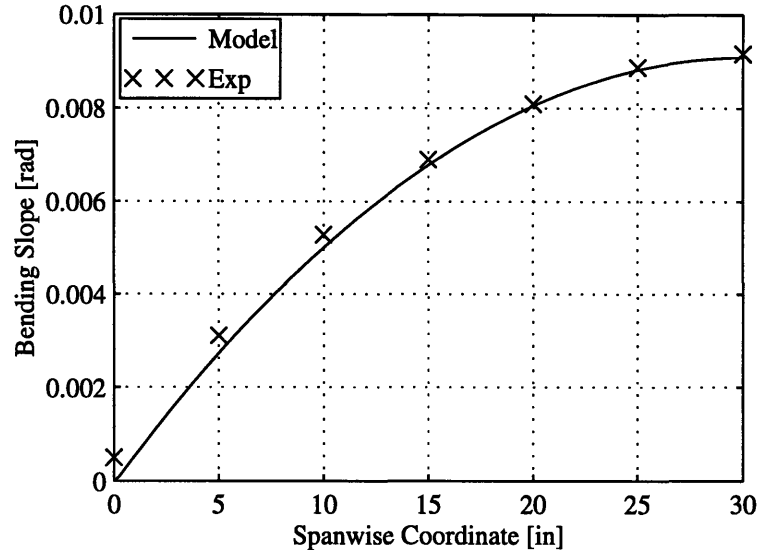


Figure 4-13. Anti-Symmetric Layup Beam - Bending Slope for a Unit Tip Shear Load, \bar{Q}_z (Top $[0/45]_3$ & Bottom $[0/45]_3$)

The model accurately predicts the bending slope for all three cases of the shear loading of the anti-symmetric beams. For the first anti-symmetric beam test (top: $[15]_6$ & bottom: $[15]_6$) the maximum bending slope prediction error is 6.5%, for the second beam (top: $[0/30]_3$ & bottom: $[0/30]_3$) the maximum bending slope error prediction is 10.7%, and for the third anti-symmetric beam (top: $[0/45]_3$ & bottom: $[0/45]_3$) the maximum error is 5%.

4.2.5 Results Discussion

For all the different box beam cases examined in this section, the correlation between the model results and the experimental results was satisfactory. Even in the cases where the model predictions were wrong, result trends were predicted correctly and the errors were never in excess of 14% (based on model predictions at beam tip). The worst correlation is for beam twist in the $[45]_6$ symmetric beam, loaded by a unit tip shear force. The displacement predictions obtained with the ABE (from this study) compare favorably with the analytical results presented by Smith [Smith and Chopra, 1990]. In all cases the ABE predictions were more accurate than the predictions by Smith [Smith and Chopra, 1990]. These correlations validate the model and associated ABE for the prediction of passive, single cell, composite beam displacements. In the next section of Chapter 4 the goal is to validate the adaptive prediction capabilities of the model and ABE.

4.3 Actuated Beam Model Verification

In Section 2.3 the model and adaptive code displacement simulation capabilities were validated for the response of passive, single cell, composite beams. This validation was done by comparing code predictions with experimental results. The next step in the model verification process is to verify the model displacement simulation capabilities for actuated, single cell, composite beams. There is no previously published results available. The cost and time to obtain experimental results for actuated, composite, beams is very high. An alternative verification method for model and ABE code is a finite element analysis (FEA) of the actuated beam system with a commercial FEA package.

The goal of this section is to verify the displacement simulation capabilities of the developed model and code. To keep the analysis realistic, an existing Chinook CH-47D helicopter blade is analyzed for blade twist when the blade is twist actuated with planar, anisotropic actuators.

4.3.1 Chinook CH-47D Blade

The Chinook CH-47D helicopter is a 50000 lb transport helicopter manufactured by Boeing-Vertol. This helicopter is being considered for helicopter blade control with in-plane, distributed, anisotropic actuators. The helicopter has two in-line, tandem rotors with three blades per rotor. Rotor radius is 30 feet and the chord of the blades is 32 inches. A structural blade description was obtained from Sandford [Sandford, 1978].

The CH-47D blade consists of the closed fiberglass "D"-spar with the aft fairing made from honeycomb with fiberglass skins. The spar is the main load carrying member and is considered as a possible platform to attain helicopter blade control. By incorporating anisotropic actuation plies in the main spar, the blade can be actuated in twist to accomplish aeroservoelastic blade control during forward flight. Thus the spar needs to be analyzed for the incorporation of anisotropic actuation plies.

The spar is manufactured from unidirectional SP250 E-Glass (glass fibers with an epoxy matrix) packs (multiple plies) at 0° enclosed between weaved SP250 E-Glass wraps biased at 45°. The heel of the 'D'-spar is composed from alternate layers of 90° unidirectional plies and weaved E-Glass elements biased at 45°. To protect the leading edge of the blade during flight, a titanium nose cap is fitted to the blade from 20% blade span to the blade tip. In order to twist the blade, anisotropic actuation plies must be included at $\pm 45^\circ$ in the spar

to obtain twist for the blade (see Chapter 3). For this study, it is assumed that it is possible to change the weaved cross-ply E-Glass wraps in the spar into $\pm 45^\circ$ anisotropic actuation plies without severe blade strength degradation. The number of $\pm 45^\circ$ actuation plies in the blade should be such that blade structural properties remain virtually unchanged. For this study, the number of actuation plies is based on the requirement that the blade torsional stiffness should remain constant. The first step to model the adaptive blade is to construct a representative model of the passive spar. Thereafter, the 45° cross-ply E-Glass wraps in the model can be changed into actuation plies and finally the system can be analyzed for twist response with the adaptive beam finite element.

4.3.2 Approximate Blade Description

The spar of the CH-47D blade is approximated as a rectangular SP250 E-Glass composite beam with a titanium skin. Laminate construction remains constant around the contour. A schematic of the spar approximation is shown in Figure 4-14. The dimensions of the approximate spar are determined from the torsional stiffness of the actual blade. It is assumed for the blade approximation that the spar wall laminate has the following layup:

$$\text{Spar Laminate: } [Ti_4 / \pm 45_4 / 0_{10} / \pm 45_2]. \quad (4.37)$$

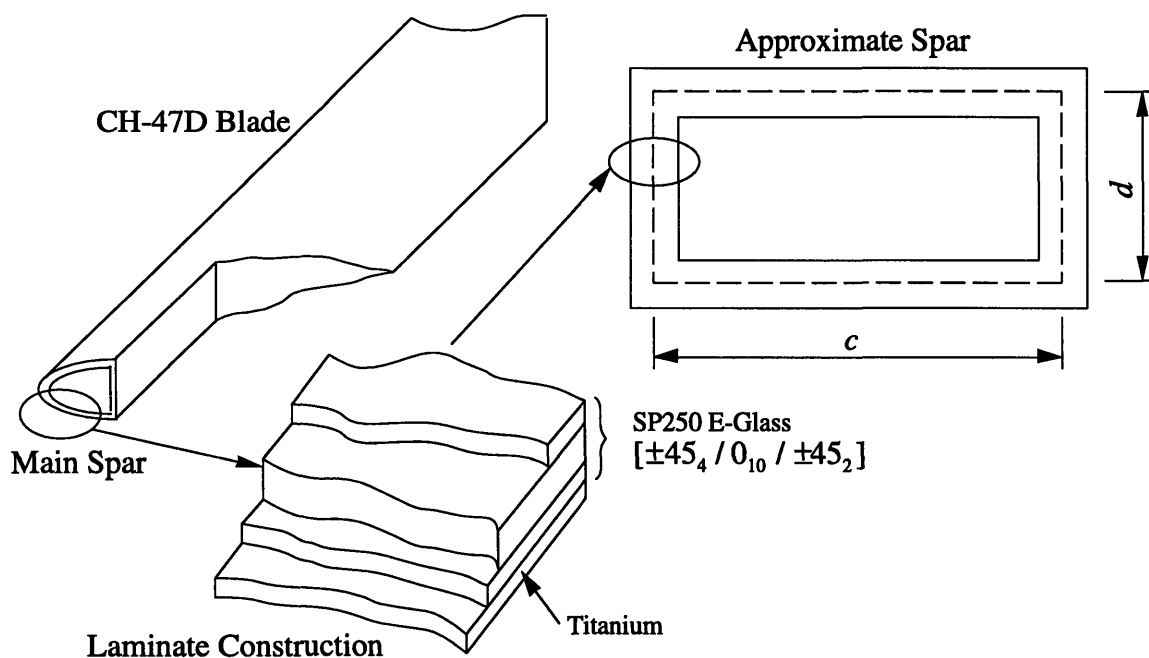


Figure 4-14. CH-47D Blade Spar Approximation

Ply thicknesses are taken from [Sandford, 1978] at a nominal value of 0.254 mm (10 mils) per ply for all of the different material plies. The relevant mechanical properties of the material plies are given in Table 4-5 [Sandford, 1978].

TABLE 4-5. CH-47D SPAR MATERIAL PLY PROPERTIES

Property	Titanium	SP250-Glass 0°
E_1	103.4 GPa (15 Msi)	43.4 GPa (6.3 Msi)
E_2	103.4 GPa (15 Msi)	12 GPa (1.74 Msi)
ν	0.3	0.3
G	42.8 GPa (6.2 Msi)	3.6 GPa (0.52 Msi)
t	0.254 mm (10 mils)	0.254 mm (10 mils)

The approximate dimensions are prescribed by the requirement that the approximate spar should maintain the torsional stiffness of the actual blade. For the original spar, the torsional stiffness, K_{44} , is $246.8 \times 10^3 \text{ Nm}^2$ ($86 \times 10^6 \text{ lbin}^2$) at 62.5% blade span. If it is assumed that the membrane response of the laminate dominates the response of the beam (see Chapter 3), the torsional stiffness of the approximate beam is (equation (3.58)):

$$K_{44} = \frac{4c^2 d^2 (t_{\text{eff}} G_{\text{eff}})}{2(c+d)} = \frac{4c^2 d^2 (t_{Ti} G_{Ti} + t_0 G_0 + t_{45} G_{45})}{2(c+d)}, \quad (4.38)$$

where subscripts Ti , 0, and 45 refer to the titanium, the 0° SP250 E-Glass plies, and the E-Glass plies at $\pm 45^\circ$. The value for the beam height, d , is taken from the actual blade and the chord is selected accordingly. The final values for the blade chord and height are:

$$c = 0.283 \text{ m (11.14 in)}, \text{ and } d = 0.075 \text{ m (2.94 in)}, \quad (4.39)$$

This combination of beam dimensions results in a good approximation of the actual CH-47D blade torsional stiffness as well as the blade flapwise bending stiffness at 62.5% blade span. The comparison of model and actual blade flapwise bending and torsional stiffnesses is summarized in Table 4-6.

TABLE 4-6. CH-47D MODEL AND ACTUAL BLADE STIFFNESSES

Stiffness	Actual Blade [Sandford, 1978]	Model Blade	Error
Flapwise Bending (EI_{flap})	229.6 kNm ² (80x10 ⁶ lbin ²)	227.6 kNm ²	0.87 %
Torsional (GJ)	246.8 kNm ² (86x10 ⁶ lbin ²)	225.3 kNm ²	8.7 %

In the next section the approximate blade model is used as a basis for a twist actuated blade which is used to verify the adaptive capabilities of the ABE.

4.3.3 Actuated Blade

It is assumed that the CH-47D helicopter blade spar is actuated with “imaginary” anisotropic actuators with the same stiffness properties as the 0° E-Glass plies. These anisotropic actuators strain 220 $\mu\epsilon$ in the longitudinal (0°) actuator direction and 0 $\mu\epsilon$ in the transverse direction when actuated. The radius of the actual CH-47D rotor is 9.14 m (360 in), but only 6.86 m (270 in) of the blade is fully developed airfoil. For the study it is assumed that only the fully developed airfoil section can be used for actuation. For the actuated spar, the $\pm 45^\circ$ SP250 E-Glass plies in the approximate spar are changed into alternating $\pm 45^\circ$ “imaginary” anisotropic actuation plies. This ensures that the blade torsional stiffness remains constant. The final laminate construction for the approximate twist actuated spar is shown in Figure 4-15:

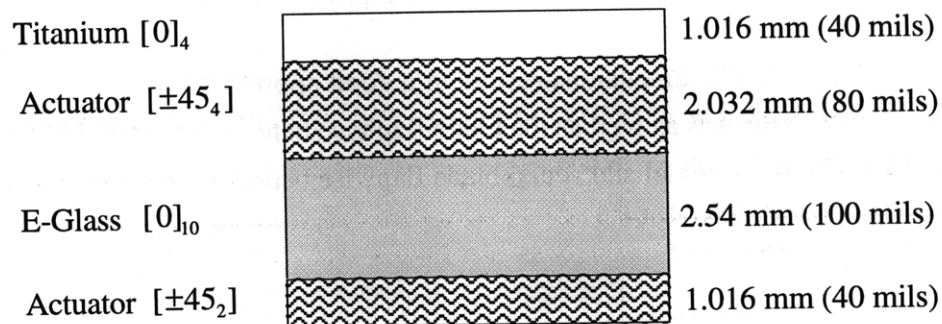


Figure 4-15. CH-47D Actuated Spar Laminate Construction

This concludes the description of the approximate actuated spar of the CH-47D blade. In the next section the twist results for this actuated spar are presented. The twist results are obtained from the adaptive beam finite element simulation and a commercial FEA of the actuated spar.

4.3.4 CH-47D Blade Spar Twist Results

To verify the adaptive beam model displacement simulation capabilities, a set of trustworthy twist results of the actuated spar are needed. The ANSYS² FEA package is used to obtain these twist results. The actuated spar is modeled with composite plate elements. Actuation strains of the anisotropic actuators are modeled in the ANSYS analysis with directional thermal expansion coefficients which result in the same actuator strain state for a unit temperature increase in the spar. The ANSYS Code is confined to Appendix B. The ANSYS beam model was constructed from plate elements with a length of 0.127 m (5 in) per element. The top and bottom panels were modeled with 6 elements per panel (chordwise direction), whereas the side panels were modeled with 2 elements per panel. Therefore the top and bottom elements dimensions were 0.127 x 0.047 m (5 x 1.86 in) and the side panel dimensions were 0.127 x 0.037 (5 x 1.47 in). The total number of plate elements used in the ANSYS model was 864. The ANSYS model of the twist actuated CH-47D blade is shown in Figure 4-16. For the ABE model the actuation strains were modeled by piezoelectric actuation material properties such that an applied unit voltage would result in 220 $\mu\epsilon$ in the longitudinal (0°) direction and 0 $\mu\epsilon$ in the transverse direction. The elements used for the ABE model each had a length of 0.127 m (5 in) for a total of 54 elements in the beam finite element model. Results from the ANSYS twist analysis and the twist predictions obtained with the adaptive beam finite element model are shown in Figure 4-17.

²ANSYS 5.0, Swanson Analysis Systems, Houston, PA

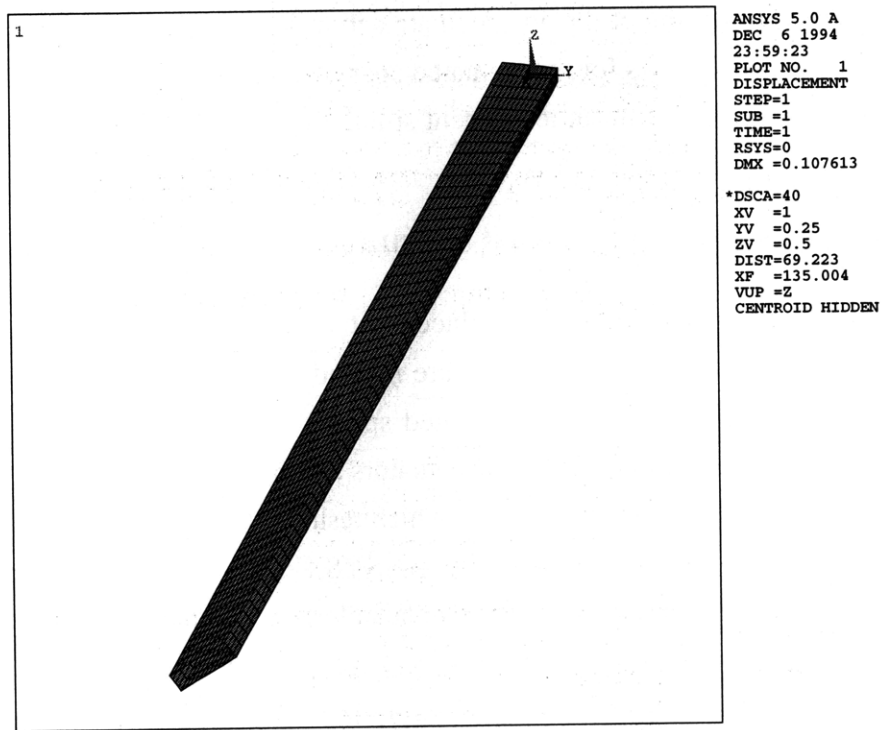


Figure 4-16. ANSYS Model of the Twist Actuated CH-47D Blade

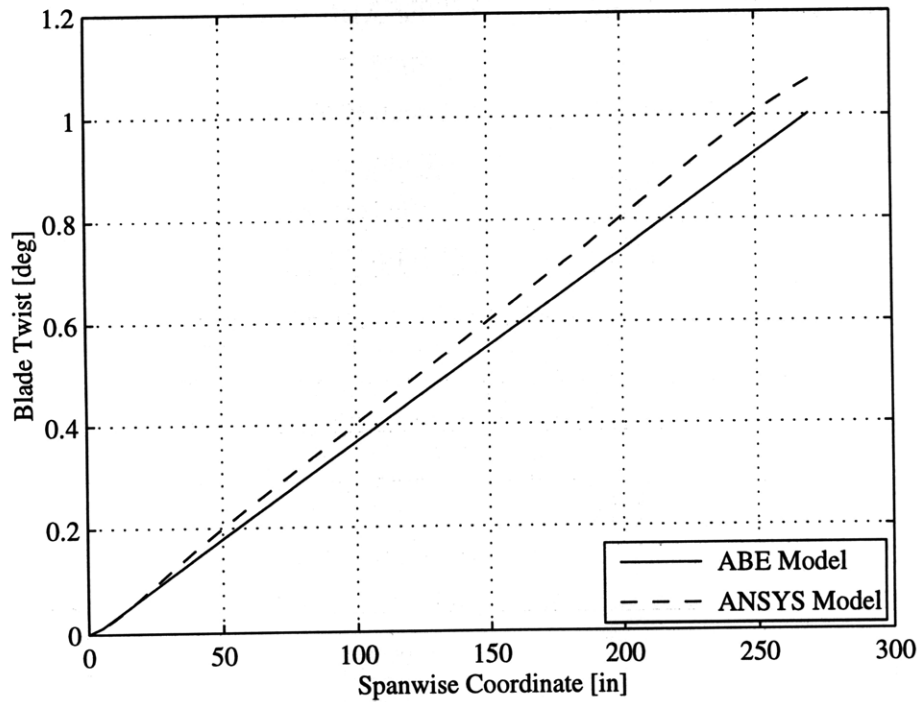


Figure 4-17. CH-47D Actuated Spar Twist

There is close agreement between the model twist predictions and the ANSYS results. The maximum error between the model and ANSYS results is 6%. A possible explanation for the small discrepancy between the model and ANSYS FEA results is the number of plate elements used in the analysis. Due to storage capacity limitations, the number of plate elements that could be used in the ANSYS analysis was limited to 500. On the other hand the ABE model only had 54 elements, which proves the efficiency of the ABE. The correlation of the actuated spar twist validates the model and associated ABE for the prediction of twist actuated, single cell, composite beam displacements.

4.4 Summary

In the first section of Chapter 4 an adaptive beam finite element was formulated. The element is based on the actuated composite beam model presented in Chapter 2. The ABE is a two node, one-dimensional beam element, with seven displacement degrees of freedom associated with every node. The actuation of the beam is described by two voltage degrees of freedom associated with every distinct ply section in the beam cross-section.

Section two of this chapter described the validation process of the passive response of the ABE. Previously published experimental results for composite beams loaded in bending and twisting were reproduced with the ABE. There was good correlation between the model and experimental results.

To validate the adaptive capabilities of the formulated beam finite element, the twisting of an actual helicopter blade with anisotropic actuators was predicted in the last section of Chapter 4. The first part of this section was used to construct a simplified model of the blade spar and to apply twist actuation to the spar. By analyzing the twist actuated spar with a commercial FEA package, twist results were generated to validate the adaptive beam model. The adaptive capabilities of the element was validated by the good agreement between model and FEA twist results

Chapter 5 ***Experimental Beam Manufacturing and Testing***

The goal of this study is to develop a model of anisotropically actuated, single cell, composite beams to be used in the design of a full scale individual blade control (IBC) mechanism. Before the full scale device can be designed, the concept has to be proven with a prototype device. A prototype device not only proves the concept but also acts as a means of validating the accuracy of the adaptive beam model.

In the first part of Chapter 5 the manufacturing and testing of passive composite box beams are described. This work is similar to the experimental results presented in Chapter 4 but this additional work was completed for two reasons. The first and most important reason for this experimental work is to gain experience with composite beam design, composite manufacturing, and testing techniques. This type of experience is indispensable once the final prototype is being developed. The second reason for this work is to act as yet another check on the passive capabilities of the composite beam model.

The ultimate goal of the study is to pave the way for implementation of a full scale helicopter blade control mechanism using distributed, anisotropic actuators. Part two of Chapter 5 concentrates on the development and testing of a "proof of concept" twist actuated, scale model helicopter blade. This section describes the IDEPFC actuators used for the model blade, the structural material used for construction, the manufacturing of the blade, and finally the testing of a scale model blade for actuated blade twist.

5.1 Manufacture of Passive Composite Box Beams

Smith [Smith and Chopra, 1990] tested the static response of passive composite box beams under external tip shear loading and applied tip torque. This experimental work was completed to validate a passive composite box beam model (similar to model presented in Chapter 2). Producing a set of similar experimental results serves the purpose of a secondary check on the passive capabilities of the actuated composite beam model and it acts as learning experience to be used during construction of the "proof of concept" anisotropic actuated composite beam.

Two classes of box beams were chosen for the experimental model validation. These classes are:

- Cross-ply layup beams with no structural couplings, and
- Symmetric layup beams with bending-twist coupling.

The laminate chosen for the cross-ply beams was $[0/90]_5$. This design resulted in a composite beam without any structural couplings. Symmetric beams are beams with opposite beam panels being mirror images (see Figure 4-6). This type of beam exhibits bending-torsion coupling with secondary extension-shear coupling. For this beam, the laminates chosen for the top and bottom beam panels were $[45]_4$ and $[-45]_4$ with the sides made from the $[0/90]_5$ laminate. This design maximized the passive beam bending-torsion coupling.

The procedure for passive box beam manufacturing is:

- Flat panel laminate manufacturing,
- Beam panel and edge-fitting preparation,
- Mandrel assembly and secondary curing.

5.1.1 Laminate Manufacturing

The flat composite panels were manufactured from the carbon reinforced plastic (CRFP) AS4/3501-6 pre-preg from Hercules³. This graphite/epoxy material comes in pre-preg form and a 37% resin content pre-preg was used for the laminates. After cutting the plies from the pre-preg tape, the $[0/90]_5$ and $[45]_4$ layups were assembled. Laminates were cured according to a standard 3501-6 net resin curing cycle.

³Hercules Inc., Wilmington, DE.

TABLE 5-1. AS4/3501-6 PLY PROPERTIES

E_1	142 GPa
E_2	9.81 GPa
ν_{12}	0.3
ν_{21}	0.021
G_{12}	6.0 GPa
t_{ply}	0.127 mm

The autoclave cure was completed in the autoclave facility at the Technology Laboratory for Advanced Composites (TELAC) at MIT. Cured AS4/3501-6 ply properties are given in Table 5-1 [Hercules].

5.1.2 Laminate Panel and Edge-fitting Preparation

The passive box beams were constructed from four laminate panels. The cured, flat laminate panels, 305x356 mm (12x14 inches), were cut into beam panels with the horizontal milling machine equipped with a diamond cutting wheel. These panels formed the top, bottom and side panels for each of the beams. Dimensions of the top and bottom panels were 49x350 mm and the side panel dimensions were 24x350 mm. The outer edges of the beam panels were lightly sanded to ensure a good bond during secondary curing.

It was decided to use aluminum edge-fittings to connect the beam panel for construction of the passive box beams. Aluminum edge-fittings had the least influence possible on the response of the beams. Aluminum T6061-T6 plate was used to manufacture the edge-fittings. The edge-fitting cross-section is shown in Figure 5-1. The length of these edge-fittings was 360 mm with a thickness of 0.81 mm and a flange width of 4 mm. Properties of the T6061-T6 plate are given in Table 5-2 [Blake, 1985]. These properties were used in the model of the experimental, passive, box beams.

TABLE 5-2. T6061-T6 ALUMINUM PROPERTIES

E	69 GPa
ν	0.3
G	26 GPa

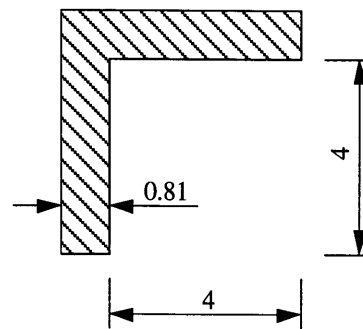


Figure 5-1. Aluminum Edge-Fitting Cross-Section (Dimensions in mm)

5.1.3 Mandrel Assembly and Secondary Cure

The next step in the manufacturing procedure was the assembly of the laminate panels and the edge-fittings onto the aluminum mandrel for secondary curing. The aluminum mandrel was machined from a block of T6061-T6. A schematic of the mandrel is shown in Figure 5-2. The cut-outs at the corners of the mandrel were machined to make it easier to remove the mandrel from the cured box beam after secondary panel bonding cure.

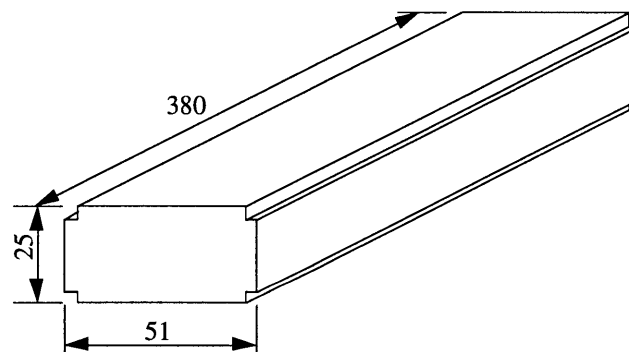


Figure 5-2. Aluminum Mandrel used for Passive Box Beam Manufacture
(Dimensions in mm)

Mandrel assembly proceeded as follows. The mandrel was wrapped in a single layer of Guaranteed Non-Porous Teflon⁴ (GNPT) and taped down with flash tape⁵ at the ends of the mandrel. This step ensured that the mandrel could be removed after secondary curing and protected the mandrel from any excess epoxy. In the second step of assembly, the AS4/3501-6 laminate panels were taped to the mandrel with flash tape. Step three of the procedure involved applying a thin layer of bonding epoxy to the edges of the laminates.

⁴GNPT, American Durafilm Co. Inc., Holliston, MA.

⁵Flash Tape, Northern Fiberglass Co. Inc., Hampton NH.

The epoxy used for secondary beam construction, was a high temperature potting compound⁶ with good shear transfer capabilities. Another layer of bonding epoxy was applied to the inside of the aluminum edge-fittings to ensure that a good bond was established between the aluminum edge-fittings and the composite panels. After placing the fittings in the correct position, the fittings were taped to the mandrel with flash tape. To prevent any excess bonding epoxy leaking to the outside, the whole assembly was wrapped in a layer of GNPT.

The thickness of the edge-fittings prevented the application of an even pressure to the assembly during secondary curing. To overcome this problem, aluminum spacers, of the same thickness as the edge-fittings, were taped down to the exposed areas on top of the composite panels. A crucial part in beam construction was to ensure that bonding layers were thin. This was accomplished by placing thick aluminum top plates on the sides of the of the mandrel assembly. In order to apply an even pressure to the top cover, a layer of high temperature resistant silicone rubber⁷ was placed on the cover followed by yet another aluminum top plate. Pressure was applied to the assembly with five C-clamps. An exploded schematic of one side of the mandrel assembly is shown in Figure 5-3.

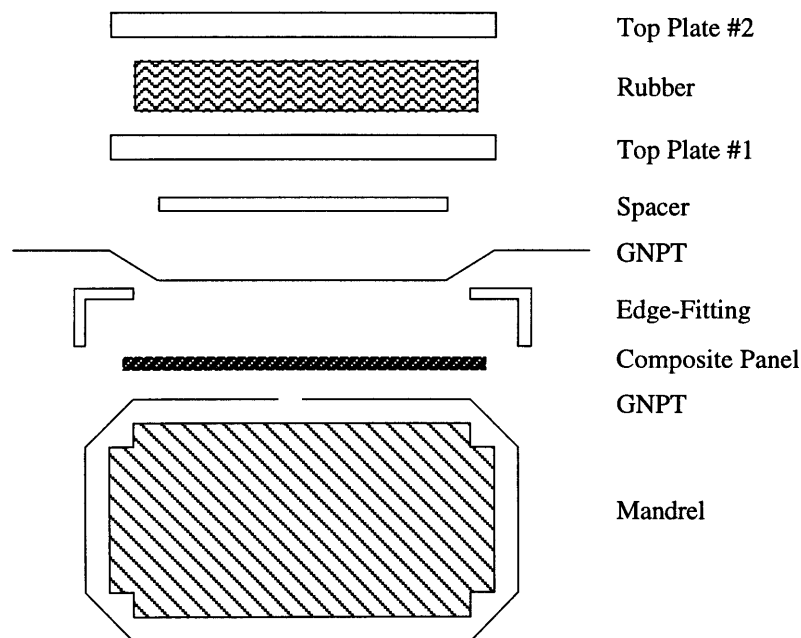


Figure 5-3. Mandrel Manufacturing Assembly

⁶EPOCAST 1636 A&B, CIBA-GEIGY Corp., Los Angeles, CA

⁷Silicone Rubber, Medium Hardness, 1/4", Greene Rubber Co., Woburn, MA.

Secondary curing was completed by heating the mandrel assembly in the post-curing oven, in TELAC, from room temperature to 180°F and keeping the temperature at that level for an hour. The secondary curing was completed by turning the oven off and letting the assembly cool to room temperature. This curing cycle resulted in a bonding layer which was more brittle than anticipated. On the advice of the manufacturers, the secondary curing cycle was reduced to 45 minutes at 180°F with the rest of the curing cycle remaining the same. By cooling the assembly in a refrigerator, the mandrel was easily removable from the composite box beam. The cross-section of the experimental beams and the associated model are shown in Figure 5-4. For the box beam model, the experimental cross-section was simplified by ignoring the composite laminate contributions underneath the aluminum edge-fittings. This simplification is based on the small influence of these parts on beam response and the indeterminacy in the unmodeled epoxy shear bonding layer. Experimental box beam dimensions and properties used for the modeling are given in Table 5-3. In the next section, the experimental setup and procedure are described. The section is concluded with the comparison of the model and experimental results.

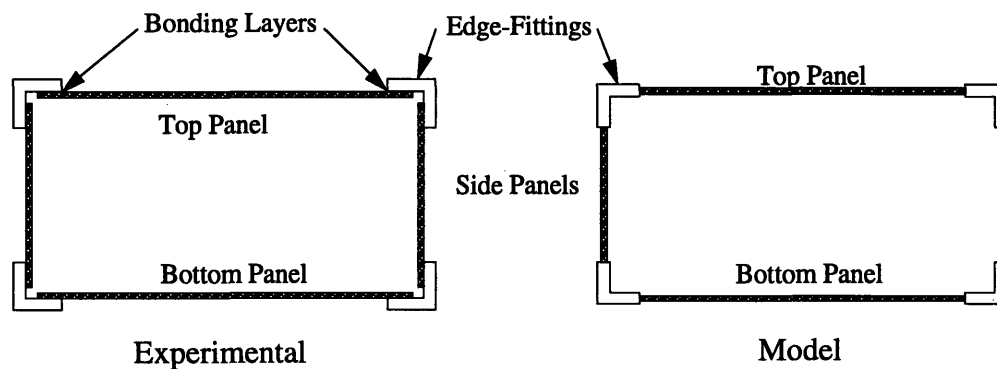


Figure 5-4. Experimental and Model Box Beam Cross-Sections

TABLE 5-3. EXPERIMENTAL BOX BEAM DIMENSIONS AND LAYUPS

Beam	Length (test length)	Chord	Height	Layup: Top & Bottom	Layup: Sides
Cross-Ply	292 mm	52 mm	26 mm	$[0/90]_s$	$[0/90]_s$
Symmetric	292 mm	52 mm	26 mm	Top: $[45]_4$ Bottom: $[-45]_4$	$[0/90]_s$

5.2 Box Beam Experimental Setup and Results

The composite box beams were tested as cantilevered beams in bending as well as in torsion. These loads correspond to the beam loadings that were used by Smith [Smith and Chopra, 1990] but are also the loadings for which the most beam displacement was observed which increased displacement measurement accuracy. Finally, experimental displacement results from these tests are used to validate the beam model results.

5.2.1 Experimental Setup

The experimental setup consisted of three distinct parts. These parts were the base and mountings, the force application system, and finally the displacement measurement system. In the next parts of the section the different components of the experimental setup is described in detail.

The base for the experimental setup was a large block of aluminum with tapped holes in the top surface onto which the different components were mounted. The box beams were mounted vertically onto the base by means of a base mount. This mount served as the “rigid” cantilevered connection between the base and the box beams. The mount was machined from aluminum with a solid 50 mm (two inch) section extending from the base. The cross-section of this part was a replica of the manufacturing mandrel cross-section. Two thick steel plates, with a width of 50 mm (two inches), were used to clamp the box beam down once it was slid onto the mount extension. This mount ensured that the beam cross-section was maintained during loading and enforced the cantilevered boundary conditions. A similar clamp and insertion was used at the free end of the beam to apply loads. In this case the insertion only extended 5 mm into the beam cross-section and smaller clamps were used. All loads were directly applied to the free end clamps. This maintained the beam cross-section during loading and caused an even pressure distribution during loading. A schematic of the base and mounts are shown in Figure 5-5.

A pulley system was built to apply the tip shear load as well as the tip twist moment. For the shear load, a single pulley was used to transform the weight of a mass to a horizontal shear force at the beam tip. Initially, the same concept was used to apply a tip twist moment. Two shear loads displaced equal distances from the beam centroid were used as a means to obtain a tip moment. This method obstructed the beam tip displacement measurements and it required that two masses be used, via the pulleys, at the same time.

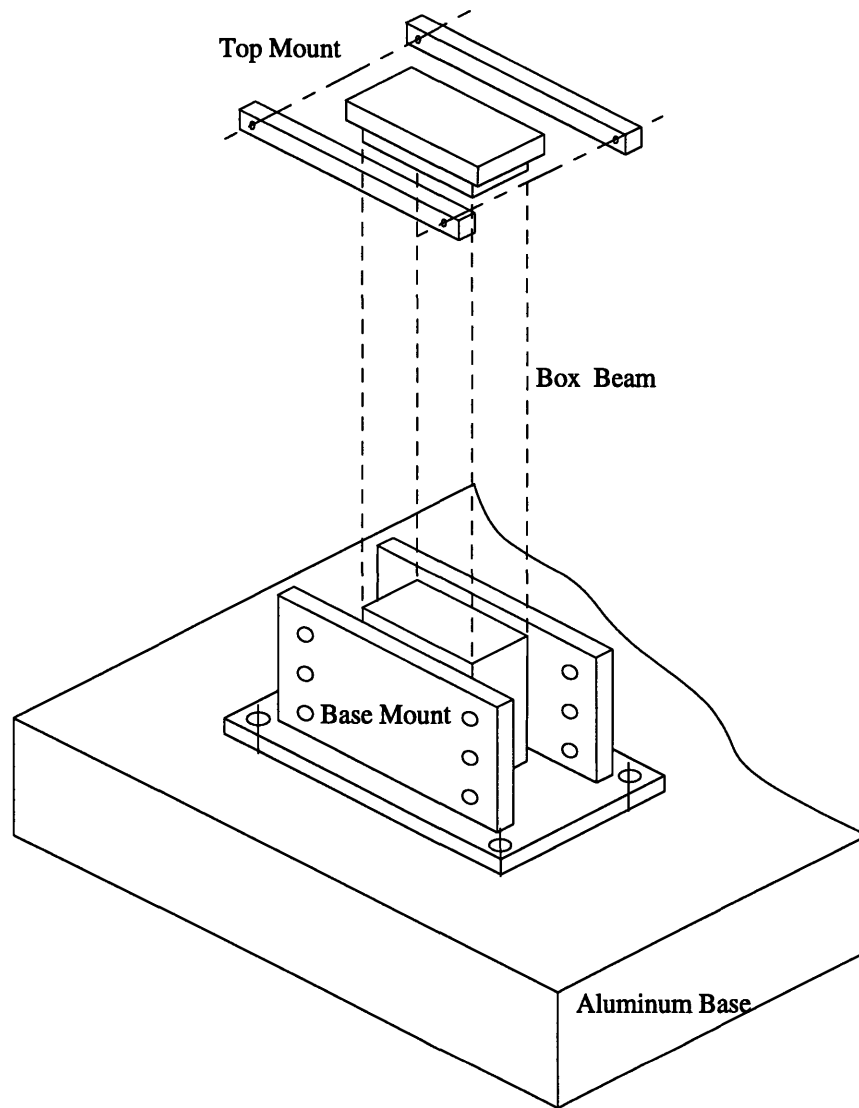


Figure 5-5. Experimental Setup Base, Base Mount, and Top Mount

A pulley system was designed that transforms the weight of a single mass into a tip moment. This system relies pulleys, strings and the application of the weight right in the middle of two supporting pulleys. The force and moment application systems are shown in Figure 5-6. In all tests, a force transducer⁸, in the force application path, was used to measure the applied loads.

⁸Model 208A02/448D, PCB, Depew, NY.

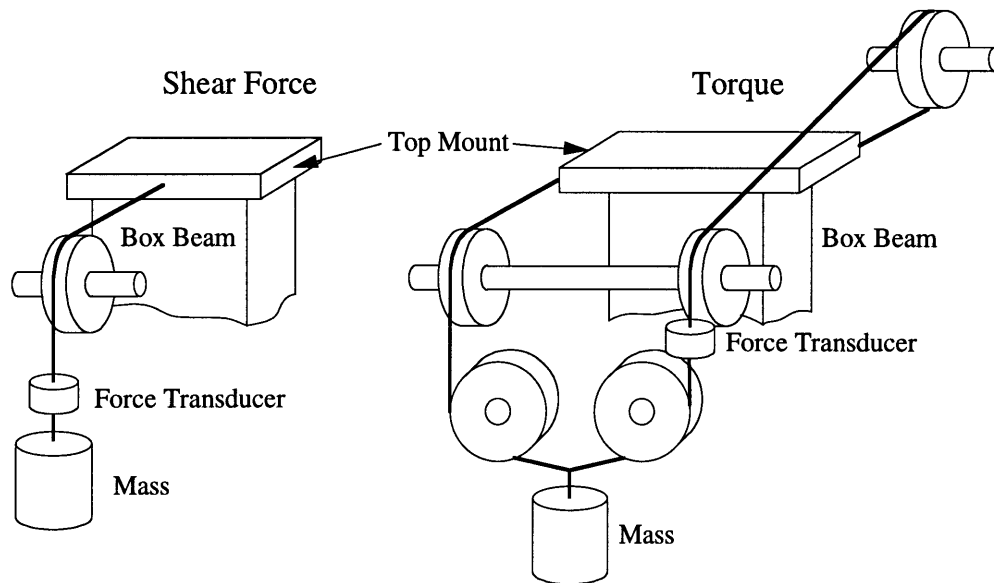


Figure 5-6. Beam Shear Force and Torque Application Systems

Displacement measurements were taken all along the length of the beam with a pair of movable laser displacement sensors⁹. The laser displacement sensors were mounted on a sliding block which in turn was mounted on a vertical shaft. The vertical shaft was fixed in a movable mounting block. A schematic of the measurement system is shown Figure 5-7.

⁹LB12/72, Keyence Corp., Fair Lawn, NJ.

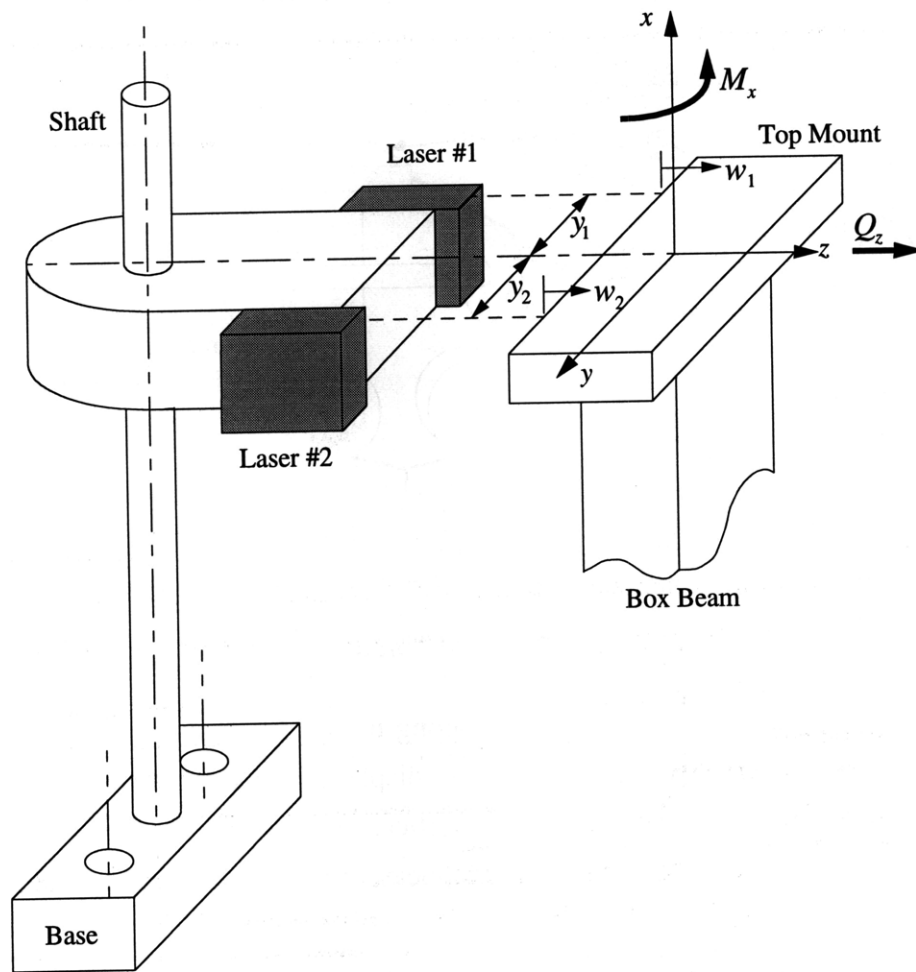


Figure 5-7. Laser Displacement Measurement System

The displacement measurements at any point along the beam were used to calculate the bending of the beam centroidal axis as well as the twist of the beam cross-section. Beam bending displacement was determined by taking the average of the laser displacement sensors measurements (assuming equidistant displacement measurements from beam axis):

$$W = \frac{w_1 + w_2}{2}, \text{ with } y_1 = y_2 \quad (5.1)$$

where W is the beam transverse displacement as defined in Section 2.3.2. Other variables are defined in Figure 5-7. The cross-sectional twist was determined from the simple trigonometric relation:

$$\phi = \arctan\left(\frac{w_2 - w_1}{y_2 + y_1}\right) \quad (5.2)$$

where ϕ is the cross-sectional twist defined in Section 2.3.2. Displacements w_1 and w_2 were determined by taking the no-load measurements and then measurements with the loads applied to the beam tip. The data acquisition system that was used consisted of a computer¹⁰ equipped with data acquisition software¹¹ and a data acquisition card¹². In the next section, the results from the beam bending and twisting tests are presented together with the model predictions based on the assumed beam cross-section shown in Figure 5-4 and the beam dimensions given in Table 5-3..

5.2.2 Cross-ply Beam Results

The cross-ply beam was constructed from $[0/90]_5$ laminate panels. For these tests only bending displacement or twist angles were measured as no coupling were expected between the different modes of deformation. Beam properties and dimensions are given in Table 5-1 to 5-3 and the cross-section construction is shown in Figure 5-4. The box beam, finite element model had 146 elements. Cross-ply beam transverse displacement results are shown in Figure 5-8. For this test a 55 N shear force was applied in the z-direction, at the free end of the beam.

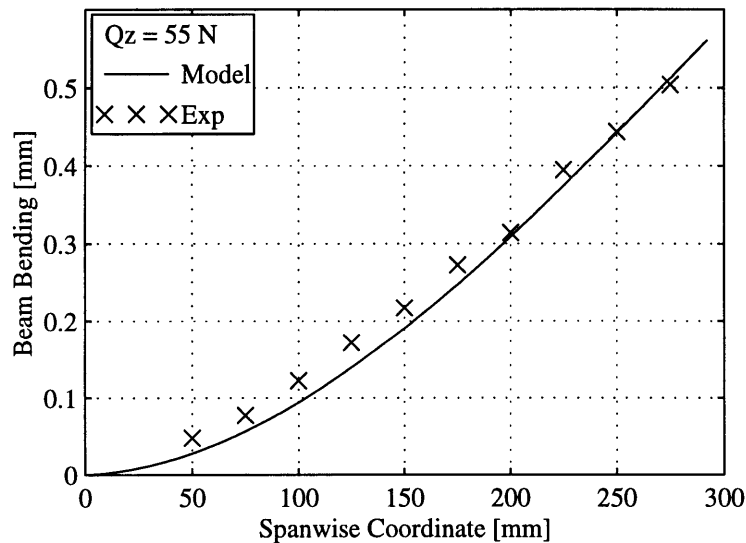


Figure 5-8. Cross-Ply Beam Transverse Displacement, W , for a Tip Shear Load

¹⁰Quadra 950, Macintosh, Apple Computer, Cupertino, CA.

¹¹LabView 3, National Instruments, Austin, TX.

¹²NB-MIO-16, National Instruments, Austin, TX.

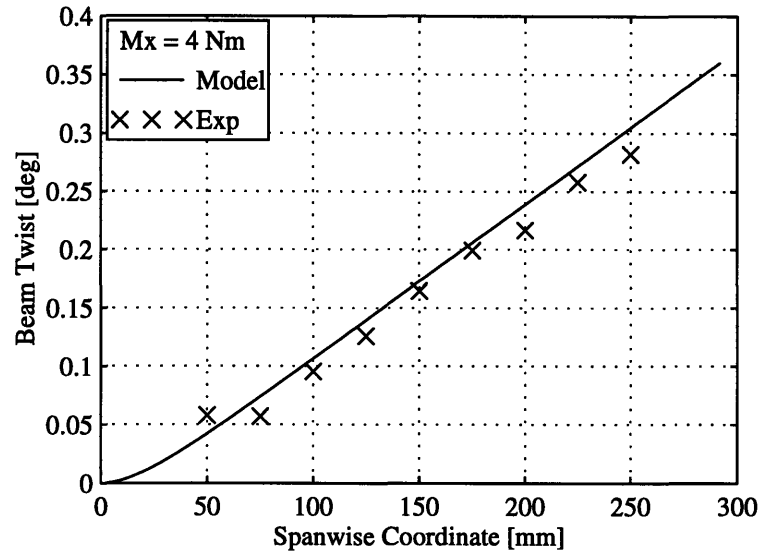


Figure 5-9. Cross-Ply Beam Twist, ϕ , for a Tip Torque

There is close agreement between the model predictions and the experimental results. The maximum error between model and experimental results is 5% (error defined as a percentage of predicted tip displacement). This agreement validates the model for cross-ply beam transverse displacement predictions.

Cross-ply beam twisting results are shown in Figure 5-9. For this test a 4 Nm tip moment was applied to the beam.

The model twist prediction agrees with the experimental results. The maximum modeling error is 6%. An interesting fact is the experimental verification of the restrained warping effect at the cantilevered end of the beam.

5.2.3 Symmetric Beam Results

Symmetric beam properties were given in Table 5-3. As described in Section 5.1, the symmetric beam exhibits bending-twist coupling. The degree of bending-twist coupling was maximized by using the $[45]_4$ composite laminate panels for the top and bottom panels of the beam. The finite element model of the symmetric box beam had 146 elements (same geometric model as for cross-ply box beam). In the first test, a 55 N transverse shear load was applied to the tip of the beam. Beam transverse displacement and twist results are shown in Figure 5-10.

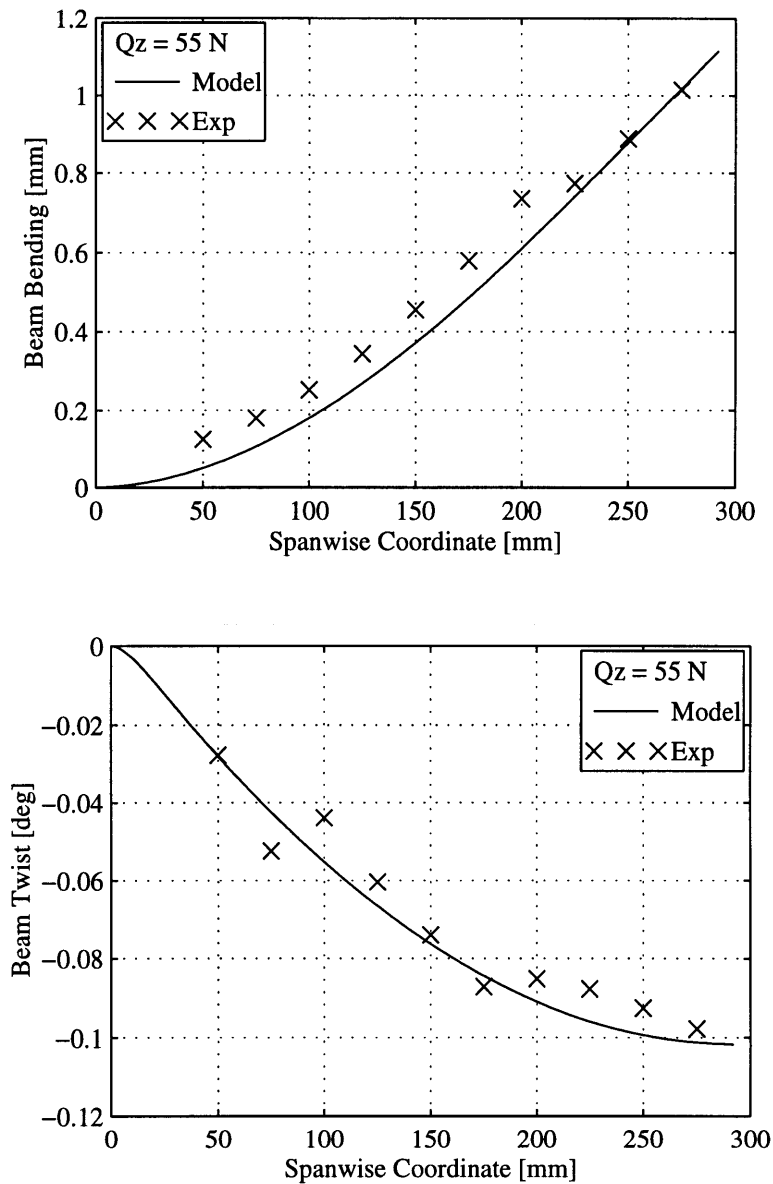


Figure 5-10. Symmetric Beam Transverse Displacement, W , and Twist, ϕ , for a Tip Shear Force

These experimental results show bending-torsion coupling for the symmetric beam. The beam bending maximum error is 11% and the maximum twisting error is 10%. Errors between the model and experimental results are within the bounds expected for this experimental setup. At the cantilevered end of the beam, displacements get so small that it is difficult to resolve the displacement and twist with confidence. Model and experimental results agreement validates the model for symmetric beam displacement predictions.

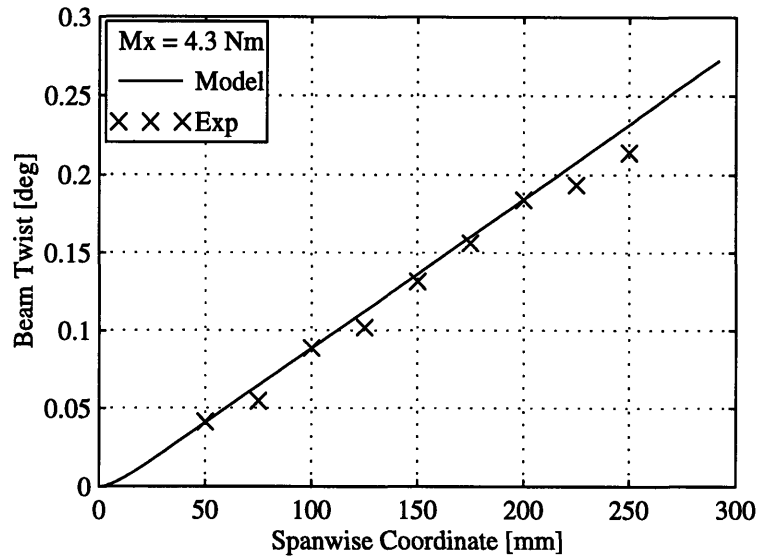


Figure 5-11. Symmetric Beam Twist, ϕ , for a Tip Moment

As a secondary symmetric beam test, a 4.3 Nm tip torque was applied to the beam. The magnitude of this tip moment is small compared to the shear load applied in the previous test (based on resulting beam displacements). For this reason the beam transverse displacements could not be resolved with confidence. Twist results from this test are shown in Figure 5-11.

Model and experimental results agree closely. The maximum error between the experimental and model predictions are 6%. As for the case of twisting the cross-ply beam, the symmetric box beam twist shows restrained warping behavior at the cantilevered end.

In all the test cases examined in this experimental section, the correlation between the model and the experimental results was satisfactory. This correlation increases the confidence in the validity of the composite, single cell, beam model. The experience gained through this experimental work proved to be invaluable during the construction of the twist actuated model helicopter blade. In the next section of Chapter 5 the experimental actuated model helicopter blade work is presented.

5.3 Twist Actuated Model Helicopter Blade

Although the theoretical analysis might predict that distributed, anisotropic actuators can be used for individual blade control to accomplish vibration attenuation for helicopters, the concept needs to be proven in practice. To prove the concept of distributed twist actuation of single cell, composite beams, a model helicopter blade was manufactured with IDEPFC actuators embedded in the blade. This blade was tested for twist actuation performance. The experimental work also served as a validation of the adaptive single cell composite beam model and the associated finite element code formulated in Chapters 2 and 4. In the first parts of this section, the passive and active materials used for model blade construction are described in detail. Following these material descriptions, the manufacturing and experimental setup are described. To validate the adaptive capabilities of the ABE, formulated in Chapter 3, for future blade control mechanism design a model of the twist actuated model blade is used for twist predictions. The twist actuated, model helicopter blade section is concluded with the presentation of the experimental twist results and a comparison of the experimentally observed and predicted twist results.

5.3.1 IDEPFC Actuators

The objective of the experimental work is to show that it is possible to twist a composite beam structure with IDEPFC actuators. The IDEPFC actuators used in the adaptive model blade were manufactured at MIT's Active Materials and Structures Laboratory (AMSL) according to the manufacturing procedures described by Bent [Bent and Hagood, 1995].

Electrodes for the actuators were manufactured by etching 12.7 μm (0.5 mils) Copper/Kapton thin film¹³ using an interdigitated electrode mask with appropriate dimensions and electrode finger orientation. It was shown in Chapter 3 that the induced shear, and therefore the induced twist in a beam, is maximized by anisotropic actuators with the primary actuation axis oriented at 45° relative to the beam spanwise axis. A decision was made to manufacture the actuators with the fibers running at 45° relative to the span of the actuator instead of orienting the actuators during the embedding process. Therefore a non-standard interdigitated electrode mask was designed with the electrode fingers running at 45° relative to the span of the electrode. The electrode pattern used in the adaptive blade is shown in Figure 5-12. The span of the electrodes was limited by the maximum area that could be etched at once with the photolithography process (5x5 in).

¹³0.5 mil Copper/Kapton, Southwall Technologies, Palo Alto, CA.

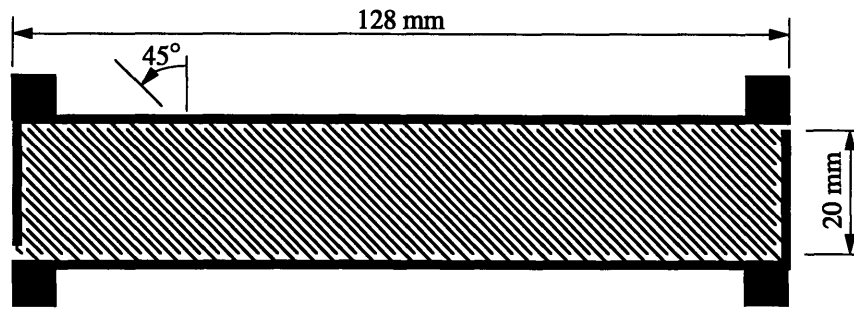


Figure 5-12. Electrode Pattern of the 45° IDEPFC Actuators used for the Adaptive Model Blade

Fibers used for the IDEPFC actuators were PZT-5H fibers¹⁴ with a fiber diameter of 130 μm (5.1 mil). Actuators were manufactured with a 56% ceramic fiber volume fraction in the active ply (80% transverse ceramic line fraction [Bent and Hagood, 1995]). The matrix material for the IDEPFC actuators was the Epon 9405¹⁵ epoxy system doped with 75% mass fraction, 1 μm PZT-5H particles¹⁶ to improve the matrix dielectric. The actuators were poled during manufacturing, prior to embedding in the blade, at an applied field of 1300 V/mm, in air at room temperature.

In order to construct an accurate model of the twist actuated model blade it is necessary to have accurate material properties for the IDEPFC actuators. Due to the fact that the IDEPFC material system is still under development, a complete set of experimentally determined IDEPFC actuator material properties is not currently available. In the absence of experimentally determined properties, the IDEPFC actuator model developed by Bent [Bent and Hagood, 1994] was used to predict the properties of the actuators.

The accuracy of the model property predictions are not only a function of the model but also a function of accuracy of actuator constituent material property values (piezoelectric fibers, matrix material, and electrodes) used for the model. For the IDEPFC actuators the material properties are mainly determined by the material properties of the piezoelectric fibers used in the actuators. The properties of these fibers are not yet determined, therefore two different fiber material property sets were used for the modeling of the IDEPFC actuators. For the first set of actuator properties it was assumed that piezoelectric fibers have the same material properties as the bulk ceramic PZT-5H material [Berlincourt]. The

¹⁴PZT-5H Fibers, CeraNova Corp., Hopedale, MA.

¹⁵Epon 9405 Resin and EpiCure 9470 Agent, Shell Chemical Co., Short Hills, NJ.

¹⁶PZT-5H Powder, Morgan Matroc Inc., Bedford, OH.

estimated matrix material and electrode properties were used to complete the input to the IDEPFC actuator model. For a more detailed description of the actuator model details the reader is referred to Bent [Bent and Hagood, 1995]. Model predicted IDEPFC actuator properties were given in Table 3-2. The IDEPFC actuator properties in Table 3-2 include the effect of the 12.7 μm (0.5 mil) electrodes on either side of the active ply for a total actuator thickness of 169 μm (6.65 mil).

As stated before, the accuracy of the IDEPFC material properties are mainly a function of the piezoelectric fiber material properties. It is possible to get better estimates of fiber material properties with the experimental mechanical and electrical testing of laminated IDEPFC actuators and iterating on model input material data until the experimental and model predictions match. This type of procedure was implemented with the tensile testing of IDEPFC actuators laminated with #120 E/Glass by Rodgers [Rodgers et al., 1996]. These actuators were different than the actuators used for the twist actuated model blade, but shared the same constituent materials. A schematic of the actuators used for the fiber property updating is shown in Figure 5-13. The actuators were laminated with #120 E/Glass to prevent a system response which was either dominated by the actuator or the material used for lamination. From the mechanical tests it was possible to estimate the properties of the PZT-5H fibers used for the blade IDEPFC actuators. The updated IDEPFC model properties, which are based on the experimentally updated fiber properties, are given in Table 5-4. Experimentally updated actuator stiffness properties were lower than the model properties. The reduction in IDEPFC material properties was associated with a deviation of piezoelectric fiber stiffness properties from the bulk PZT-5H values. The updated IDEPFC actuator properties were based on a single test, and therefore it is impossible to make any statements on the accuracy of these updated material properties.

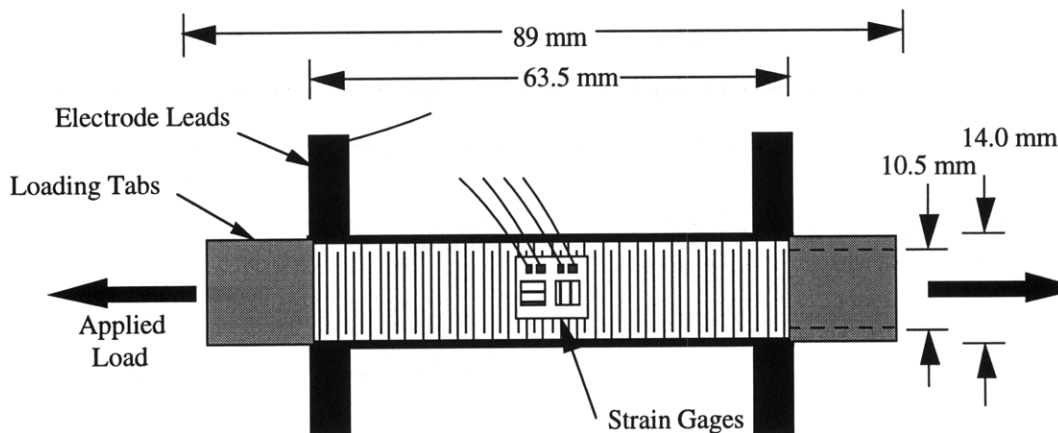


Figure 5-13. IDEPFC Actuators used for Updating of Piezoelectric Fiber Material Properties [Rodgers et al., 1996]

TABLE 5-4. IDEPFC STIFFNESS PROPERTIES

	Q_{11} [GPa]	Q_{12} [GPa]	Q_{22} [GPa]	Q_{66} [GPa]
Basic Model	44.5	6.56	18.5	5.5
Updated Model	32.8	6.26	17.3	5.5

During the testing of the twist actuated model blade the applied field levels would be much higher than the levels for which the actuation constants in Table 5-4 are valid. At maximum applied field levels the IDEPFC actuators would be operating at field levels close to the coercive field where the actuator response is non-linear [Chan and Hagood, 1994]. Therefore it was decided to model the actuation constants of the IDEPFC with a linear approximation of the large field strain response of the actuators used for the fiber property updating (1000 $\mu\epsilon$ at a total applied field of 2630 V/mm). The small field as well as the large field actuation constants for the IDEPFC actuators, used for the modeling of the twist actuated blade, are given in Table 5-5. It should be noted again that the actuators used for fiber updating were different than the actuators used for the twist actuated model blade, but it was assumed that the strain response of the fiber updating actuators at large fields, would be more realistic than the small field actuation model values (based on Table 5-4) extrapolated to large applied fields. It should be noted that the piezoelectric actuation constants, d_{31eff} and d_{32eff} , are the effective in-plane, constants for the IDEPFC actuators.

TABLE 5-5. IDEPFC ACTUATION PROPERTIES

	Field Levels	d_{32eff} [pvm/V]	d_{32eff} [pvm/V]
Basic Model	Low	147 ¹⁷	-61.3 ¹⁷
Updated Model	Low	144 ¹⁷	-60 ¹⁷
Experimental	High	381 ¹⁸	-160 ¹⁸

This concludes the section on the IDEPFC actuators used for the twist actuation of the scale model helicopter blade. In the next section the composite material used as passive construction material for the actuated model blade are discussed in more detail.

5.3.2 E-Glass Properties

High quality composite laminates are normally formed in an autoclave where the curing process can be precisely controlled and a pressure can be applied to consolidate the laminate during curing. This autoclave curing process is very costly and time consuming for non-standard flat panel cures. It was decided to manufacture the model blade around a foam-core and pressed inside a mold to obtain the correct blade cross-section. This manufacturing procedure would have required special fixtures if the cure was to be done in the autoclave. Therefore it was decided to manufacture the blade from a wet layup, room temperature curing composite material system. The fiber material was Style #120 E-Glass¹⁹ and the matrix was "SAFE-T-POXY"²⁰. E-Glass is a specific type of glass fiber and #120 E-Glass is a woven ply format of E-Glass with the woven fibers running perpendicular to each other.

The mechanical properties of the #120 E-Glass/SAFE-T-POXY (referred to as E-Glass henceforth) composite material system are not readily available. Therefore, in-house tensile and shear tests were done to determine the mechanical properties. The #120 E-Glass weave is a crowfoot weave and for the tests, the transverse weave direction was taken as the transverse material direction (90°). For the tests, two flat panels were manufactured with the following layups: $[0]_6$ and $[90]_6$. The laminates were manufactured by placing a sheet of GNPT on an aluminum top plate (12x13.5in) which was followed by the six sheets of #120 E-Glass. Between every layer of E-Glass, a layer of SAFE-T-POXY was

¹⁷Linear, small field, PZT-5H actuation properties used for model.

¹⁸Large field linear approximation with $E_{max}=1840$ V/mm and $E_{min}=-790$ V/mm.

¹⁹#120 E-Glass, BGF Industries, 301 N Elm St., Greensboro, NC.

²⁰Epolite Resin 2410 and Hardner 2184, Hexel, 201 E Abram St., TX.

applied with a brush. The epoxy was applied until the E-Glass layer was soaked with epoxy. Another sheet of GNPT was applied to the top of this layup followed by another aluminum top plate. Finally some weights were put on the top plate to apply pressure during curing. Curing was completed by leaving the laminate overnight at room temperature. The thickness of the cured laminate panels was used as an indication of the fiber volume fraction laminates. By ensuring that the thicknesses, of the laminates used model blade construction and the laminates used for property determination, were the same (or very close) the fiber volume fraction remain constant between different manufacturing techniques.

Tensile testing coupons were cut from the laminate panels according to TELAC standards [Lagace et al., 1991]. Two 50×350 mm coupons were cut from each of the panels. Fiberglass end-tabs were bonded to the coupons using SAFE-T-POXY. These tabs acted as gripping areas during tensile testing and ensured that if the laminate failed during testing, that it would be in the gage section. The coupons were tested in the TELAC MTS testing machine²¹ to determine the extensional (Young's) moduli in both material directions (0° and 90°) and the poisson's ratios. Longitudinal (0°) and transverse (90°) strains were measured using surface bonded T-strain gages²².

The shear modulus of the E-Glass was determined by testing 50×350 mm coupons (two from each laminate) in twisting with a custom built twisting setup. This experimental setup applies a tip torque without restraining axial movement. By measuring the amount of twist and applied torque, an estimate for the shear modulus could be obtained from thin section torsion theory [Megson, 1990]:

$$G = \frac{M_x l}{\phi_{tip} J} = \frac{M_x l}{\frac{1}{3} w t^3 \phi_{tip}} \quad (5.3)$$

where w is the coupon width, t is the coupon thickness, and l is the gage section length.

TABLE 5-6. CURED E-GLASS (#120) PROPERTIES

E_1 [GPa]	E_2 [GPa]	ν_{12}	ν_{21}	G_{12} [GPa]	t_{ply} [mm]
14.8	13.6	0.19	0.17	1.9	0.2

²¹MTS 800, MTS, Minneapolis, MN.

²²CEA-06-125UT-120, Measurements Group, Raleigh, NC.

The shear stiffness determined from this test was not very accurate. The inaccuracy was caused by a non-linear stiffening effect due to the clamped conditions at the edges of the laminates. Another contributing factor was thicknesses of the tested laminates. From equation (5.3) it can be seen that small variations of the laminate thickness greatly effects the estimate of the material's shear stiffness. The cured E-Glass properties are given in Table 5-6.

5.3.3 Non-Active Scale Model Blade Manufacturing

A non-active model blade was designed and manufactured to develop a thoroughly tested manufacturing procedure for the twist actuated model blade. To keep the experimental work relevant, the non-active model blade was designed as a 1/16th scale model of the CH-47D blade [Sandford, 1978] with a NACA0012 airfoil instead of the VR7 airfoil. This was done because a 50 mm NACA0012 mold was already available. This mold prescribed the 1/16th scale factor.

Helicopter blades can be scaled in two different fashions [Bielawa, 1992]. These are Mach-scaling and Froude-scaling. A Mach scaled blade is a blade which is tested at the same Mach numbers as the full scale article and which has the same dynamic response (rotating natural frequencies and mode-shapes) as the full scale article. For the Mach scaled blade the same stress and strains are the same for the model and the full scale article during dynamic testing. On the other hand a Froude scaled model blade is scaled to have the same static, gravitational, blade, displacement response as the full scale article. For a model blade the Froude scaled blade stiffnesses differ from the Mach scaled model blade by the length scaling factor used.

The non-active model blade, used as a manufacturing procedure development for the twist actuated model blade, was designed around a combination of Mach and Froude Scaling. For this study, the primary interest is in the static twist response of an actuated model blade. The static twist response of the model blade is governed by the torsional stiffness of the blade. Therefore only the torsional stiffness (expressed in standard engineering terms as GJ) was scaled and no attention was paid to the flapwise and chordwise bending stiffnesses of the blade as well as the mass distribution of the model blade. The Mach and Froude model blade scaling parameters are summarized in Table 5-7.

The torsional stiffness of a Froude scaled blade is $1/16^{\text{th}}$ of that of a Mach scaled model blade. The blade length in Table 5-7 is the blade length from the hinge point, at the rotor hub, to the tip of the blade. The Froude model blade torsional stiffness was used to determine a lower bound on the wall thickness of the non-active model blade.

TABLE 5-7. NON-ACTIVE MODEL BLADE SCALING PARAMETERS

	CH-47D	Mach	Froude	Mach Model	Froude Model
Length [m]	7.72	1/16	1/16	0.483	0.483
Chord [m]	0.81	1/16	1/16	0.05	0.05
GJ [Nm ²]	246.8×10^3	$(1/16)^4$	$(1/16)^5$	3.76	0.235

From thin walled, closed section, torsion theory the torsional constant for the NACA0012 airfoil is [Boresi, 1985; Megson, 1990]:

$$J = \frac{4A^2}{\Gamma} t \quad (5.4)$$

where A is the cross-sectional area, Γ is the cross-sectional contour length, and t is the thickness of the blade wall. Equation (5.4) can be used to solve for the wall thickness of the blade in terms of the blade torsional stiffness and the construction material's shear modulus:

$$t = \frac{\Gamma(GJ)}{4A^2G} \quad (5.5)$$

Equation (5.5) was used to determine the thickness of the non-active Froude model blade wall for the 50mm NACA0012 cross-section made from E-Glass:

$$t_{\text{Froude}} = 0.07 \text{ mm} \quad (5.6)$$

This thickness is smaller than the thickness of a single cured E-Glass ply (see Table 5-5). Therefore it was decided to manufacture the non-active model blade from a single E-Glass ply with the understanding that the blade torsional stiffness would be 186% higher than the design value for a Froude scaled blade, but still lower than the Mach scaled model blade torsional stiffness.

The non-active model blade was manufactured by cutting a foam-core²³ to the correct airfoil with a hot wire foam cutter. In the second process, the foam-core was coated with a layer of SAFE-T-POXY, followed by a layer of #120 E-Glass with the 0° material angle aligned with the span of the foam-core. To ensure that the E-Glass was completely wetted, the assembly was coated with another layer of the epoxy. The final step was to cure the model blade by leaving it overnight at room temperature. Due to the limitations on the thickness of the construction material, the center of gravity (CG) of the non-active blade was at an incorrect chord location (CG located close to mid-chord as opposed to quarter-chord). The incorrect CG location excluded the non-active model blade from dynamic spin stand testing, but it served the purpose of providing a model on which to base the twist actuated model blade manufacturing.

5.3.4 Twist Actuated Model Blade Manufacturing

The adaptive model blade was based on the non-active model blade. Two layers of E-Glass were used to construct the adaptive model blade instead of only one for the non-active blade. Six IDEPFC actuators (described in Section 5.3.1) were embedded in the top and bottom skins of the blade (three on each side). The actuators in the top skin were aligned with fibers running at 45° with respect to the spanwise dimension and bottom actuators were aligned at -45°. These actuator orientations maximize the induced shear in the blade walls and therefore the induced twist. The actuators were centered at 30% chord with the first actuator placed as close as possible to the blade root.

²³STYROFOAM, Sterling Industries, Waltham, MA.

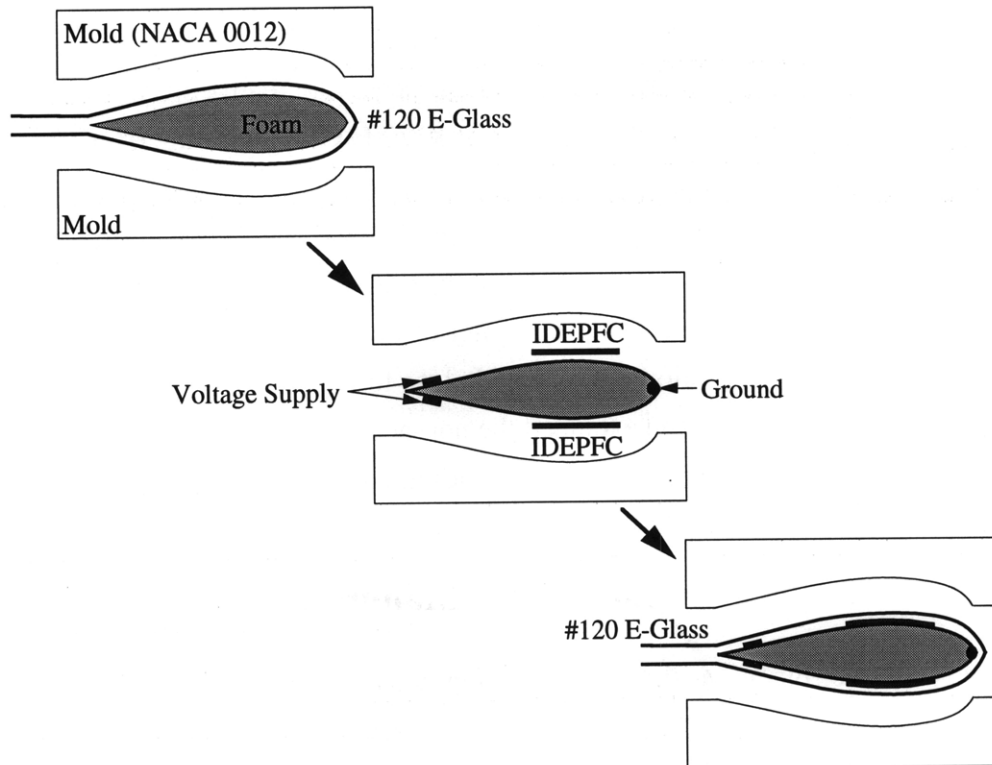


Figure 5-14. Twist Actuated Model Blade Manufacturing

The blade was constructed by curing the first layer of E-Glass on the foam-core, inside a 50 mm NACA0012 clamped mold. The clamped mold ensured the correct blade cross-section. Curing was completed with a 150°F, 2 hour cure in the TELAC post-cure oven. In the next step, the IDEPFC actuators were bonded the top and bottom surfaces of the blade with SAFE-T-POXY. Bonding was completed with the 150°F, 2 hour curing cycle in the clamped mold. Clamping the mold ensured a thin bonding layer. In the third step, the electrical leads were attached to the actuators. The actuators were connected in parallel. Separate high voltage leads were bonded on the aft section of the blade and a common ground was bonded to the leading edge. This connection ensured that the actuators could be actuated independently (should any of the actuators fail during actuation). Electrical connections between the leads and the actuators were established with conductive epoxy²⁴. The conductive epoxy was cured at 100°C for one hour. Finally, the last ply of wet E-Glass was applied to the assembly and the whole blade was cured in the clamped mold (same curing cycle as before was used). A schematic of the manufacturing process is shown in Figure 5-14. The completed blade is shown in Figure 5-15.

²⁴Epotek 410E, Epoxy Technology, Inc., Billerica, MA.

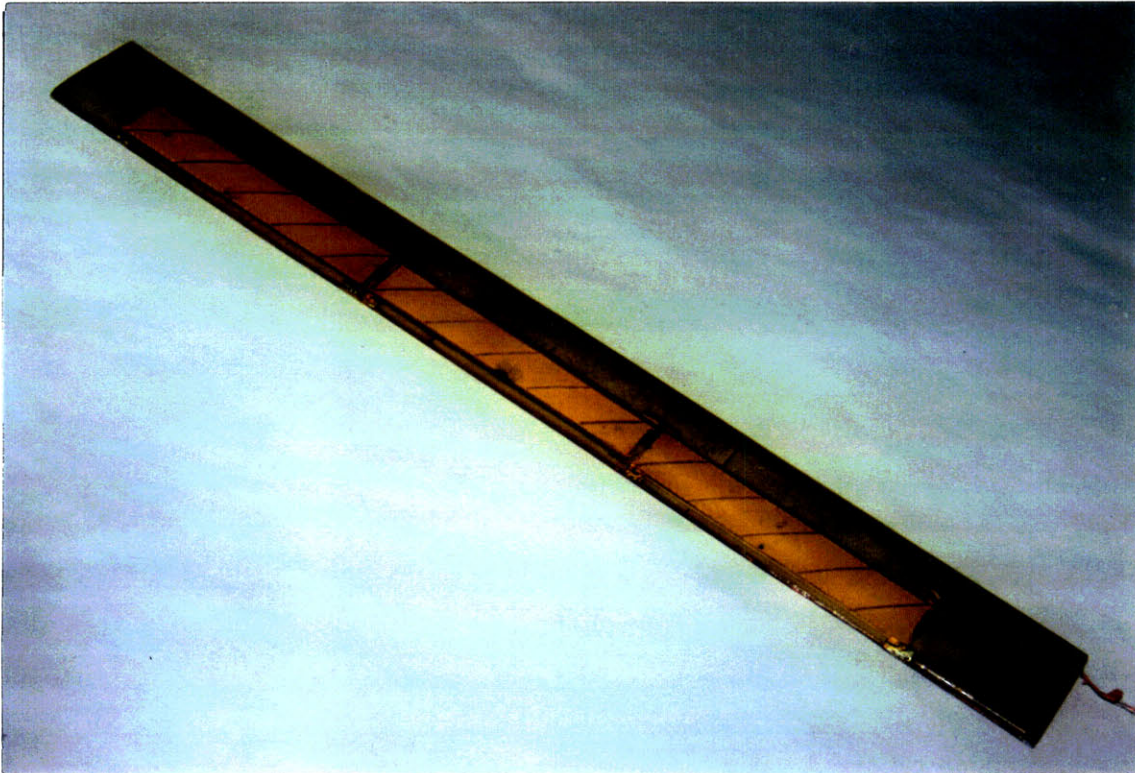


Figure 5-15. Twist Actuated Model Helicopter Blade

The adaptive model helicopter blade was modeled using the adaptive beam element (ABE) developed in Chapter 4. A schematic of the active blade with dimensions and actuator locations are shown in Figure 5-16. The blade model ignored the root attachment of the blade as this part did not influence the twist behavior of the blade. Two different elements were used for the modeling of the blade. The first element was the non-actuated blade element which represented the non-actuated sections of the blade. In the element, the blade cross-section was approximated with twenty linear pieces. The second element used the same cross-sectional description as the first element but with the IDEPFC actuators included in the blade wall. The model torsional stiffness of the actuated model blade sections was 1.85 Nm^2 . This torsional stiffness is 51% of the Mach scaled model helicopter blade torsional stiffness (3.76 Nm^2). Therefore it can be concluded that the adaptive model helicopter blade is somewhere in between a Mach and Froude scaled model blade (based on the torsional stiffness). In the next section the experimental setup and testing of the blade are discussed.

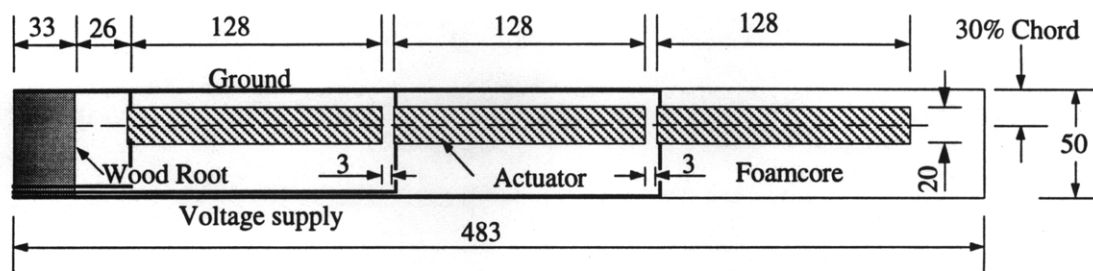


Figure 5-16. Adaptive Model Blade with Dimensions and Actuator Locations
(Dimensions in mm)

5.3.5 Experimental Setup

The model blade was mounted vertically for the twist actuation tests, by clamping the root of the blade in the base mount (see Section 5.2.1). The IDEPFC actuators were actuated in shear by applying a sinusoidal voltage with a DC offset to the actuators. The DC voltage offset was such that the minimum voltage was always kept at 0V. A function generator²⁵ was used to supply the desired voltage signal which was fed through an amplifier²⁶ to obtain the required high voltage driving signal.

Two twist actuation tests were completed on the blade. For the first test, an angular indicator was mounted to the tip of the blade. This indicator was longer than the blade chord to improve the angular resolution of the measurement system. To complete the experimental setup, a protractor was fixed, in the plane of the angular indicator, centered at the blade twist center. An endview of this experimental setup is shown in Figure 5-17. Results obtained from this experimental setup are denoted as "Exp-1" in the results section (Section 5.3.6).

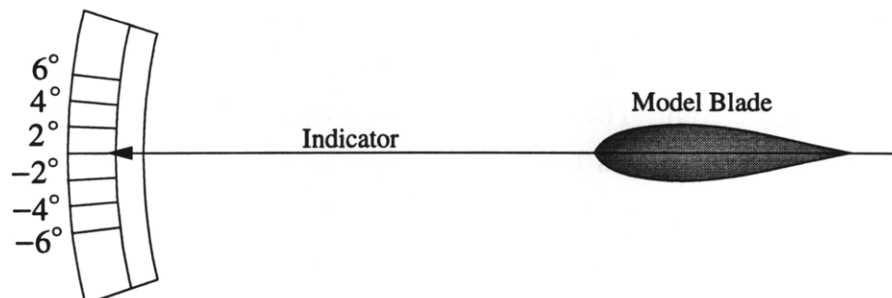


Figure 5-17. Angular Indicator Twist Measurement Setup

²⁵PM5138, Phillips, Hamburg, Germany.

²⁶Model 664, Trek, Medina, NY.

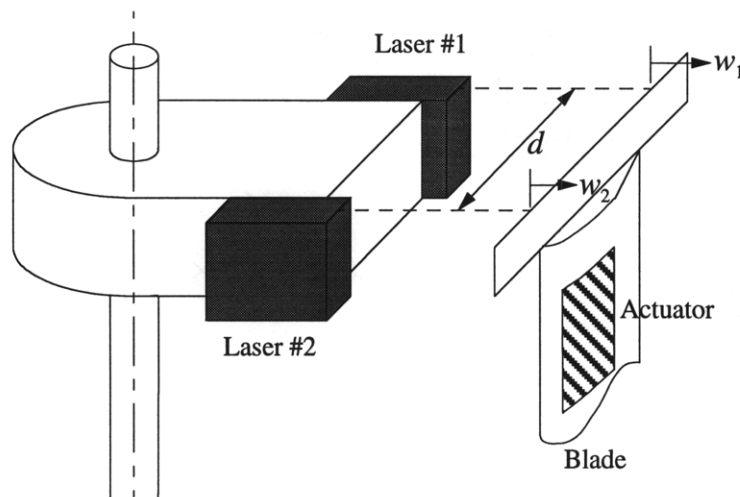


Figure 5-18. Laser Twist Measurement Setup

The twist measurements from the angular indicator experimental setup are not very accurate. To improve the accuracy of the tip twist measurements the tip twist was measured with the movable laser displacement setup described in Section 5.2.1 (see equation (5.7)). The complete experiment setup is shown in Figure 5-18. Results obtained from this measurement system are denoted as "Exp-2" in the results presentation.

$$\phi = \arctan\left(\frac{w_2 - w_1}{d}\right) \quad (5.7)$$

5.3.6 Actuated Model Blade Twist

The results for the twist actuation tests are shown in Figure 5-18. Actuation tests were completed with a excitation voltage frequency of 0.5 Hz. The voltage amplitude was increased in steps of 200V to a maximum voltage level of 2000 V. For the first test, the angular indicator setup was used to measure tip twist. Results from test are marked as "Exp-1" in Figure 5-19.

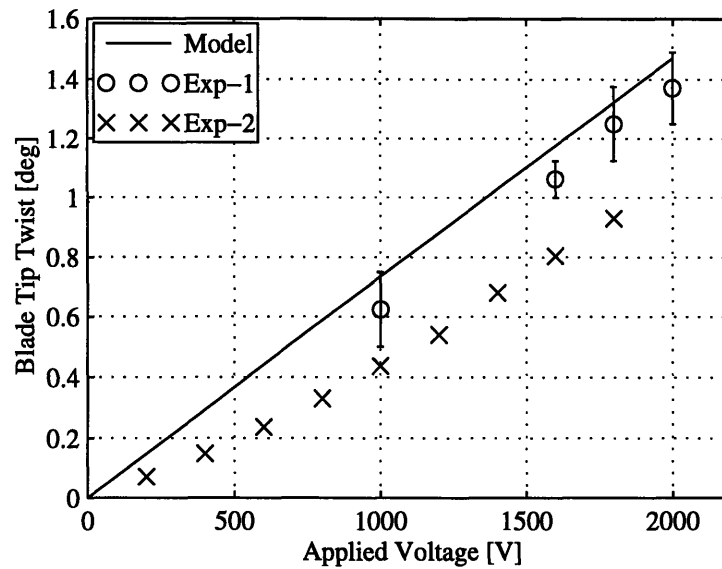


Figure 5-19. Tip Twist of the Active Blade as a Function of Applied Voltage

Five of the actuators failed at voltage levels of 2100V during this test. Failure occurred due to dielectric breakdown between two adjacent electrode fingers. Some of the damaged areas showed localized delaminations. It was decided to repair the blade and repeat the twist actuation tests using the laser displacement twist measurement setup. The damaged actuators were repaired by removing the damaged areas. These areas were removed by drilling holes in the blade and filling the hole with quick setting epoxy to prevent further electrical breakdown. One of the repaired actuators failed again, but this time failure occurred at 2000V. Results from the second test are marked as "Exp-2" in Figure 5-19.

For the first test, the blade tip twist was 1.4° at the maximum voltage level of 2000 volts. At 1800V the tip twist was 1.3° . The error bars for these experimental results represent the maximum and minimum twist measured for each applied voltage. In the second test the maximum voltage level was restricted to 1800V due to repeated actuator failure at 2000 V. At this voltage level the blade tip twist was 0.9° . The big difference between the first and the second tests is due damage to the blade during actuator failure. The maximum experimentally measured twist level of 1.4° represent 46% of the twist requirement as stated by Shaw [Shaw and Albion, 1981].

There is good agreement between the model tip twist predictions and the experimental results for the first twist test. The maximum error between the model and "Exp-1" results is 7%. The small discrepancy between the model and experimental results may be due to

unmodeled bonding layers and the uncertainty in actuation properties. Twist levels can be increased by improving the IDEPFC actuation system or by embedding more actuator plies in the skins. With these experimental results, the concept of twist actuation has been validated and the analytical model has been verified. Therefore the validated analytical model can be used for further detail designs of a twist actuated composite beams for helicopter blade control.

5.4 Summary

In the first part of Chapter 5 the construction of two passive box beams were described. Each of the passive composite box beams was from a different class of beams. The first of the beams was a cross-ply beam without any structural couplings and the second beam was a symmetric box beam with bending-torsion coupling. Both the beams were tested for displacement response by applying a tip shear force as well as a tip torque. There was close agreement between model and experimental results. Result correlations validate the model and finite element passive capabilities.

In the second part of Chapter 5 the manufacturing and testing of a twist actuated model helicopter blade were described. A model helicopter blade was manufactured from E-Glass and a foam-core. To actuate the blade in twist, IDEPFC actuators were embedded in the skin of the blade. The model blade was successfully twisted with the embedded IDEPFC actuators. Twist results prove the capability of IDEPFC actuators to induce twist and prove the concept of anisotropically actuated, single cell, composite beams. Adaptive capabilities of the beam model and associated beam finite element were validated by the correlation between predicted and experimental results. From the experimental twist results it can be concluded that it is feasible to use IDEPFC actuators for main spar twist actuation to accomplish HHC through IBC.

The final chapter of this thesis is divided into two parts: conclusions and recommendations. Conclusions based on the results from the study are presented first. This section also serves as a summary of the work done for the study. In the second part, recommendations are made for future work in this field.

6.1 Conclusions

The major objective of this study was to develop a model for the static displacement response of distributed, anisotropically actuated, single cell, composite beams. This study objective was driven from the possible application of distributed, anisotropic actuation materials to accomplish helicopter blade control. A model for this type of beam was successfully developed by expanding an existing single cell, composite beam model. The effect of anisotropic actuation was included in the model through augmenting the constitutive relations used to model beam construction material behavior. The model accounts not only for cross-sectional displacements, rotations, and twist but also for the twist rate at the specific beam cross-section. The non-classical inclusion of the twist rate accounts for the twist related, out-of-plane warping of the cross-section which can be an important effect in single cell, composite beams. In the final part of the study this model was validated through the experimental testing of both passive and twist actuated composite beams.

The set of governing equations which describe the static displacement response of anisotropically actuated, single cell, composite beams is a system of 14th order, coupled, ordinary, differential equations with associated boundary conditions. The complex nature of this boundary value problem excludes analytical solutions except for very simple cases. A high order adaptive beam finite element was developed to solve the actuated beam displacement problem effectively. This adaptive beam element was formulated from the model derived in the first part of this study. There are 14 displacement degrees of freedom in the element associated with two displacement nodes. The voltages in the beam are described by the voltage at the top and bottom of every discrete ply region in the beam cross-section. Therefore, the number of voltage degrees of freedom are twice the number of discrete ply regions. This beam element requires substantial numerical effort to determine the element equations, but once that is complete, the element is very effective in modeling the response of the beams. Another advantage of the element is that it provides physical insight into the problem. Modeling the beam with plate elements would lead to a set of equations which are difficult to interpret in terms of what physical mechanisms are acting in the beam, but with the beam element these mechanisms can be directly identified. The adaptive beam element was validated through extensive correlation with both analytical results as well as experimental results. Experimental results for passive beams were obtained from previously published results as well as the testing of passive beams constructed for this study. Results used for validation of adaptive element capabilities were generated with a commercial finite element analysis code as well as through the testing of a twist actuated model helicopter blade. This element can be used for the effective design of helicopter blade control mechanisms which utilize distributed, planar, anisotropic actuation materials to induce strain.

In the second chapter of this study a twist parameter study was used to show that certain actuation and stiffness anisotropy combinations are better for inducing twist in composite, single cell, beams. For this study some assumptions were made for the geometry and construction of twist actuated composite beams. These assumptions were used to obtain a simple relation for the non-dimensional tip twist of an actuated composite beam. The results from the study indicate that two combinations of material anisotropies exist which are inherently good for inducing twist. The first of these combinations is an anisotropic actuation material with the same stiffness in the longitudinal and transverse directions but transverse contraction when the material expands in the longitudinal direction when actuated. The second material combination is an actuation material with expansion in both

directions when actuated with zero transverse stiffness. In the final part of the parameter study it was shown that the two different anisotropic actuator technologies, IDEPFC and DAP elements, have favorable material anisotropies for twist actuation. The actuated non-dimensional twist parameters are similar for these two material systems although IDEPFC actuators and DAP elements have completely different stiffness and actuation anisotropies. Therefore, based on the non-dimensional twist parameter, IDEPFC actuators and DAP elements will induce the same levels of twist in helicopter blades. This analysis does not take the primary induced strain capability of the actuator material system into account. If the induced strain capability is included in a twist performance comparison, IDEPFC actuators will produce higher levels of twist than DAP elements.

In the experimental part of this study, the concept of distributed twist actuation of composite beams was proven with a twist actuated composite model helicopter blade. IDEPFC anisotropic actuator patches were embedded in the top and bottom skins of a model helicopter blade made from E-Glass. The IDEPFC actuators were embedded with the material fibers running at 45° for the top actuator and -45° for the bottom actuator relative to the blade spanwise axis. This actuator configuration maximized the induced twist in the model blade. The beam torsional stiffness was comparable with that of a dynamically scaled model helicopter blade. Therefore actuated twist results were representative of twist levels that could be expected for full scale helicopter blades. The model blade twist levels were on the order of 1° for voltage actuation levels of 2000V. These twist levels are in the range needed to accomplish HHC by direct blade pitch control. Therefore it can be concluded that it is feasible to investigate the application of distributed, anisotropic actuation for helicopter blade control

In summary, an accurate model of anisotropically actuated, single cell, composite beams was developed. This model was used to construct an adaptive beam finite element which was validated with experimental results. The twist parameter study was used to determine optimal anisotropic actuators material properties for the induced twist. The twist concept was proven with a prototype actuated model helicopter blade. All that remains now is to pull all these tools together in the development of helicopter blade control schemes which utilize the distributed anisotropic actuation concept.

6.2 Recommendations

The control of helicopter vibrations through IBC is a dynamic control problem and not a static problem. In the dynamic displacement domain, the response of an actuated composite beam are far more complex than the static case. There are non-linear aerodynamic forcings which interact with the beam elastic deformations. The inertial response of the beam also plays a role. The full aeroelasticity problem must be solved in this case. Therefore it is necessary to expand the current static adaptive model to the complete dynamic case.

The second recommendation is for the improvement of the anisotropic actuator material systems. These systems have a high material density and in the helicopter environment mass is a driving factor. Thus active materials with lower densities are required. The control authority of current anisotropic actuation material systems is limited by the material stiffness and actuation strains. An increase of these properties will greatly advance the applicability of anisotropic actuation for helicopter blade control.

From the parameter study it was evident that certain material anisotropies are more suited for twist actuation. By driving actuator development towards these material anisotropy combinations, the twist available from an actuated composite beam can be maximized. As a third recommendation for future IDEPFC material development: a specific goal for IDEPFC material technology would be to increase the transverse stiffness of the actuator (up to the point where the transverse stiffness is the same as the normal stiffness) while increasing the amount of transverse contraction for normal expansion during actuation. If this is impossible, different combinations of realizable anisotropies should be investigated to determine the optimum IDEPFC actuator for the blade twist application.

During the manufacturing of the model helicopter blade, difficulties were experienced with embedding the IDEPFC actuators effectively in the composite structure. Thick bonding layers reduced the effectiveness of the actuators. The fourth recommendation is for development of an effective means for attaining thin bonding layers when embedding conformable actuators on curved surfaces. One possible solution is a pressurized autoclave cure adapted for helicopter blade construction.

The final recommendation is geared towards future concepts for helicopter blade control using twist actuated, single cell, composite beams. During the course of this study three

different concepts were identified for helicopter blade control. The first of these concepts follows directly from this study: twisting the main spar, or any substructure in a helicopter blade, to obtain blade twist.

The second concept is that of a trailing edge flap which spans the complete length of the beam. This trailing edge flap could be driven with a twist actuated beam located in the aft section of the blade. An advantage of this concept is that less actuation material is needed to deform the lifting structure, as opposed to the main spar which is very stiff.

The third blade control concept using twist actuated beams is a variant of the trailing edge flap concept. Instead of having a flap which spans the length of the blade, a small discrete flap, on the out-board aft-section of the blade, can be rotated with a twist actuated beam embedded in the main spar. This concept requires little actuation material for operation because the base structure can be designed to be less torsionally stiff than the main spar while it moves the CG forward towards the quarter-chord instead of aft as would done by the complete span flap.

References

- Allik, H. and Hughes, T.J.R., "Finite Element Method for Piezoelectric Vibration", *International Journal of Numerical Methods in Engineering*, Vol. 2, 1970, pp. 151-157.
- Barrett, R.M., "Actuation Strain Decoupling through Enhanced Directional Attachment in Plates and Aerodynamic Surfaces", *Proceedings of the 1st European Conference on Smart Structures and Materials*, Glasgow, United Kingdom, May 1992, pp 383-386.
- Barret, R.M., "Modeling Techniques and Design Principles of a Low Aspect Ratio Aeroservoelastic Wing", *Proceedings of the 1993 North American Conference on Smart Structures and Materials*, Albuquerque, NM, 1993, pp. 107-118, SPIE Paper No. 1917-10.
- Bauchau, O.A., "A Beam Theory for Anisotropic Materials", *Transactions of the ASME*, Vol. 52., June 1985, pp. 416-422.
- Bent, A.A., Hagood, N.W. and Rodgers, J.P., 1993, "Anisotropic Actuation with Piezoelectric Fiber Composites", *Journal of Intelligent Material Systems and Structures*, Vol.6 No.3, May 1995, pp. 338-349.
- Bent, A.A. and Hagood, N.W., 1995, "Improved Performance in Piezoelectric Fiber Composites using Interdigitated Electrodes.", *Proceedings of the 1995 North American Conference on Smart Structures and Materials*, San Diego, CA., SPIE Paper No. 2441-50.
- Berlincourt, D., Krueger, H. and Near, C., "Important Properties of Morgan Matroc Piezoelectric Ceramics", TP-226, Electro Ceramics Division, Morgan Matroc, Inc., Bedford, OH.
- Blake, A., "Handbook of Mechanics, Materials, and Structures", John Wiley and Sons, New York, 1985, pp. 290.
- Boresi, A.P. and Sidebottom, O.M., "Advanced Mechanics of Materials", John Wiley and Sons, New York, 1985, pp. 169.
- Boswell, L.F., "The Finite Element Analysis of Thin Walled Box Beam Structures", *Finite Element Applications to Thin Walled Structures*, Elsevier Applied Science, 1990, pp. 157-198.
- Bueller, W.J. and Wiley, R.C., "Nickel - Base Alloys", U.S. Patent 3174851, 1965.

- Butler, J.L., "Application Manual for the Design of ETREMA Terfenol-D Magnetostrictive Transducers", ETREMA Products Inc., 1988.
- Bisplinghoff, R.L. and Ashley, H., "Principles of Aeroelasticity", Dover Publications, 1975.
- Chan, K.H. and Hagood, N.W., "Modeling of Non-Linear Piezoceramics for Structural Actuation", Proceedings of the Smart Structures and Intelligent Systems Conference, Orlando, FL., February. 1994, SPIE Proceedings, Vol. 2190, pp. 194-205.
- Chandra, R., Stemple, A.D. and Chopra, I., "Thin Walled Composite Beams Under Bending, Torsional, and Extensional Loads", Journal of Aircraft, July 1990, Vol. 27, No. 7, pp. 619-626.
- Chen, P. and Chopra, I., "Hover Testing of a Smart Rotor with Induced-Strain Actuation of Blade Twist", Proceedings of the 36th AIAA/ASME/ASCE/AHS/ASC Structures, Structural Dynamics and Materials Conference, New Orleans, LA, April 1995, pp. 2836-2853, AIAA Paper 95-1097-CP.
- Cook, R.D., Malkus, D.S. and Plesha, M.E., "Concepts and Applications of the Finite Element Analysis", John Wiley and Sons, New York, 3rd Edition, 1989.
- Crawley, E.F. and de Luis, J., "Use of Piezoelectric Actuators as Elements of Intelligent Structures", AIAA Journal, Vol.25, No. 10, 1987, pp. 1373-1385.
- Crawley, E.F. and Lazarus, K., "Induced Strain Actuation of Isotropic and Anisotropic Plates", AIAA Journal, Vol. 29, No. 6, June 1991, pp. 944-951.
- Ehlers, S.M. and Weisshaar, T.A., "Static Aeroelastic Behavior of an Adaptive Laminated Piezoelectric Composite Wing", Proceedings of the 31th AIAA/ASME/ASCE/AHS/ASC Structures, Structural Dynamics and Materials Conference, Long Beach, CA, April 1990, pp. 1611-1623, AIAA Paper No. 90-1078-CP.
- Ehlers, S.M. and Weisshaar, T.A., "Effect of Adaptive Materials on Static Aeroelastic Control", Proceedings of the 33th AIAA/ASME/AHS/ASC Structures, Structural Dynamics and Materials Conference, Dallas, TX., April 1992, AIAA Paper No. 92-2526-CP.
- Ehlers, S.M., "Active Closed Cell Beam Shape Control", Proceedings of the 35th AIAA/ASME/AHS/ASC Structures, Structural Dynamics and Materials Conference, Hilton Head SC, April 1994, pp. 320-332.
- Fenn, R.C., Downer, J.R., Bushko, D.A., Gondhalekar, V. and Ham, N.D., "Terfenol-D Driven Flaps for Helicopter Vibration Reduction", SPIE Proceedings, Vol. 1917, July 1993, pp. 407-418.
- Fripp, M., Hagood, N.W. and Luoma, L., "Distributed Structural Actuation with Electrostrictives", Proceedings of the Smart Structures and Intelligent Systems Conference, Orlando, FL., February 1994, SPIE Proceedings, Vol. 2190, pp. 575-585.
- Ghandi, K. and Hagood, N.W., "Shape memory Ceramic Actuation of Adaptive Structures", Proceedings of the 35th AIAA/ASME/AHS/ASC Structures, Structural Dynamics and Materials Conference, Hilton Head SC, April 1994, pp. 221-231, AIAA Paper No. 94-1758-CP.
- Giurgiutiu, V., Chaudhry, Z., and Rogers, C.A., "Engineering Feasibility of Induced Strain Actuators for Rotor Blade Active Vibration Control.", SPIE Proceedings, Vol. 2190, September 1994, pp. 107-122.

-
- Hagood, N.W., Chung, W.H., and von Flotow, A., "Modeling of Piezoelectric Actuator Dynamics for Active Structural Control", *Journal of Intelligent Material Systems and Structures*, July 1990, Vol. 1, pp. 327-354.
- Hagood, N.W. and Bent, A.A., "Development of Piezoelectric Fiber Composites for Structural Actuation", *Proceedings of the 34th AIAA/ASME/AHS/ASC Structures, Structural Dynamics and Materials Conference*. La Jolla, CA, April 1993, AIAA Paper No. 93-1717-CP.
- Hagood N.W., Kindel, R., Ghandi, K., and Gaudenzi, P., "Improving Transverse Actuation of Piezoceramics using Interdigitated Surface Electrodes.", *Proceedings of the 1993 North American Conference on Smart Structures and Materials*, Albuquerque, NM, SPIE Paper No. 1917-25. 1993.
- Hodges, D.H., "Review of Composite Rotor Blade Modeling", *AIAA Journal*, Vol. 28, No. 3, March 1990, pp. 561 - 565.
- Hercules, "AS4/3501-6", *Magnamite Product Data Sheet*, No. 843-1, Magna, UT.
- Hurtado, I., Van Humbeeck, J. and Moo, C., "Elastic Modulus Behavior in Dual Phase Cu-Al-Ni-Ti-(Mn) Shape Memory Alloys", *Proceedings of the Smart Structures and Materials Conference*, San Diego, CA., February 1995, SPIE Proceedings Vol. 2441, pp. 131-138.
- IEEE Std 176-1978, "IEEE Standard on Piezoelectricity", *Institute of Electrical and Electronic Engineers*, 1978.
- Jaffe, B., Cook, W.R. and Jaffe, H., "Piezoelectric Ceramics", *Academic Press*, New York, 1971.
- Jensen, D.W., Crawley, E.F. and Dugundji, J., "Vibration of Cantilevered Graphite/Epoxy Plates with Bending Torsion Coupling", *Journal of Reinforced Plastics and Composites*, Vol. 1, July 1982, pp. 254-269.
- Jones, R.M., "Mechanics of Composite Materials", *Hemisphere*, New York, 1975.
- Labace, P.A., Beaumont, M., Brewer, J.C. and Varnerin, C.F., "TELAC Manufacturing Course Class Notes", *TELAC Report No. 88-4b*, 1991.
- Lazarus, K.B. and Crawley, E.F., "Multivariable Active Lifting Surface Control Using Strain Actuation - Analytical and Experimental Results", *Proceedings of the 3rd International Conference on Adaptive Structures*, San Diego, CA, November 1992, pp. 87-101.
- Libove, C., "Stresses and Rate of Twist in Single Cell Thin Walled Beams with Anisotropic Walls", *AIAA Journal*, September 1988, Vol. 26, No. 9, pp. 1107-1118.
- Librescu, L. and Song, O., "Static Aeroelastic Tailoring of Composite Aircraft Wings Modeled as Thin Walled Beam Structures", *Achievements in Composites in Japan and the United States*, Fifth Japan-US Conference on Composite Materials, Tokyo, Japan, 1990, pp. 141-149.
- Librescu, L. and Thangjitham, S., "Analytical Studies on Static Aeroelastic Behavior of Forward Swept Composite Wing Structures", *Journal of Aircraft*, Vol. 28, No. 2, February 1991, pp. 151-157.
- Lin, C.Y., Crawley, E.F. and Heeg, J., "Open Loop and Preliminary Closed Loop Results of a Strain Actuated Active Aeroelastic Wing", *Proceedings of the 36th AIAA/ASME/ASCE/AHS/ASC Structures, Structural Dynamics and Materials*

- Conference , New Orleans, LA, April 1995, pp. 1904-1914, AIAA Paper 95-1386-CP.
- Loewy, R.G., "Helicopter Vibrations: A Technical Perspective", *Journal of the American Helicopter Society*, Vol. 29, October 1984, pp. 4-30.
- Megson, T.H.G., "Aircraft Structures for Engineering Students", John Wiley and Sons, New York, 1990, pp. 240-264.
- Meirovitch, L., "Elements of Vibration Analysis", McGraw-Hill, 1986, pp. 250.
- Reich, G.W., van Schoor, M.C., Lin, C.Y. and Crawley, E.F., "An Active Aeroelastic Wing Model for Vibration and Flutter Suppression", *Proceedings of the 36th AIAA/ASME/ASCE/AHS/ASC Structures, Structural Dynamics and Materials Conference* , New Orleans, LA, April 1995, pp. 314-324, AIAA Paper No. 95-1193-CP.
- Rehfield, L.W., "Design Analysis Methodology for Composite Rotor Blades", *Proceedings of the Seventh DOD/NASA Conference on Fibrous Composites in Structural Design*, AFWAL-TR-85-3094, June 1985, pp. V(a)-1 - V(a)-15.
- Rehfield, L.W., Atilgan, A.R. and Hodges, D.H., "Nonclassical Behavior of Thin Walled Composite Beams with Closed Cross Sections", *Proceedings of the American Helicopter Society National Technical Specialists' Meeting: Advanced Rotorcraft Structures*, Williamsburg, VA., October 1988, pp. 42-50.
- Rehfield, L.W. and Atilgan, R., "Shear Center and Elastic Axis and their usefulness for Composite Thin Walled Beams", *Proceeding of the American Society for Composites, 4th Technical Conference*, 3-5 October 1989, pp. 179-188.
- Rodgers, J.P. and Hagood, N.W., 1995, "Manufacture of Adaptive Composite Plates Incorporating Piezoelectric Fiber Composite Plies", *Proceeding of the 36th AIAA/ASME/ASCE/AHS/ASC Structures, Structural Dynamics and Materials Conference* , New Orleans, LA, April 1995, pp. 2824-2835. AIAA Paper No. 95-1096-CP.
- Rodgers, J.P., Bent, A.A., Pizzochero, A., and Hagood, N.W., "Preliminary Characterization of Interdigitated Electrode Piezoelectric Fiber Composites for Rotor Blade Applications", To be presented at the SPIE Conference on Smart Structures and Intergrated Systems, San Diego, CA, 26-29 February, 1996.
- Sandford, A., "YCH-47D Fiberglass Rotor Blade Loads and Structural Analysis", Boeing-Vertol Report No. 145-SS-607.1.1, April 1978.
- Shaw, J. and Albion, N., "Active Control of the Helicopter Rotor for Vibration Reduction", *Journal of the American Helicopter Society*, July 1981, pp. 32-39.
- Shaw, J., Albion, N., Hanker, E. and Teal, R., "Higer Harmonic Control: Wind Tunnel Demonstration of Fully Effective Vibratory Hub Force Suppression", *Proceedings of the 41st Annual Forum of the AHS*, 1985, pp. 1-15.
- Shirk, M.H., Hertz, T.J., and Weisshaar, T.A., "Aeroelastic Tailoring - Theory, Practise and Promise", *Journal of Aircraft*, January 1986, Vol. 23, No. 1, pp 6-18.
- Smith, E.C. and Chopra, I., "Formulation and Evaluation of an Analytical Model for Composite Box Beams", *Proceedings of the 31st AIAA/ASME/AHS/ASC Structures, Structural Dynamics and Materials Conference*, April 1990, pp. 759-782. AIAA Paper No. 90-0962-CP.

-
- Song, O., Librescu, L and Rogers, C.A., "Application of Adaptive Technology to Static Aeroelastic Control of Wing Structures", *AIAA Journal* , Vol. 30, No. 12, December 1992, pp. 2882-2889.
- Song, O. and Librescu, L., "Vibrational Behavior of Rotating Helicopter Blades Incorporating Adaptive Capabilities", *SPIE Conference on Smart Structures and Intelligent Systems*, 1993.
- Spangler, R.L. and Hall, S.R., "Piezoelectric Actuators for Helicopter Rotor Control", *Proceedings of the 31st AIAA/ASME/ASCE/AHS/ASC Structures, Structural Dynamics and Materials Conference*, Long Beach, CA, April 1990, pp. 1589-1599. AIAA Paper No. 90-1076-CP.
- Wada, B.K., Fanson, J.L. and Crawley, E.F., "Adaptive Structures", *Proceedings of the ASME Winter Annual Meeting*, San Francisco, CA, December 1989. pp. 1-8.
- Walz, C. and Chopra, I., "Design and Testing of a Helicopter Rotor Model with Smart Trailing Edge Flaps", *Proceedings of the 35th AIAA/ASME/AHS/ASC Structures, Structural Dynamics and Materials Conference*, Hilton Head SC, April 1994, pp. 309-319.
- Wang, K.W., Kim., Y.S. and Shea, D.B., "Structural Vibrational Control via Electrorheological-Fluid-Based Actuators with Adaptive Viscous and Frictional Damping", *Journal of Sound and Vibration*, Vol. 177, No. 2, pp. 227-237.
- Webster's College Dictionary, Random House, New York, 1992.
- Weisshaar, T.A., "Divergence of Forward Swept Composite Wings", *Journal of Aircraft*, Vol. 17, 1980, pp. 442-448.
- Weisshaar, T.A. and Foist, B.L., "Vibration Tailoring of Advanced Composite Lifting Structures", *Journal of Aircraft*, February 1985, Vol. 22, No. 2, pp. 141-147.
- Weisshaar, T.A., "Aeroelastic Tailoring - Creative Use of Unusual Materials", *Proceedings of the 28th AIAA/ASME/ASCE/AHS/ASC Structures, Structural Dynamics and Materials Conference*, Monterey, CA, April 1987, AIAA Paper No. 87-0976-CP.
- Zienkiewicz, O.C., "The Finite Element Method in Engineering Science", McGraw-Hill, London, 1971.

Appendix A

MATLAB Code

Beam.m

```
% BEAM
%
% Composite Box Beam Analysis
%
% BEAM do the analysis of a composite single cell box beam.
%   The analysis consists of mass, cg, pitch inertia as well
%   as a finite element analysis to determine displacements given
%   a certain load condition. Properties may vary around the
%   circumference of the beam and any cross sectional shape can
%   be handled. The cross sectional shape is built from linear
%   pieces(panels) and in every panel the properties must be constant.
%   The elements used in the analysis constructed earlier by the m-file
%   "elem.m"

%-----
%
%   Author: Andries J. du Plessis
%   Original:   March 29 1994
%   Modified:   October 1995
%   Copyright:  MIT-SERC-AMSL (c) 1994
%-----

clear;
clg;
clc;

%-----
%---- Define the beam -----
%-----
%---- [Element-Names]
elements = ['modelBn'
           'modelBa'
           'modelBn'
           'modelBa']
```

```

        'modelBn'
        'modelBa'
        'modelBn'];

%----- [Beam length for specific element   Element length];
def = [ 0.026  0.003
        0.124  0.004
        0.006  0.003
        0.124  0.004
        0.006  0.003
        0.124  0.004
        0.039  0.003];

numel = size(elements,1); % Number of different element types used in analysis
n = def(:,1)./def(:,2);
%----- Point Loads at the end of the beam
Fp = [0 0 0 0 0 0]; %-----[N Qy Qz Mx My Mz Qw]'

%-----
%----- Construct spanwise location vectors for analysis -----
%-----
nod = 1;
x = [0];
for i = 1:numel,
    for j = 1:n(i),
        if nod == 1
            xi = 0;
            xe = def(i,2);
            xp = [xi;xe];
            x = [x;xe];
            nod = nod + 1;
        else
            xi = xi+def(i,2);
            xe = xe+def(i,2);
            xp = [xp; xi; xe];
            x = [x;xe];
            nod = nod+1;
        end
    end
end

%-----
%----- Read element properties and construct global variables --
%-----
%----- Global variables
%     Prop - matrix with mass/length, CG, etc.
%     K - Stiffness matrix
%     F - Element forcing
Prop = zeros(length(xp),4); % - [Area, mass/length, CG, pitch inertia]
K = sparse(7*nod,7*nod);
F = zeros(7*nod,1);
nodc1 = 1;
nodc2 = 14;
pc = 1;
for i = 1:numel,
    fin = sprintf('%s',deblank(elements(i,:))); % Inputfile
    eval(['load ' fin]);
end

```

```

if dx ~= def(i,2)
error('Specified element length do not correlate with length read');
end
for j = 1:n(i),
    Prop(pc:pc+1,:) = [cprop;cprop];
    K(nodc1:nodc2,nodc1:nodc2)=K(nodc1:nodc2,nodc1:nodc2)+Ke;
    F(nodc1:nodc2,1)=F(nodc1:nodc2,1)+Fq+Fa;
    nodc1 = nodc1+7;
    nodc2 = nodc2+7;
    pc = pc+2;
end
end
rcs=(nod-1)*7+1;
F(rcs:7*nod,1)=F(rcs:7*nod,1)+Fp; %----- Add the point loads

%-----
%----- Force Displacement Analysis -----
%-----

%----- Remove the constraints for the cantilevered beam
uu=K(8:7*nod,8:7*nod)\F(8:7*nod,1);
u = [0;0;0;0;0;0;uu];
U = zeros(nod,1);
V = zeros(nod,1);
W = zeros(nod,1);
Phi = zeros(nod,1);
By = zeros(nod,1);
Bz = zeros(nod,1);
Phi_x = zeros(nod,1);
W_x = zeros(nod,1);
for i=2:nod,
    U(i) = u(7*(i-1)+1,1);
    V(i) = u(7*(i-1)+2,1);
    W(i) = u(7*(i-1)+3,1);
    Phi(i) = u(7*(i-1)+4,1);
    By(i) = u(7*(i-1)+5,1);
    Bz(i) = u(7*(i-1)+6,1);
    Phi_x(i)= u(7*(i-1)+7,1);
    W_x(i) = (W(i)-W(i-1))/(x(i)-x(i-1));
end

%-----
%----- Result Plotting -----
%-----

%----- Properties
figure(1)
subplot(4,1,1)
plot(xp,Prop(:,1));
xlabel('x-coordinate [m]');
ylabel('Cross Sectional Area [m^2]');
grid
subplot(4,1,2)
plot(xp,Prop(:,2));
xlabel('x-coordinate [m]');
ylabel('Mass/Unit Length [kg/m]');
grid
subplot(4,1,3)

```

```
plot(xp,Prop(:,3));
xlabel('x-coordinate [m]');
ylabel('CG-Location [m]');
grid
subplot(4,1,4)
plot(xp,Prop(:,1));
xlabel('x-coordinate [m]');
ylabel('Pitch Inertia [kgm^4]');
grid

%----- Displacements
figure(2)
subplot(2,1,1);
%plot(x*1000,W*1000);
plot(x,W);
xlabel('x-coordinate [mm]');
ylabel('Bending Displacement [mm]');
grid
subplot(2,1,2);
plot(x,Phi*180/pi);
%plot(x,Phi)
xlabel('x-coordinate [mm]');
ylabel('Twist [deg]');
grid
```

Elem.m

```

% ELEM
%
% Composite Box Beam Analysis - Element
%
% ELEM do the analysis of a composite single cell box beam element.
%   The analysis consists of mass, cg, pitch inertia as well
%   as a finite element structural matrix. Properties may vary around the
%   circumference of the beam and any cross sectional shape can
%   be handled. The cross sectional shape is built from linear
%   pieces(panels) and in every panel the properties must be constant.
%   The result from this m-file is the cross sectional properties for
%   the element as well as the element stiffness matrix.
%   The output from this m-file are read into the global finite element
%   program.

%-----
%
%   Author:      Andries J. du Plessis
%   Original:    March 29 1994
%   Modified:    October 16 1995
%   Copyright:   MIT-SERC-AMSL (c) 1994
%-----

clear;
clg;
clc;

%-----
%---- Read Input -----
%-----
inputf = input('What is the name of the input file? (No extensions!) :','s');
fout = sprintf('%s.out',inputf);
idout = fopen(fout,'wt');
eval(inputf);

%---- Input Set Printing
fprintf(idout,'Input File: %s\n',inputf);
fprintf(idout,'----- \n\n');
fprintf(idout,'Cross Section\n');
fprintf(idout,'----- \n');
fprintf(idout,' Y Z \n');
fprintf(idout,' %6.1f %6.1f \n',yz);
fprintf(idout,'\n');
fprintf(idout,'Materials\n');
fprintf(idout,'----- \n');
for i = 1:m,
    for j = 1:n,
        fprintf(idout,'%2d ',mat(i,j));
    end
    fprintf(idout,'\n');
end
fprintf(idout,'\n');
fprintf(idout,'Thicknesses\n');

```

```

fprintf(idout,'-----\n');
for i = 1:m,
    for j = 1:n,
        fprintf(idout,'%7.5f ',thick(i,j));
    end
    fprintf(idout,'\n');
end
fprintf(idout,'\n');
fprintf(idout,'Angles of Plies\n');
fprintf(idout,'-----\n');
for i = 1:m,
    for j = 1:n,
        fprintf(idout,'%5.1f ',ang(i,j));
    end
    fprintf(idout,'\n');
end
fprintf(idout,'\n');
fprintf(idout,'Voltages Top & Bottom Plies\n');
fprintf(idout,'-----\n');
for i = 1:m,
    for j = 1:2*n,
        fprintf(idout,'%5d ',volt(i,j));
    end
    fprintf(idout,'\n');
end
fprintf(idout,'\n');
fprintf(idout,'Distributed Forces\n');
fprintf(idout,'-----\n');
fprintf(idout,'%4.1f %4.1f %4.1f %4.1f %4.1f %4.1f %4.1f\n',q);
fprintf(idout,'\n');

%-----
%---- Cross Sectional Properties -----
%-----

%---- Geometric Properties of Panels and Cross Section -----
%---- Lengths of linear panel pieces
leng = zeros(m,1);
for i = 1:m,
    leng(i) = sqrt((yz(i+1,1)-yz(i,1))^2+(yz(i+1,2)-yz(i,2))^2);
end
%---- Derivatives of linear panel pieces
deriv = zeros(m,2);
for i=1:m,
    deriv(i,1) = (yz(i+1,1)-yz(i,1))/leng(i);
    deriv(i,2) = (yz(i+1,2)-yz(i,2))/leng(i);
end
%---- Normal projections of the linear panels
normp = zeros(m,1);
for i=1:m;
    normp(i) = -yz(i,1)*deriv(i,2)+yz(i,2)*deriv(i,1);
end

%---- Cross section perimeter length
c = sum(leng);

%---- Cross sectional area

```

```

A=0;
for i = 1:m,
    dA = 0.5*normp(i)*leng(i);
    A = A + dA;
end

%----- Physical Properties of the Panels and Cross Section -----
%----- Panel mass/unit length (rho*thickness - mass/unit area)
pmassl = zeros(m,1);
for i = 1:m,
    for j = 1:n,
        if thick(i,j)>0
            rho = matprop(2,mat(i,j));
            mul = rho*thick(i,j);
            pmassl(i) = pmassl(i) + mul;
        end;
    end
    mul= 0;
end

%----- Cross sectional mass per unit length
mass = leng'*pmassl; %----- Based on a per unnit length piece of the beam

%----- Cross Section CG
sumcg =0;
for i=1:m,
    dcg = leng(i)*pmassl(i)*(yz(i+1,1)+yz(i,1))/2;
    sumcg = sumcg+dcg;
end
CG = sumcg/mass;

%----- Cross Section Pitch Inertia
%----- Based on a unit length of the beam
Iner = 0;
for i = 1:m,
    dI = leng(i)*pmassl(i)*(((yz(i+1,2)+yz(i,2))/2)^2+((yz(i+1,1)...
        + yz(i,1))/2)^2) + leng(i)^3*pmassl(i)/12;
    Iner = Iner+dI;
end
cprop = [A mass CG Iner];

%----- Stiffness and Actuation Properties of Panels and Cross Section -----
%----- Panel laminate properties
%----- Panel plate stiffness and stress actuation properties
pstiff = zeros(m,6);
pstract = zeros(m,3);
pGeff = zeros(m,1);
for i = 1:m,
    k = 0.0;
    layup = [];
    prop = [];
    E = [];
    for j = 1:n,
%-----Exclude the layers with zero thickness/properties etc.
        if thick(i,j) > 0
            k = k+1;
            layup(k,1) = ang(i,j);

```

```

    prop(k,1) = thick(i,j);
    prop(k,2:7) = matprop(1,mat(i,j));
    prop(k,8:9) = matprop(3,mat(i,j));
    %----- Be sure to use the right thicknesses (eg:IDEPFC) for Field E
    E(k,1) = (volt(i,2*j-1)-volt(i,2*j))/((45e-3)*0.0254); %thick(i,j);
  end
end
[L,P,Geff] = panstif(prop,layup); % Can rewrite this not to transfer [L]
pstiff(i,1:6) = [L(1,1) L(1,2) L(1,3) L(2,2) L(2,3) L(3,3)];
pstract(i,1:3) = (P*E);
pGeff(i) = Geff;
end

%----- Warping Function for the Cross Section -----
%----- Warping specified at the cordinates around the contour
[psi,alf]=warpfunc(A,c,leng,normp,pGeff);

%----- Cross sectional stiffness
ord = 4; %----- Order of guassian integration
[Kc,Fac] = Cstiff(yz,leng,deriv,A,pstiff,pstract,ord,psi,alf);

%-----
%----- Element Property Output -----
%-----
fprintf(idout,'Cross Sectional Properties\n');
fprintf(idout,'-----\n');
fprintf(idout,'Area [m^2]: %7.4f\n',A);
fprintf(idout,'Perimeter Length [m]: %7.4f\n',c);
fprintf(idout,'Mass [kg/m]: %7.4f\n',mass);
fprintf(idout,'Pitch Inertia [kgm^2]: %10.6f\n',Iner);
fprintf(idout,'CG [m]: %7.4f\n',CG);
%-----
%----- Element Stiffness -----
%-----
%----- Integration to obtain element stiffness matrix
ord = 4; % Order of Gaussian integration (2<n<5)
Ke = elemstif(dx,yz,leng,deriv,A,pstiff,psi,alf,ord);
%-----
%----- Element Electrical Forcing -----
%-----
%----- Integration to obtain electrical forcing
ord = 4; % Order of Gaussian integration (2<n<5)
Fa = elecmech(dx,yz,leng,deriv,A,pstract,psi,alf,ord);
%-----
%----- Distributed Loading -----
%-----
%----- Integration of the distributed loading to obtain nodal loads
ord = 3; % Order of Gaussian integration (2<n<5)
Fq = distrib(dx,q,ord);
%-----
%----- FEM Property Output -----
%-----
output = [inputf ' dx cprop Ke Fq Fa'];
eval(['save ' output]);

```


Inputf.m

```

% INPUTF
%
% Input file for the element analysis
%
% INPUTF defines the element cross section, materials, layups used in the
%   different linear panels and the actuation

%-----
%
%   Author:      Andries J. du Plessis
%   Original:    October 17 1995
%   Modified:    October 31 1995
%   Copyright:   MIT-SERC-AMSL (c) 1994
%-----

%----- Element General Properties -----
dx = 0.004; %----- Element length in analysis

%----- Cross-Section Coordinates -----
yz = 1e-3*[-15    0
           -12.5  1.77
            -10   2.34
             -5   2.86
              0   3
              5   2.90
             10   2.65
            12.5  2.48
             15   2.28
             20   1.83
             25   1.31
             30   0.72
             35   0
             30  -0.72
             25  -1.31
             20  -1.83
             15  -2.28
            12.5 -2.48
             10  -2.65
              5  -2.90
              0  -3
             -5  -2.86
            -10  -2.34
            -12.5 -1.77
            -15   0];

%----- Laminate Panels -----
% mat = [material plies in panels] %-----Size(panels,max #plies)
% Index of Materials - Look in matprop.m to get the current values
mat = [ 4  4  0
       4 14  4
       4 14  4
       4 14  4
       4 14  4
       4 14  4

```



```
0 0 0
0 0 0
0 0 0
0 0 0
0 0 0
0 45 0
0 45 0
0 45 0
0 45 0
0 45 0
0 45 0
0 0 0];

%volt = [Voltages at the top and bottom of every ply]
V = -1800;
volt = [0 0 0 0 0 0
        0 0 0 0 0 0
        0 0 V 0 0 0
        0 0 V 0 0 0
        0 0 V 0 0 0
        0 0 V 0 0 0
        0 0 0 0 0 0
        0 0 0 0 0 0
        0 0 0 0 0 0
        0 0 0 0 0 0
        0 0 0 0 0 0
        0 0 0 0 0 0
        0 0 0 0 0 0
        0 0 0 0 0 0
        0 0 0 0 0 0
        0 0 0 0 0 0
        0 0 0 0 0 0
        0 0 0 0 0 0
        0 0 0 0 0 0
        0 0 0 0 0 0
        0 0 0 0 0 0
        0 0 0 0 0 0
        0 0 0 0 0 0
        0 0 0 0 0 0];

%----- Element loading -----
%----- Distributed loading (assume constant distributed loads)
q = [0 0 0 0 0 0]'; %----- [qx qy qz mx my mz qw]';
```

Matprop.m

```

function outp=matprop(tipe,varb)
%   MATPROP: Subroutine that returns the material properties
%   based on material selection which is done during the
%   initialization phase. The output from this subroutine
%   gives the stiffness matrix [C], the inplane actuation matrix [d],
%   and the density. Other options would be to include the dielectric
%   for use when the full coupled electro-mechanical problem are
%   considered.
%   Type 1 - [C]
%   Type 2 - Density
%   Type 3 - Electrical
%
%   Units : SI except were specified otherwise

%-----
%
%   Author:      Andries J. du Plessis
%   Original:    August 8 1995
%   Modified:    October 31 1995
%   Copyright:   MIT-AMSL (c) 1995
%-----

if varb<0
    error('Material specification positive number')
elseif varb > 15
    error('Unspecified material used')
end

% Index of Materials
%   0 - Air
%   1 - Steel
%   2 - Aluminum
%   3 - AS/4-3501-6
%   4 - E-Glass (Wet layup used for 1/16th model blade)
%   5 - Capton Electrode
%   6 - AS4 (Smith values in English)
%   7 - T300 Tape
%   8 - Kevlar 49 Style 120
%   9 - S2-Glass used by Boeing
%   10 - E/Glass used by Boeing
%   11 - Titanium (BIN)
%   12 - SP250 E/Glass (BIN)
%   13 - IDEPFC U-Series Model values
%   14 - IDEPFC U-Series experimentally augmented values
%   15 - IDEPFC (BIN)
%
%   rho  d31  d32  EI  Et  vlt  Glt  0  0
materl=[7800 0 0 205e9 205e9 0.3 77e9 0 0 %--1-Steel
2800 0 0 69e9 69e9 0.33 26e9 0 0 %--2-Al 6061-T6
1520 0 0 142e9 9.81e9 0.3 6e9 0 0 %--3-AS4/3501-6
1800 0 0 14.8e9 13.6e9 0.19 1.9e9 0 0 %--4-#120E-Glass(wet)
1100 0 0 1e9 1e9 0.3 0.7e9 0 0 %--5-Electrode
0.055 0 0 20.59e6 1.42e6 0.42 0.87e6 0 0 %--6-AS4-Smith(BIN)

```

```
1522 0 0 124e9 10.3e9 0.34 4.8e9 0 0 %--7-T300 Tape
1370 0 0 29e9 29e9 0.05 2.1e9 0 0 %--8-Kevlar49/120
1855 0 0 43.4e9 12e9 0.28 3.6e9 0 0 %--9-S2 Glass
1855 0 0 17.9e9 17.9e9 0.15 4.1e9 0 0 %--10-E-Glass/120
0.16 0 0 15e6 15e6 0.3 6.2e6 0 0 %--11-Titanium(BIN)
0.067 0 0 6.3e6 1.74e6 0.3 0.52 0 0 %--12-SP250 E/G (BIN)

% rho d31 d32 Q11 Q12 Q13 Q22 Q23 Q33 Plane Stress Props!!!
4810 147e-12 -61e-12 44.5e9 6.56e9 0 18.5e9 0 5.5e9 %--13-IDEPFC
4810 381e-12 -160e-12 32.8e9 6.26e9 0 17.3e9 0 5.5e9 %--14-IDEPFC_exp
0.17 5.79e-9 -2.43e-9 6.45e6 0.95e6 0 2.68e6 0 0.8e6]; %--15-IDEPFC (BIN)

if tipe == 1
    if varb < 12
        Q = plyp(materl(varb,4:7));
        outp = [Q(1,1) Q(1,2) Q(1,3) Q(2,2) Q(2,3) Q(3,3)];
    else
        outp = materl(varb,4:9);
    end
end

if tipe == 2
    outp = materl(varb,1);
end

if tipe == 3
    outp = materl(varb,2:3);
end
```

Panstif.m

```

function [L,P,Geff] = panstif(prop,layup)
% PANSTIF
%
% Panel stiffness
%
% PANSTIF determines the stiffness of a composite panel with the usage of
%   CLPT. Certain stiffnesses are ignored in the analysis due to the
%   plane nature of the problem. The reduced stiffnesses determined
%   through static condensation on the original stiffness matrix.
%   The effective electric properties are also determined
%   in this function.
%   Assumption: Layup is such that there will always be a ply
%   boundary at the midplane.
%   Q - Plane stress lamina properties
%
%-----
%
%   Author:      Andries J. du Plessis
%   Date:        April 4 1994
%   Modified:    October 10 1995
%   Copyright:   MIT-SERC-AMSL (c) 1994
%
%-----
%----- Error messages
if nargin ~= 2
    error('Need property matrix and layups to determine panel stiffness');
end

[mx,nx] = size(prop);
[my,ny] = size(layup);
if mx~=my
    error('Property matrix and Layup matrix do not correlate');
end
n = length(prop(:,1));
A = zeros(3);
B = zeros(3);
D = zeros(3);
%----- Ply location matrices (relative to midline plane)
zu = zeros(1,n);
zl = zeros(1,n);
thick = 0.0;
for i = 1:n,
    thick = thick + prop(i,1);
end
zu(1) = thick/2;
zl(1) = zu(1)-prop(1,1);
for i=2:n,
    zu(i) = zu(i-1)-prop(i-1,1);
    zl(i) = zl(i-1)-prop(i,1);
end
%----- Stiffness calculation
for i=1:n,
    Q = [prop(i,2) prop(i,3) prop(i,4);
        prop(i,3) prop(i,5) prop(i,6);

```

```

        prop(i,4) prop(i,6) prop(i,7)];
% Q = plyp(prop(i,2:5));
Qr = plyrp(Q,layup(i)); % Rotate the ply properties
z1 = zu(i)-zl(i);
z2 = (1/2)*(zu(i)^2-zl(i)^2);
z3 = (1/3)*(zu(i)^3-zl(i)^3);
A = A+Qr*z1;
B = B+Qr*z2;
D = D+Qr*z3;
end
if A(2,2)~=0
    A(2,2)=0.00001;
end
%----- Stiffness reduction
L = zeros(3);
L(1,1) = A(1,1) - (A(1,2)^2)/A(2,2);
L(1,2) = A(1,3) - (A(1,2)*A(2,3))/A(2,2);
L(1,3) = B(1,1) - (A(1,2)*B(1,2))/A(2,2);
L(2,1) = L(1,2);
L(2,2) = A(3,3) - (A(2,3)^2)/A(2,2);
L(2,3) = B(1,3) - (A(2,3)*B(1,2))/A(2,2);
L(3,1) = L(1,3);
L(3,2) = L(2,3);
L(3,3) = D(1,1) - (B(1,2)^2)/A(2,2);
for i=1:3,
    for j=1:3,
        if abs(L(i,j))<0.00001
            L(i,j)=0.0;
        end
    end
end
%----- Electrical properties
P = zeros(3,n);
GAM = zeros(3,1);
PI = zeros(3,1);
for i=1:n,
% Q = plyp(prop(i,2:5));
% e = Q*([0 0 prop(i,6); 0 0 prop(i,7); 0 0 0]);
Q = [prop(i,2) prop(i,3) prop(i,4);
     prop(i,3) prop(i,5) prop(i,6);
     prop(i,4) prop(i,6) prop(i,7)];
e = Q*([0 0 prop(i,8); 0 0 prop(i,9); 0 0 0]);
er = vectrr(e,layup(i));
z1 = zu(i)-zl(i);
z2 = (1/2)*(zu(i)^2-zl(i)^2);
GAM = er*[0 0 1]'*z1; % Only have field applied in the n-direction
PI = er*[0 0 1]'*z2; % Only have field applied in the n-direction
P(1,i) = GAM(1)-GAM(2)*A(1,2)/A(2,2);
P(2,i) = GAM(3)-GAM(2)*A(2,3)/A(2,2);
P(3,i) = PI(1)-GAM(2)*B(1,2)/A(2,2);
end
%----- Effective sheat stiffness for warping function
Geff=L(2,2)+((2*L(1,2)*L(1,3)*L(2,3)-L(1,2)^2*L(3,3)-L(1,1)*L(2,3)^2)...
/(L(1,1)*L(3,3)-L(1,3)^2));

```

Warpfunc.m

```

function [psi,alf]=warpfunc(A,c,leng,normp,Geff);
% WARPF
%
% Warping function around the circumference
%
% WARPF determines the warping function around the circumference of the
% composite boxbeam. The function does allow for variations in the
% stiffness around the circumference of the boxbeam.
% phi - matrix that contain warping function slopes and constants
% in the four panels
% alf - warping parameter (differs in every panel)
% Geff - Effective shear stiffness for the panel

%-----
%
% Author:      Andries J. du Plessis
% Date:       March 29 1994
% Modified:   October 10 1995
% Copyright:  MIT-SERC-AMSL (c) 1994
%-----

m = length(leng);

%----- Calculate the warping parameter
alfsum = sum(leng./Geff);
alf = (1./Geff)/alfsum;
%----- Calculate the interim warping function
psie = zeros(m,2);
psie(1,:) = [0 leng(1)*(-2*A*alf(1)+normp(1))];
for i = 2:m,
    psie(i,1)=psie(i-1,2);
    psie(i,2)=leng(i)*(-2*A*alf(i)+normp(i))+psie(i,1);
end
%----- Adjust the warping function to reflect symmetry and intergral req.
kint = sum((0.5*(psie(:,1)+psie(:,2))).*leng);
Kpsi = kint/c;
psi(:,1) = psie(:,1)-Kpsi;
psi(:,2) = psie(:,2)-Kpsi;

```


Cstiff.m

```

function [Kc,Fac] = Cstiff(yz,leng,deriv,A,pstiff,pstract,n,psi,alf);
% Cstiff
%
% Cross sectional stiffness
%
% Cstiff:function that do the integration to obtain the cross section
% stiffness.Integration is done with Gauss Quads with variable
% order of integration.
% A - Area
% pstiff - reduced plate stiffness
% pstract - reduced induced stress actuation
% psi - warping function description
% alf - extra constants used in warping function description
% n - order of the gaussian integration

%-----
%
% Author:      Andries J. du Plessis
% Date:       March 31 1994
% Modified:   October 12 1995
% Copyright:  MIT-SERC-AMSL (c) 1994
%-----

m = length(leng);

%----- Read Abiscissa and Weights for order n gaussian integration
AW = gausstab(n);

% ----- Integration for the Panels
Kc=zeros(7,7);
Fac = zeros(7,1);
dF = zeros(7,1);
for i = 1:m, %----- Integration across all the panels
    J = leng(i)/2; %---- Jacobian for transformation to [-1,1]
    %---- Determine the slope and intersection on [-1,1]
    myg = (yz(i+1,1)-yz(i,1))/2;
    cyg = (yz(i+1,1)+yz(i,1))/2;
    mzg = (yz(i+1,2)-yz(i,2))/2;
    czg = (yz(i+1,2)+yz(i,2))/2;
    mpsig = (psi(i,2)-psi(i,1))/2;
    cpsig = (psi(i,2)+psi(i,1))/2;
    alfa = alf(i);
    dy = deriv(i,1);
    dz = deriv(i,2);
    L11 = pstiff(i,1);
    L12 = pstiff(i,2);
    L13 = pstiff(i,3);
    L22 = pstiff(i,4);
    L23 = pstiff(i,5);
    L33 = pstiff(i,6);
    Nxxa = pstract(i,1);
    Nxxa = pstract(i,2);
    Mxxa = pstract(1,3);

```

for j = 1:n, %---- Gaussian integration of order n, 1-Dimensional

$$y = \text{myg} * \text{AW}(j,1) + \text{cyg};$$

$$z = \text{mzg} * \text{AW}(j,1) + \text{czg};$$

$$p = \text{mpsig} * \text{AW}(j,1) + \text{cpsig};$$

$$\begin{aligned} dk(1,1) &= L11; \\ dk(1,2) &= L12 * dy; \\ dk(1,3) &= L12 * dz; \\ dk(1,4) &= L12 * (-2 * A * \text{alfa}); \\ dk(1,5) &= L11 * z + L13 * dy; \\ dk(1,6) &= -L11 * y + L13 * dz; \\ dk(1,7) &= L11 * p; \end{aligned}$$

$$\begin{aligned} dk(2,1) &= dk(1,2); \\ dk(2,2) &= L22 * dy^2; \\ dk(2,3) &= L22 * dz * dy; \\ dk(2,4) &= L22 * (-2 * A * \text{alfa}) * dy; \\ dk(2,5) &= (L12 * z + L23 * dy) * dy; \\ dk(2,6) &= (-L12 * y + L23 * dz) * dy; \\ dk(2,7) &= L12 * p * dy; \end{aligned}$$

$$\begin{aligned} dk(3,1) &= dk(1,3); \\ dk(3,2) &= dk(2,3); \\ dk(3,3) &= L22 * dz^2; \\ dk(3,4) &= L22 * (-2 * A * \text{alfa}) * dz; \\ dk(3,5) &= (L12 * z + L23 * dy) * dz; \\ dk(3,6) &= (-L12 * y + L23 * dz) * dz; \\ dk(3,7) &= L12 * p * dz; \end{aligned}$$

$$\begin{aligned} dk(4,1) &= dk(1,4); \\ dk(4,2) &= dk(2,4); \\ dk(4,3) &= dk(3,4); \\ dk(4,4) &= L22 * (-2 * A * \text{alfa})^2; \\ dk(4,5) &= (L12 * z + L23 * dy) * (-2 * A * \text{alfa}); \\ dk(4,6) &= (-L12 * y + L23 * dz) * (-2 * A * \text{alfa}); \\ dk(4,7) &= L12 * p * (-2 * A * \text{alfa}); \end{aligned}$$

$$\begin{aligned} dk(5,1) &= dk(1,5); \\ dk(5,2) &= dk(2,5); \\ dk(5,3) &= dk(3,5); \\ dk(5,4) &= dk(4,5); \\ dk(5,5) &= (L11 * z + L13 * dy) * z + (L13 * z + L33 * dy) * dy; \\ dk(5,6) &= (-L11 * y + L13 * dz) * z + (-L13 * y + L33 * dz) * dy; \\ dk(5,7) &= L11 * z * p + L13 * dy * p; \end{aligned}$$

$$\begin{aligned} dk(6,1) &= dk(1,6); \\ dk(6,2) &= dk(2,6); \\ dk(6,3) &= dk(3,6); \\ dk(6,4) &= dk(4,6); \\ dk(6,5) &= dk(5,6); \\ dk(6,6) &= (-L11 * y + L13 * dz) * (-y) + (-L13 * y + L33 * dz) * dz; \\ dk(6,7) &= L11 * (-y) * p + L13 * dz * p; \end{aligned}$$

$$\begin{aligned} dk(7,1) &= dk(1,7); \\ dk(7,2) &= dk(2,7); \\ dk(7,3) &= dk(3,7); \end{aligned}$$

```
dk(7,4) = dk(4,7);
dk(7,5) = dk(5,7);
dk(7,6) = dk(6,7);
dk(7,7) = L11*p^2;

dF(1) = Nxxa;
dF(2) = Nxxa*dy;
dF(3) = Nxxa*dz;
dF(4) = Nxxa*(-2*A*alfa);
dF(5) = Nxxa*z+Mxxa*dy;
dF(6) = Nxxa*(-y)+Mxxa*dz;
dF(7) = Nxxa*p;

Kc = Kc + AW(j,2)*dk*J;
Fac = Fac + AW(j,2)*dF*J;

end
end
```

Elemstif.m

```

function K = elemstif(l,yz,leng,deriv,A,pstiff,psi,alf,n)
% ELEMSTIF
%
% Element Stiffness Integration
%
% ELEMSTIF:function that do the integration to obtain the element stiffness.
%     Integration is done with Gauss Quads with variable order of
%     integration.

%-----
%
%     Author: Andries J. du Plessis
%     Date:      March 31 1994
%     Modified:  October 12 1995
%     Copyright: MIT-SERC-AMSL (c) 1994
%-----

m = length(leng);

%----- Read Abiscissa and Weights for order n gaussian integration
AW = gausstab(n);

% ----- Integration for the Panels
K=zeros(14,14);
Bu = zeros(3,14);
for i = 1:m, %----- Integration across all the panels
    J = l*leng(i)/4; %---- Jacobian for transformation to [-1,1]
    %----- Determine the slope and intersection on [-1,1]
    myg = (yz(i+1,1)-yz(i,1))/2;
    cyg = (yz(i+1,1)+yz(i,1))/2;
    mzg = (yz(i+1,2)-yz(i,2))/2;
    czg = (yz(i+1,2)+yz(i,2))/2;
    mpsig = (psi(i,2)-psi(i,1))/2;
    cpsig = (psi(i,2)+psi(i,1))/2;
    alfa = alf(i);
    dy = deriv(i,1);
    dz = deriv(i,2);
    dk= [pstiff(i,1) pstiff(i,2) pstiff(i,3)
         pstiff(i,2) pstiff(i,4) pstiff(i,5)
         pstiff(i,3) pstiff(i,5) pstiff(i,6)];
    for j = 1:n, %----- First part of 2-D Gaussian integration.
        xj = (l*AW(j,1)+l)/2;
        for k = 1:n, %----- Second part of 2-D Gaussian integration.
            y = myg*AW(k,1)+cyg;
            z = mzg*AW(k,1)+czg;
            p = mpsig*AW(k,1)+cpsig;
            Bu(1,1) = -1/l;
            Bu(2,1) = 0;
            Bu(3,1) = 0;
            Bu(1,2) = 0;
            Bu(2,2) = -1/l*dy;
            Bu(3,2) = 0;
            Bu(1,3) = 0;

```

```
Bu(2,3) = -1/l*dz;
Bu(3,3) = 0;
Bu(1,4) = p*([12/l^3 -6/l^2]*[xj 1]');
Bu(2,4) = -2*A*alfa*([6/l^3 -6/l^2]*[xj^2 xj]');
Bu(3,4) = 0;
Bu(1,5) = -1/l*z;
Bu(2,5) = dz*([-1/l 1]*[xj 1]');
Bu(3,5) = -1/l*dy;
Bu(1,6) = 1/l*y;
Bu(2,6) = dy*([1/l -1]*[xj 1]');
Bu(3,6) = -dz/l;
Bu(1,7) = p*([6/l^2 -4/l]*[xj 1]');
Bu(2,7) = -2*A*alfa*([3/l^2 -4/l 1]*[xj^2 xj 1]');
Bu(3,7) = 0;
Bu(1,8) = 1/l;
Bu(2,8) = 0;
Bu(3,8) = 0;
Bu(1,9) = 0;
Bu(2,9) = 1/l*dy;
Bu(3,9) = 0;
Bu(1,10) = 0;
Bu(2,10) = 1/l*dz;
Bu(3,10) = 0;
Bu(1,11) = p*([-12/l^3 6/l^2]*[xj 1]');
Bu(2,11) = -2*A*alfa*([-6/l^3 6/l^2]*[xj^2 xj]');
Bu(3,11) = 0;
Bu(1,12) = 1/l*z;
Bu(2,12) = dz*([1/l 1]*[xj 0]');
Bu(3,12) = 1/l*dy;
Bu(1,13) = -1/l*y;
Bu(2,13) = -dy*([1/l -1]*[xj 0]');
Bu(3,13) = dz/l;
Bu(1,14) = p*([6/l^2 -2/l]*[xj 1]');
Bu(2,14) = -2*A*alfa*([3/l^2 -2/l]*[xj^2 xj]');
Bu(3,14) = 0;

K = K + AW(j,2)*AW(k,2)*Bu'*dk*Bu*J;

Bu = zeros(3,14);
end
end
end
```

Elecmech.m

```

function T = elecmech(l,yz,leng,deriv,A,pstract,psi,alf,n)
% ELECMECH
%
% Panel electro-mechanical coupling matrix construction
%
% ELECMECH:function that do the integration to obtain the coupling matrices.
%   Integration is done with Gauss Quads with variable order of
%   integration.
%   A - Area
%   pstract - reduced induced stress actuation
%   psi - warping function description
%   alf - extra constants used in warping function description
%   n - order of the gaussian integration

%-----
%
%   Author:      Andries J. du Plessis
%   Date:        April 4 1994
%   Modified:    October 12 1995
%   Copyright:   MIT-SERC-AMSL (c) 1994
%-----

m = length(leng);

%----- Read Abiscissa and Weights for order n gaussian integration
AW = gausstab(n);

% ----- Integration for the Panels
T = zeros(14,1);
Bu = zeros(3,14);
for i = 1:m, %----- Integration across all the panels
    J = l*leng(i)/4; %----- Jacobian for transformation to [-1,1]
    %----- Determine the slope and intersection on [-1,1]
    myg = (yz(i+1,1)-yz(i,1))/2;
    cyg = (yz(i+1,1)+yz(i,1))/2;
    mzg = (yz(i+1,2)-yz(i,2))/2;
    czg = (yz(i+1,2)+yz(i,2))/2;
    mpsig = (psi(i,2)-psi(i,1))/2;
    cpsig = (psi(i,2)+psi(i,1))/2;
    alfa = alf(i);
    dy = deriv(i,1);
    dz = deriv(i,2);
    dk= [pstract(i,1)
         pstract(i,2)
         pstract(i,3)];
    for j = 1:n,
        xj = (l*AW(j,1)+1)/2;
        for k = 1:n,
            y = myg*AW(k,1)+cyg;
            z = mzg*AW(k,1)+czg;
            p = mpsig*AW(k,1)+cpsig;
            Bu(1,1) = -1/l;
            Bu(2,1) = 0;

```

```

Bu(3,1) = 0;
Bu(1,2) = 0;
Bu(2,2) = -1/l*dy;
Bu(3,2) = 0;
Bu(1,3) = 0;
Bu(2,3) = -1/l*dz;
Bu(3,3) = 0;
Bu(1,4) = p*([12/l^3 -6/l^2]*[xj 1]');
Bu(2,4) = -2*A*alfa*([6/l^3 -6/l^2]*[xj^2 xj]');
Bu(3,4) = 0;
Bu(1,5) = -1/l*z;
Bu(2,5) = dz*[-1/l 1]*[xj 1]';
Bu(3,5) = -1/l*dy;
Bu(1,6) = 1/l*y;
Bu(2,6) = dy*[1/l -1]*[xj 1]';
Bu(3,6) = -dz/l;
Bu(1,7) = p*([6/l^2 -4/l]*[xj 1]');
Bu(2,7) = -2*A*alfa*[3/l^2 -4/l 1]*[xj^2 xj 1]';
Bu(3,7) = 0;
Bu(1,8) = 1/l;
Bu(2,8) = 0;
Bu(3,8) = 0;
Bu(1,9) = 0;
Bu(2,9) = 1/l*dy;
Bu(3,9) = 0;
Bu(1,10) = 0;
Bu(2,10) = 1/l*dz;
Bu(3,10) = 0;
Bu(1,11) = p*([-12/l^3 6/l^2]*[xj 1]');
Bu(2,11) = -2*A*alfa*([-6/l^3 6/l^2]*[xj^2 xj]');
Bu(3,11) = 0;
Bu(1,12) = 1/l*z;
Bu(2,12) = dz*[1/l 1]*[xj 0]';
Bu(3,12) = 1/l*dy;
Bu(1,13) = -1/l*y;
Bu(2,13) = -dy*[1/l -1]*[xj 0]';
Bu(3,13) = dz/l;
Bu(1,14) = p*([6/l^2 -2/l]*[xj 1]');
Bu(2,14) = -2*A*alfa*[3/l^2 -2/l]*[xj^2 xj]';
Bu(3,14) = 0;

T = T + AW(j,2)*AW(k,2)*Bu'*dk*J;
Bu = zeros(3,14);

```

```

end
end
end

```

Distrib.m

```

function dBn = distrib(l,q,n);
% DISTRIB
%
% Distributed force integration
%
% DISTRIB: function that do the integration to obtain the constant element
%       nodal loads for the analysis. Forcing constant along length.
%       Integration is done with Gauss Quads with variable order of
%       integration.
%       l - length of element
%       q - vector that obtain the distributed loading
%       n - order of the gaussian integration
%-----
%
%       Author: Andries J. du Plessis
%       Date:      April 7 1994
%       Modified:  October 2 1995
%       Copyright: MIT-SERC-AMSL (c) 1994
%-----
%----- Read Abiscissa and Weights for order n gaussian integration
AW = gausstab(n);
%----- Integration
J = 1/2;
dBn = zeros(14,1);
N = zeros(7,14);
for j = 1:n,
    xj = (l*AW(j,1)+l)/2;
    N(1,1) = [-1/l 1]*[xj 1]';
    N(2,2) = [-1/l 1]*[xj 1]';
    N(3,3) = [-1/l 1]*[xj 1]';
    N(4,4) = [2/l^3 -3/l^2 1]*[xj^3 xj^2 1]';
    N(4,7) = [1/l^2 -2/l 1]*[xj^3 xj^2 xj]';
    N(5,5) = [-1/l 1]*[xj 1]';
    N(6,6) = [-1/l 1]*[xj 1]';
    N(7,4) = [6/l^3 -6/l^2]*[xj^2 xj]';
    N(7,7) = [3/l^2 -4/l 1]*[xj^2 xj 1]';
    N(1,8) = [1/l 1]*[xj 0]';
    N(2,9) = [1/l 1]*[xj 0]';
    N(3,10) = [1/l 1]*[xj 0]';
    N(4,11) = [-2/l^3 3/l^2]*[xj^3 xj^2]';
    N(4,14) = [1/l^2 -1/l]*[xj^3 xj^2]';
    N(5,12) = [1/l 1]*[xj 0]';
    N(6,13) = [1/l 1]*[xj 0]';
    N(7,11) = [-6/l^3 6/l^2]*[xj^2 xj]';
    N(7,14) = [3/l^2 -2/l]*[xj^2 xj]';

    dBn = dBn + AW(j,2)*N'*q*J;
    N = zeros(7,14);
end

```


Plyrp.m

```

function Qr = plyrp(Q,deg)
% PLYRP
%
% Rotated ply properties [Jones p.48]
% Qr - rotated ply properties
% Q - properties in the ply coordinate system
% deg - angle of major ply direction relative to structural axis. See [Jones]

%-----
%
% Author: Andries J. du Plessis
% Date: March 29 1994
% Copyright: MIT-SERC-AMSL (c) 1994
%-----

%----- Error messages
if nargin~=2
    error('Too few arguments');
end
if abs(deg)>180
    error('Angle of ply incorrectly specified');
end
[mx,nx]=size(Q);
if((mx~=3)&(nx~=3))
    error('Stiffness property matrix incorrect');
end

%----- Rotation
Qr = zeros(3);
the = (pi/180)*deg;
c = cos(the);
s = sin(the);
T = [c^2 s^2 2*s*c
      s^2 c^2 -2*s*c
      -s*c s*c (c^2-s^2)];
R = [1 0 0
      0 1 0
      0 0 2];
Qr = inv(T)*Q*R*T*inv(R);

```

Gausstab.m

```
function AW = gausstab(n);
% GAUSSTAB - Look up table for abscissa and weights for the gaussian
% quadrature integration scheme. Only allow for orders 2 to 5.

%-----
%
% Author: Andries J. du Plessis
% Date: March 31 1994
% Copyright: MIT-SERC-AMSL (c) 1994
%-----

if n == 2
    AW = [1/sqrt(3) 1
          -1/sqrt(3) 1];
end
if n == 3
    AW = [0 8/9
          sqrt(0.6) 5/9
          -sqrt(0.6) 5/9];
end
if n == 4
    AW = [0.3399810436 0.6521451549
          -0.3399810436 0.6521451549
          0.8611363116 0.3478548451
          -0.8611363116 0.3478548451];
end
if n == 5
    AW = [0.0000000000 0.5688888889
          0.5384693101 0.4786286705
          -0.5384693101 0.4786286705
          0.9061798459 0.2369268850
          -0.9061798459 0.2369268850];
end
```

The ANSYS code consisted of three different files which was run as a batch to obtain the blade twist. A flowchart of the code is shown in Figure C-1. CH47D.mod is the main part of the code which does grid and area definition as well as meshing of the model. In the main code the composite element construction is defined by calling the routines CH47Dlr.mod and CH47Dm.mod. The subroutine CH47Dlr.mod defines the construction of the plate elements whereas CH47Dm.mod defines the ply materials used for elements.

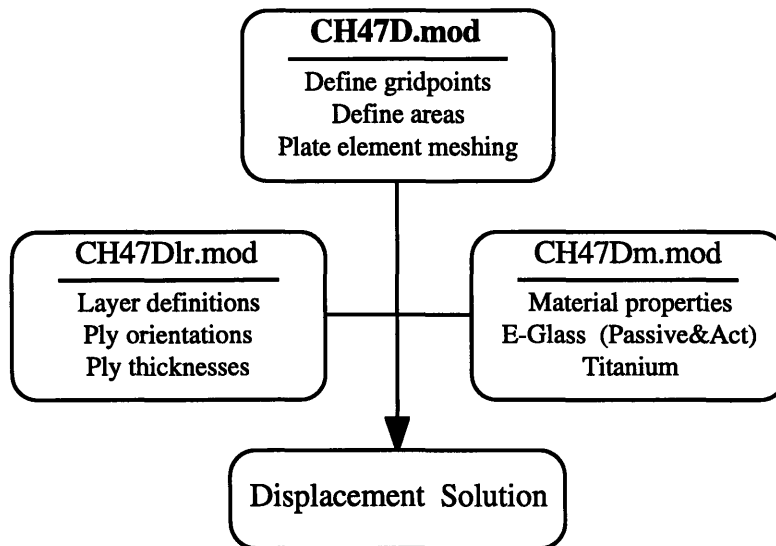


Figure C-1. ANSYS Code Flowchart

CH47D.mod

```

/COM, ANSYS REVISION 5.0
/COM,
/COM, CH47-D Blade Finite Element Model
/COM,
/COM, This file contains the model of a CHINOOK 47-D
/COM, actuated helicopter blade. The objective of this model
/COM, is to verify actuation results obtained through a
/COM, higher order actuated beam model done with MATLAB
/COM,
/COM, A.J. du Plessis 11-20-94
/COM, MIT-SERC (copywrite)

/FILNAME,test
/TITLE,CH47-D Actuated Blade
/UNITS,BIN

/com,
/com, Start preprocessor and set element types: SHELL 91
/com,
/prep7
antype,static
ET,1,91 !Element used for the top panel of the blade
!ET,2,91 !Element used for the righthand panel of the blade
!ET,3,91 !Element used for the bottom panel of the blade
!ET,4,91 !Element used for the lefthand panel of the blade
/com,
/com, Load #-layers per element and the real constant set
/com, used for every element (material, orientation, thickness)
/com,
*ulib,ch47lr.mod,/home/ajduples/Ansys/
*use,LAYERS
*use,RCSET
/com,
/com, Load material properties
/com,
*ulib,ch47m.mod,/home/ajduples/Ansys/
*use,ACTEG1,1 ! Active E-Glass at -45 deg
*use,ACTEG2,2 ! Active E-Glass at 45 deg
*use,EGLASS,3 ! Non active E-Glass at 0 deg
*use,TITA,4 ! Titanium outerskin
/com,
/com, GEOMETRIC MODELING -----
/com,
del = 1e-5 ! Defined tolerance for "selecting" purposes
bleng = 270 ! Blade length (Other dimensions defined in the
! keypoint assignment

/com, Define keypoints
k,1,0,-5.57,1.47
k,2,0,5.57,1.47
k,3,0,5.57,-1.47
k,4,0,-5.57,-1.47
K,5,bleng,-5.57,1.47
K,6,bleng,5.57,1.47
K,7,bleng,5.57,-1.47

```

```
K,8,bleng,-5.57,-1.47
```

```
/VUP,ALL,Z  
/VIEW,,1,.25,.5  
/psym,esys,1
```

```
/com, Define areas used in the analysis  
A,1,5,6,2  
A,2,6,7,3  
A,3,7,8,4  
A,4,8,5,1
```

```
/com, Meshing of the different areas  
/com, Area 1 - Top Panel  
real,1  
type,1  
asel,,area,,1  
esize,,3  
lesize,1,,,12  
lesize,3,,,12  
amesh,1
```

```
/com, Area 2 - Righthandside Panel  
/com,real,2  
/com,type,2  
asel,,area,,2  
esize,,1  
lesize,6,,,12  
amesh,2
```

```
/com, Area 3 - Bottom Panel  
/com,real,3  
/com,type,3  
asel,,area,,3  
esize,,3  
lesize,9,,,12  
amesh,3
```

```
/com, Area 4 - Lefthandside Panel  
/com,real,4  
/com,type,4  
asel,,area,,4  
esize,,1  
amesh,4
```

```
nummrg,all,1e-6 ! Merge all coincident nodes/keypoints/etc.  
/com,wsort ! Sort node numbering for the best wavefront  
finish
```

```
/com,  
/com, MODELING COMPLETE -----  
/com,
```

```
/com,  
/com, SOLUTION PHASE -----  
/com,
```

```
/solu

/com, Geometric boundary conditions
nse1,s,loc,x,-del,del
d,all,all
nse1,all
esel,all

/com, Apply the "temperature" loading for every layer at every node
BFE,ALL,TEMP,1,1,1,1,1 ! T=1 to get induced strain of 220e-6 [strain]
BFE,ALL,TEMP,5,1,1,1,1
BFE,ALL,TEMP,9,1,1,1,1
BFE,ALL,TEMP,13,1,1,1,1
BFE,ALL,TEMP,17,1,1,1,1
BFE,ALL,TEMP,21,1,1,1,1
BFE,ALL,TEMP,25,1,1,1,1
BFE,ALL,TEMP,29,1,1,1,1
BFE,ALL,TEMP,33,1,1,1,1
BFE,ALL,TEMP,37,1,1,1,1
BFE,ALL,TEMP,41,1,1,1,1
BFE,ALL,TEMP,45,1,1,1,1
BFE,ALL,TEMP,49,1,1,1,1
BFE,ALL,TEMP,53,1,1,1,1
BFE,ALL,TEMP,57,1,1,1,1
solve
save
finish
/com,
/com, SOLUTION FINISHED -----
/com,

/com,
/com, OUTPUT RESULTS -----
/com,
/post1
set
/psym,esys,0
pldisp,1
/com, Create a graphics file with the output plot
/com,/show,plots,plt
/com,pldisp
/com, Select nodes along vertice
/com,nse1,s,loc,y,5.57-del,5.57+del
/com,nse1,r,loc,z,1.47-del,1.47+del
/com,nsort,loc,x,1
/com, Output current selected nodes and displacements to a data file
/com,/output,data,dat
/com,nlist
/com,prnsol,u
/com,/output
/com,finish
/com,/eof
```

CH47Dlr.mod

LAYERS

/com,

/com, Number of layers in every panel

/com,

keyo, 1, 3,14 !Number of layers in the top Panel

keyo, 2, 3,14 !Number of layers in the righthand Panel

keyo, 3, 3,14 !Number of layers in the bottom Panel

keyo, 4, 3,14 !Number of layers in the lefthand Panel

/EOF

RCSET

/com,

/com, Real constant set to be used with every element

/com, (Material,Orientation(deg),layer thickness)

/com, 1st Real Constant Set

R,1,1,-45,.01,.01,.01

RMORE,2,45,.01,.01,.01

RMORE,1,-45,.01,.01,.01

RMORE,2,45,.01,.01,.01

RMORE,3,0,.1,.1,.1

RMORE,1,-45,.01,.01,.01

RMORE,2,45,.01,.01,.01

RMORE,1,-45,.01,.01,.01

RMORE,2,45,.01,.01,.01

RMORE,1,-45,.01,.01,.01

RMORE,2,45,.01,.01,.01

RMORE,1,-45,.01,.01,.01

RMORE,2,45,.01,.01,.01

RMORE,4,0,.04,.04,.04

/eof

/com, 2nd Real Constant Set

R,2,1,-45,.01,.01,.01

RMORE,2,45,.01,.01,.01

RMORE,1,-45,.01,.01,.01

RMORE,2,45,.01,.01,.01

RMORE,3,0,.1,.1,.1

RMORE,1,-45,.01,.01,.01

RMORE,2,45,.01,.01,.01

RMORE,1,-45,.01,.01,.01

RMORE,2,45,.01,.01,.01

RMORE,1,-45,.01,.01,.01

RMORE,2,45,.01,.01,.01

RMORE,1,-45,.01,.01,.01

RMORE,2,45,.01,.01,.01

RMORE,4,0,.04,.04,.04

/com, 3rd Real Constant Set

R,3,1,-45,.01,.01,.01

RMORE,2,45,.01,.01,.01

RMORE,1,-45,.01,.01,.01

RMORE,2,45,.01,.01,.01

RMORE,3,0,.1,.1,.1,.1
RMORE,1,-45,.01,.01,.01,.01
RMORE,2,45,.01,.01,.01,.01
RMORE,1,-45,.01,.01,.01,.01
RMORE,2,45,.01,.01,.01,.01
RMORE,1,-45,.01,.01,.01,.01
RMORE,2,45,.01,.01,.01,.01
RMORE,1,-45,.01,.01,.01,.01
RMORE,2,45,.01,.01,.01,.01
RMORE,4,0,.04,.04,.04,.04

/com, 4th Real Constant Set
R,4,1,-45,.01,.01,.01,.01
RMORE,2,45,.01,.01,.01,.01
RMORE,1,-45,.01,.01,.01,.01
RMORE,2,45,.01,.01,.01,.01
RMORE,3,0,.1,.1,.1,.1
RMORE,1,-45,.01,.01,.01,.01
RMORE,2,45,.01,.01,.01,.01
RMORE,1,-45,.01,.01,.01,.01
RMORE,2,45,.01,.01,.01,.01
RMORE,1,-45,.01,.01,.01,.01
RMORE,2,45,.01,.01,.01,.01
RMORE,1,-45,.01,.01,.01,.01
RMORE,2,45,.01,.01,.01,.01
RMORE,4,0,.04,.04,.04,.04

/EOF

CH47Dm.mod

```

ACTEG1
/com,
/com, Active E-Glass at -45 degrees
/com,
mp,ex,ARG1,6.3e6
mp,ey,ARG1,1.74e6
mp,ez,ARG1,1.74e6
mp,alpx,ARG1,1,220e-6 ! "Equivalent" Thermal Strian Induced
! Sign determined from the actuation desired
mp,alpy,ARG1,0
mp,alpz,ARG1,0
mp,nuxy,ARG1,0.3
mp,nuyz,ARG1,0
mp,nuxz,ARG1,0
mp,gxy,ARG1,0.52e6
mp,gyz,ARG1,1e8 ! I don't have values for Gyz - Fudge it
mp,gxz,ARG1,1e8 ! Ditto
! Other properties not assigned any values as they are not
! needed in the analysis or SHELL 91 don't use them (stiffness)
/EOF

```

```

ACTEG2
/com, Active E-Glass at 45 deg
mp,ex,ARG1,6.3e6
mp,ey,ARG1,1.74e6
mp,ez,ARG1,1.74e6
mp,alpx,ARG1,-220e-6 ! "Equivalent" Thermal Strian Induced
! Sign determined from the actuation desired
mp,alpy,ARG1,0
mp,alpz,ARG1,0
mp,nuxy,ARG1,0.3
mmp,nuyz,ARG1,0
mp,nuxz,ARG1,0
p,gxy,ARG1,0.52e6
mp,gyz,ARG1,1e8 ! I don't have values for Gyz - Fudge it
mp,gxz,ARG1,1e8 ! Ditto
/EOF

```

```

EGLASS
/com, E-Glass Properties
mp,ex,ARG1,6.3e6
mp,ey,ARG1,1.74e6
mp,ez,ARG1,1.74e6
mp,alpx,ARG1,0 ! NO Induced Strain
mp,alpy,ARG1,0
mp,alpz,ARG1,0
mp,nuxy,ARG1,0.3
mp,nuyz,ARG1,0
mp,nuxz,ARG1,0
mp,gxy,ARG1,0.52e6
mp,gyz,ARG1,1e8 ! I don't have values for Gyz - Fudge it
mp,gxz,ARG1,1e8 ! DittoMP,EX,3,6.3e6
/EOF

```

```

TTTA

```

```
/com, Titanium Properties
mp,ex,ARG1,15e6
mp,ey,ARG1,15e6
mp,ez,ARG1,15e6
mp,alpx,ARG1,0 ! No Induced Strain
mp,alpy,ARG1,0
mp,alpz,ARG1,0
mp,nuxy,ARG1,0.3
mp,nuyz,ARG1,0
mp,nuxz,ARG1,0
mp,gxy,ARG1,6.2e6
mp,gyz,ARG1,6.2e6 ! Isotropic Material - No Fudging
mp,gxz,ARG1,6.2e6 ! Isotropic Material - No Fudging
/EOF
```

4271-94